Development of Implantable Bioartificial Kidney Based on Two-dimensional and Three-dimensional Hydrolyzed Polyacrylamide Hydrogel

Marleine Tamer

THÈSE POUR OBTENIR LE GRADE DE DOCTEUR DE L'UNIVERSITÉ DE MONTPELLIER

En Chimie et Physicochimie Des Matériaux

École doctorale SCIENCE CHIMIQUES BALARD (ED459)

Unité de recherche Institut Européen Des Membranes (UMR 5635, CNRS, UM, ENSCM)

DEVELOPMENT OF IMPLANTABLE BIOARTIFICIAL KIDNEY BASED ON TWO-DIMENSIONAL AND THREE-DIMENSIONAL HYDROLYZED POLYACRYLAMIDE HYDROGEL

Présentée par Marleine TAMER
Le 10 Décembre 2021

Sous la direction de Mikhael BECHELANY,
La codirection Maria BASSIL,
L'encadrement de Sebastien BALME et Philippe MIELE

Devant le jury composé de

M. Fabien PICAUD, Maître de Conférences, Université de Franche-Compté	Rapporteur
M. Roland HABCHI, Full Professor, Université Libanaise	Rapporteur
Mme. Sophie TINGRY, Directeur de Recherches, CNRS, Université de Montpellier	Présidente
Mme. Camille RAILLON, Chercheur CEA, Université Grenoble Alpes	Examinateur
Mme. Maria BASSIL, Full Professor, Université Libanaise	Co-Directeur
M. Mikhael BECHELANY, Directeur de Recherches CNRS, Université de Montpellier	Directeur
M. Sébastien BALME, Maître de Conférences, Université de Montpellier	Co-Encadrant
M. Mario EL TAHCHI, Full Professor, Université Libanaise	Invité
M. Philippe MIELE, Professeur, École Nationale Supérieure de Chimie de Montpellier	Invité

UNIVERSITÉ DE MONTPELLIER

Acknowledgement

I would like to extend my deepest sincerest gratitude to all the people who helped me and have shared with me the knowledge to achieve this work.

My profound gratitude and recognition are expressed, foremost, to my academic supervisors, **Dr. Maria Bassil** and **Dr. Mikhael Bechelany.** I would like to warmly thank them for believing in my potential and providing me with the right tools to strive in using my talents and curiosity during these four years. I revere their eminent support and most importantly, their humanitarian and professional values, which were reflected throughout the thesis work. Their equanimity and constant motivation inspired me to dare to aim high. Their erudite work was undoubtedly key to facing all the challenges during the research time of the thesis.

Moreover, I would like to profoundly thank **Dr. Sebastian Balme and Dr. Mario El Tahchi** for sharing with me scientific culture, competences and experience. Their hard questions incented me to widen my research from various perspectives. Additionally, I would like to thank **Dr. Philippe Miele** for his support in further scientific consultations and discussions.

I would like to give my sincere gratitude to **Dr. Frederic Cuisinier, Dr. Csilla Gergely,** and **Dr. Bela Varga** for allowing me to have an appropriate platform to work on the biological part and to get all the necessary information I need to make this thesis possible. I would also like to thank **Dr. Vincent Huon** and **Jonathan Barés** for offering me the opportunity to work in their laboratory for mechanical characterization.

I would like to thank **Mr. Fabien PICAUD,** Lecturer at University of Franche-Compté and **Mr. Roland HABCHI,** Full Professor at Lebanese University for the honor they gave it to me to evaluate my work. I also want to thank **Mrs. Sophie TINGRY,** Research Director at CNRS, University of Montpellier and **Mrs. Camille RAILLON,** CEA Researcher at Grenoble Alpes University for accepting to be members of my Ph.D. examination committee.

This thesis could not be the same without the presence of **Dr. Maya Abdallah**. who helped me and gave me her experience in the field of cell culture.

To the academic institutions, Lebanese University (LU), University of Montpellier, and Balard Chemical Sciences Doctoral School, I will always appreciate the frame you built and the opportunity you provided me to do my Ph.D. I am proud to be part of these communities, where intelligence and hard work are both appreciated.

My sincere gratitude goes to my IEM colleagues and friends, with whom I have lived amazing and unforgettable moments during my time there, **Dr. Danae Gonzalez Ortiz, Dr. Habib Belaid, Dr. Octavio Graniel Tamayo, Dr. Carlos Castilla-Martinez, Dr. Enrique Folgado, Dr. Cyril Oberlin, Dr. Wassim Sebai, Dr. Sakthivel Nagarajan, Dr. Imad Abrao Nemeir, Dr. Tianji Ma, Dr. Ghady Dakroub, Dr. Ghenwa Chawich, Dr Syreina Al Sayegh, Dr. Sara Kourani,** and the Doctors to be: **Hana Bouzit, Carole Barou, Nathan Meyer, Raphael Chabas, Fida Tanos and Joelle Hayek**.

Thanks to my second family **Dr. Konie Al Khoury, Dr. Angela Haykal, Dr. Mirella Katrib, Dr. Claudette Mansour, Dr. Rana Tanos, Raneen Khalil Ibrahim**, and the Doctors to be: **Marie Rahme, Maroun Alam, Petros Abi Youness, Georges Matta, and Cynthia Farha**, with whom I laughed, cried, suffered and enjoyed unforgettable moments throughout my four years working on my thesis. Thanks to them, Montpellier is not just the place where I complete my PhD, rather it is also the place where I met brothers and sisters.

I would also like to thank **Dr. Rodrigue Mounzer** for his scientific support in medicine and for **Father Marcelino Assal** for his spiritual support.

I express my deepest gratitude to my parents, **Elias** and **Alice**, and my three sisters**, Loraine, Joelle, and Elise,** for supporting me through adversity times, and believing in my potential. Even from miles away, I felt their presence and got their efforts in helping me to seek what I am passionate about. I am very lucky to have a family that always pushes me to march into the right career and spiritual paths. I will forever owe my achievements to my dedicated, caring, and thoughtful family.

Finally, I owe many thanks to my very special person, my husband, **Dr. Elia Zgheib**, for his true love and big support. Thanks for all the help, the scientific advices and for always showing me new directions when faced by challenges. Thank you for making the four years of my thesis work easier for me. I am grateful to have you by my side. I love you.

Table of content

List of Figures

Chapter I:

Chapter II:

Chapter III:

List of Tables

Chapter I:

Chapter II:

Chapter III:

General Introduction

The kidney plays an essential role in normal homeostasis, it maintains the normal body fluid composition for a normal cellular size and function, retains plasma volume, plays a role in red blood cell production, controls the intravascular volume, and excretes nitrogenous waste a wide range of pharmacologic and exogenous toxic compounds in the urine. The glomerulus is a complex network of capillaries responsible for the selective ultrafiltration of plasma and the clearance of small solutes such as water, sodium, and urea while excluding the passage of cells and large proteins such as albumin. The basement membrane, endothelium, and podocytes confer a net negative charge to the filtration barrier. As a result, negatively charged proteins such as albumin are less likely to pass through the filtration barrier. The glomerulus has four major components: the endothelium, the mesangium, the basement membrane, and the podocytes[1].

Each kidney filters and clears approximately 160 L of plasma per day. The kidney filtration membrane is characterized by its size and charge selectivity. Chronic Kidney Disease (CKD) refers to a wide range of conditions which damage the kidneys, and reduce their efficiency to filter the blood[1,2]. 5% to 10% of the population worldwide suffers from (CKD) and few of them receive hemodialysis treatment[3]. Hemodialysis is a treatment method in which blood purification is performed by a dialyzer machine that purifies blood by diffusion of molecules through a porous hollow fiber membrane. Since many types of equipment, such as pump and monitoring device, are required, it is necessary for the patients to receive treatments at the hospitals 3-4 times a week, lead significantly low quality of life of the patients and rising socio-economical burdens on our societies[4,5].

Many studies are made to develop an implantable or portable dialysis device, in order to alleviate the burden of dialysis treatment, by miniaturizing the whole dialysis system[5], but they still facing many limitations, such as the limited flow rate (1 ml/min ≈ 1.44 L per day) avoiding any additional pressure which might be generated in the cells membrane interface that is fragile and create cracks in the membrane[6]. In addition, the loss of blood pressure in the *in vivo* application, the short lifetime of the membrane and the decrease of filtration efficiency after 7 days[5,7], slows down the transition to the device implantation.

Poly(ether sulfone) and polyester membrane are the most used membrane for the filtration devices[5,8], characterized by their multifunctionality, including surface hydrophilicity, ion

exchange and biofouling resistance to proteins and bacteria[9]. These membranes are limited by their mirror-polished surface that can prevent protein adhesion[7].

In this work, we aim to extend the life time of the device, and increase its efficiency to maintain the performance for a long time, even years to assure the blood filtration in case of kidney failure by developing a new microfluidic "filtration units" based on hydrolyzed Polyacrylamide hydrogel. The ultimate goal of this work is to develop a biocompatible implantable bioartificial kidney that mimic the work of a natural kidney.

In this thesis, we aim to develop several "filtration units" each having a specific filtration function and serving as building blocks of the future bioartificial kidney. The "filtration unit" of this device is made by robust silicon membranes that are biocompatible and present total toxin clearance at pressure compared to blood[1,6].

In Chapter 1, the kidney anatomy is detailed by developing specially the filtration function of a kidney. The kidney structure and the blood circulation is described, going from the blood entrance to the kidney, to the filtration carried out by the glomeruli inside the nephrons. The role of podocyte cells and the basement membrane in kidney filtration is elaborated, focusing on the foot processes that block the passage of high-molecular-weight proteins.

Kidney disease refers to a wide range of conditions that damage the kidneys and reduce their efficiency in purifying blood[2,11,12]. The actual treatments such as transplantation and dialysis are detailed, and the disadvantages of this treatment are mentioned. The microfluidic bioartificial kidney is presented in this chapter as a promising approach to treat the patients in case of kidney failure. The application and the preparation methods are detailed, explaining the preparation method of PDMS layers and their assembly using Plasma Oxygen treatment, forming a small device encapsulating a specific filtration membrane.

Different types of membrane used as a filtration barrier for kidney filtration application are mentioned in Chapter 1, while focusing on Hydrolyzed Polyacrylamide hydrogel that have many advantages over other type of membranes, which can mix the filtration function of a membrane and the properties of a scaffolding material suitable for cell culture. In addition, structural and

mechanical properties of PAAM hydrogel can be easily controlled making it a good scaffold for cell, that can be affected by the stiffness and the porosity of scaffold, as mentioned in Chapter 1.

The chapter 2 will describe the design and the conception of bioarticial kidney, which is composed of several filtration units. The fabrication of filtration unit is detailed after, from the mold design, to the PDMS preparation, to the assembly of several PDMS layers. The preparation of 2D hydrogel that will be encapsulated inside the device will be detailed. The hydrogel having different crosslinker concentration were characterized by measuring the swelling degree and Young's Modulus. The filtration ability of the device is tested under different experimental conditions, using different flow rate, hydrogels having different crosslinker density. The ability of the hydrogel to mimic the kidney filtration is tested using different compounds, ions and molecules having different molecular weight.

In chapter 3, the ability of PAAM hydrogel to encapsulate cell spheroids was tested. The fabrication of a macroporous Hydrolyzed Polyacrylamide Hydrogel was detailed. Different hydrogel was prepared having different experiment parameters (volume of the mixture, oil/water ratio of the emulsion, the surfactant content, the crosslinker density, hydrolysis rate) and the effect of each parameter on the 3D PAAM Hydrogels properties is evaluated (swelling, Young's Modulus, Porosity, morphology). The formation of podocyte spheroids is tested on different hydrogel prepared in order to investigate their effect on the spheroid formation, stability, proliferation and death.

Finally, the conclusion part will summarize the main findings of this thesis. Moreover, perspectives will be proposed as possible for future work.

References

1. Bomback, A. S. *et al. National Kidney Foundation's primer on kidney diseases*. (2018).

2. N, R. *et al.* Improvements in Glomerular Filtration Rate (GFR) in Chronic Kidney Disease (CKD) Patients Using a Commercial Patented and Proprietary ProbioticPrebiotic Formulation* - 3rd Biennial Survey. *International Journal of Nephrology and Kidney Failure* **4**, (2018).

3. Levey, A. S., Inker, L. A. & Coresh, J. Chronic Kidney Disease in Older People. *JAMA* **314**, 557 (2015).

4. Ising, C. & Brinkkoetter, P. T. Prohibitin Signaling at the Kidney Filtration Barrier. in *Mitochondrial Dynamics in Cardiovascular Medicine* (ed. Santulli, G.) vol. 982 563–575 (Springer International Publishing, 2017).

5. Ota, T., Nakayama, M., Kanno, Y., Suzuki, T. & Miki, N. In vitro and in vivo tests of nanoporous membrane coated with biocompatible fluorine-doped diamond-like carbon for hemofiltration treatment. in 412–414 (IEEE, 2018). doi:10.1109/MEMSYS.2018.8346575.

6. Qu, Y. *et al.* A nephron model for study of drug-induced acute kidney injury and assessment of drug-induced nephrotoxicity. *Biomaterials* **155**, 41–53 (2018).

7. Ota, T., To, N., Kanno, Y. & Miki, N. Evaluation of biofouling in stainless microfluidic channels for implantable multilayered dialysis device. *Japanese Journal of Applied Physics* **56**, 06GN10 (2017).

8. Wilmer, M. J. *et al.* Kidney-on-a-Chip Technology for Drug-Induced Nephrotoxicity Screening. *Trends in Biotechnology* **34**, 156–170 (2016).

9. Yi, Z., Liu, C.-J., Zhu, L.-P. & Xu, Y.-Y. Ion Exchange and Antibiofouling Properties of Poly(ether sulfone) Membranes Prepared by the Surface Immobilization of Brønsted Acidic Ionic Liquids via Double-Click Reactions. *Langmuir* **31**, 7970–7979 (2015).

10. UCSF. The Kidney Project - Device. *The Regents of the University of California* https://pharm.ucsf.edu/kidney/device.

11. Webster, A. C., Nagler, E. V., Morton, R. L. & Masson, P. Chronic Kidney Disease. *The Lancet* **389**, 1238–1252 (2017).

12. Romagnani, P. *et al.* Chronic kidney disease. *Nature Reviews Disease Primers* **3**, (2017).

Chapter I: Literature Review

I. Introduction

The kidney plays an essential role in normal homeostasis, it maintains the normal body fluid composition for a normal cellular size and function, retains plasma volume, plays a role in red blood cell production, controls the intravascular volume, and excretes nitrogenous waste a wide range of pharmacologic and exogenous toxic compounds in the urine. The glomerulus is a complex network of capillaries responsible for the selective ultrafiltration of plasma and the clearance of small solutes such as water, sodium, and urea while excluding the passage of cells and large proteins such as albumin. The glomerulus has four major components: the endothelium, the mesangium, the basement membrane, and the podocytes[1]. The basement membrane, endothelium, and podocytes confer a net negative charge to the filtration barrier. As a result, negatively charged proteins such as albumin are less likely to pass through the filtration barrier.

The kidney filtration membrane is characterized by its size and charge selectivity. Chronic Kidney Disease (CKD) refers to a wide range of conditions which damage the kidneys, and reduce their efficiency to filter the blood[1,2]. 10% to 15% of the population worldwide suffers from (CKD) and few of them receive hemodialysis treatment[3]. Hemodialysis is a treatment method in which blood purification is performed by a dialyzer machine that purifies blood by diffusion of molecules through a porous hollow fiber membranes. Since many big equipment are required, it is necessary for the patients to receive treatments at the hospitals 3-4 times a week, lead significantly low quality of life of the patients and rising socio-economical burdens on the societies[4,5].

Many studies are made to develop an implantable or portable dialysis device, in order to alleviate the burden of dialysis treatment, by miniaturizing the whole dialysis system[5].

This chapter aims to explain the normal kidney anatomy and function, and the disease affecting the kidney function, and detail the history of treatments used to replace kidney function.

In this chapter, the kidney anatomy will be detailed by developing specially the filtration function of a kidney. The kidney structure and the blood circulation will be described, going from the blood entrance to the kidney, to the filtration carried out by the glomeruli inside the nephrons.

Kidney disease refers to a wide range of conditions that damage the kidneys and reduce their efficiency in purifying blood[2,6,7]. The actual treatments such as transplantation and dialysis are

detailed, and the disadvantages of this treatment are mentioned. The microfluidic bioartificial kidney is presented in this chapter as a promising approach to treat the patients in case of kidney failure. The application and the preparation methods are detailed, explaining the preparation method of PDMS layers and their assembly using Plasma Oxygen treatment, forming a small device encapsulating a specific filtration membrane.

Different type of membrane used as a filtration barrier for kidney filtration application are mentioned in Chapter 1, while focusing on Hydrolyzed Polyacrylamide hydrogel that have many advantages over other type of membranes, which can mix the filtration function of a membrane and the properties of a scaffolding materials suitable for cell culture. In addition, structural and mechanical properties of PAAM hydrogel can be easily controlled making it a good scaffold for cell, that can be affected by the stiffness and the porosity of scaffold, as mentioned in Chapter 1.

II. Kidney

1. Kidney Anatomy

a) Kidney Structure

The kidneys are one of most important organ in the body; they play a vital role in normal body function. The kidney maintains the normal body fluid composition for a normal cellular size and function, retains plasma volume, regulates blood pressure, plays a role in red blood cell production, controls the intravascular volume, and excretes nitrogenous waste a wide range of pharmacologic and exogenous toxic compounds in the urine[1,8]. The kidneys are bean-shaped organs positioned on the posterior abdominal wall on either side of the vertebral column, each weighing approximately 150 g[1,8,9].

Anatomically, the kidneys are divided into two regions: an outer region called the cortex and an inner region called the medulla (Fig. 1). The cortex and medulla are composed almost entirely of

nephrons, blood vessels, lymphatics, and nerves. Each kidney contains approximately 1 million nephrons, which are the functional unit of the kidneys. The nephron is consisting of a renal corpuscle, proximal tubule, loop of Henle, distal tubule, and collecting duct system. The renal corpuscle consists of the glomerulus, Bowman capsule (Fig. 2).

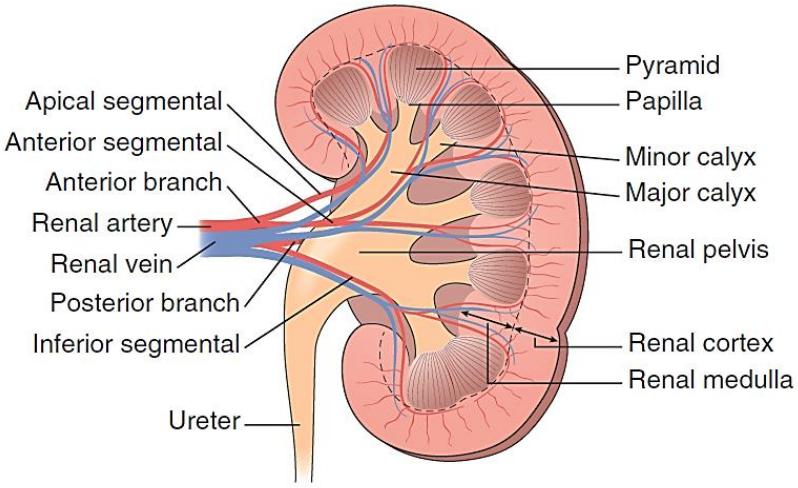

Figure 1. The anatomy of the kidney. Structure of a human kidney, cut open to show the internal structures[1].

The glomerulus, the distal tubule, and most of the proximal tubule are located in the cortex. The medulla is composed of parallel disposition of the limb of the loop of Henle and collecting ducts. The filtration process begins at the glomerulus. The glomerular filtrate flows into Bowman's capsule and enters the proximal tubule where approximately two-thirds of the filtrate is reabsorbed. Tubular fluid then flows through the thin descending limb of the loop of Henle, ascends through the thin into the thick ascending limb of the loop of Henle, and after pass through the distal convoluted tubule. The processed filtrate then flows into the cortical and medullary collecting ducts where the secretion of potassium and hydrogen ion is regulated. A highly coordinated process of solute reabsorption and secretion occurs as the filtrate passes through each part of the nephron, producing the excretion of the precise amount of water, acid-base equivalents, and electrolytes necessary to maintain homeostasis. The resulting urine passes from the papilla to the minor calyces, then to the major calyces which form the renal pelvis. The urine is carries out of the kidney through the ureter to the bladder, from which it is eliminated via the urethra. The lining of the renal pelvis, the ureter, the bladder, and the urethra are all epithelial cells that are impermeable to water, known as transitional cells[1,8].

b) Blood Circulation

The renal circulation is one of the richest vascular beds in the body, in which the renal blood flow comprises roughly 25% of the total cardiac output in resting individuals (about 1.25 L/min)[1,9]. The renal blood flow originate from the aorta and enter the kidneys in the hilum through the renal artery (Fig 1)[1,10]. The renal artery bifurcates first into segmental arteries, then branches progressively to form the interlobar artery, the arcuate artery, the interlobular artery, and the afferent arteriole, which branch off and leads into the glomerulus of Bowman's capsule, where high blood pressure in the glomerular cavity causes the fluid, solutes and waste to be filtered into the Bowman's space. From here, the glomerular capillaries come together to form the efferent arteriole, then subdivide into a second capillary network, the peritubular capillaries, which supply blood to the nephron. Blood then leaves the kidney and enters the venous circulation [1,8–11]. The venous vessels system run parallel to the arterial vessels, progressively form the interlobular vein, arcuate vein, interlobar vein, and renal vein, which courses beside the ureter[9].

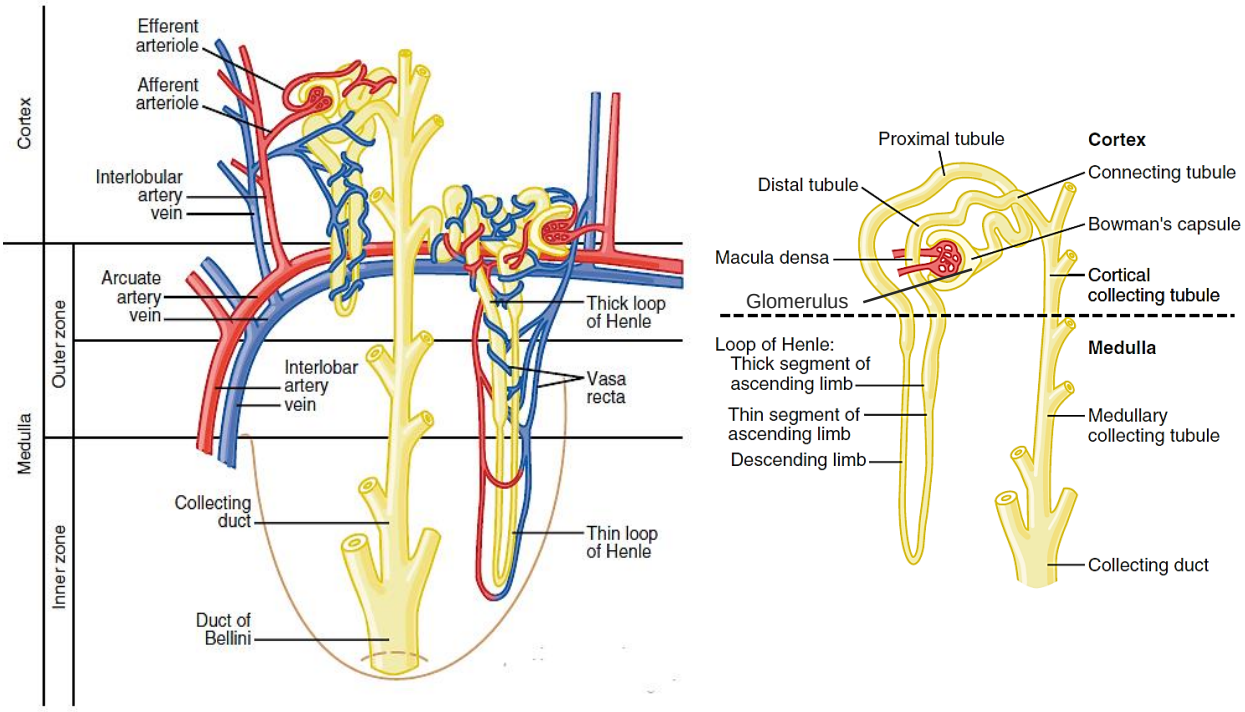

Figure 2. Diagram of **(a)** blood vessels, tubular structures and nephrons. **(b)** Single nephron and its tubular structures detailed[12].

c) Nephron

Nephrons are the basic structural and functional units of the kidneys. Each human kidney contains approximately 1.2 million nephrons, which are hollow tubes composed of a single cell layer. The nephron consists of a spherical filtering component, called renal corpuscle, proximal tubule, loop of Henle, distal tubule, and collecting duct system (Figure 2.). The renal corpuscle responsible for the initial step in urine formation, it separate protein-free filtrate from plasma, it consists of glomerular capillaries called the *glomerulus* and Bowman's capsule. The filtration barrier in the renal corpuscle through which all filtered substances must pass consists of 3 layers: the capillary endothelium of the *glomerulus*, a rather thick basement membrane, and a single-celled layer of epithelial cells[1,8,9,12].

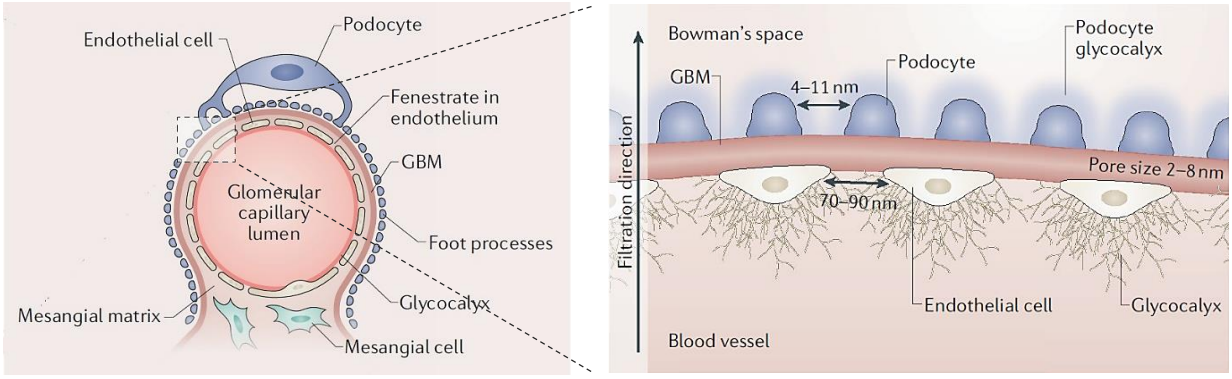

(a) **(b)**

Figure 3. **(a)** Diagram of the glomerulus showing its different section; The glomerular filtration barrier, located between the glomerular capillary lumen and the Bowman's space. The interstitium in the glomerular capillaries is composed of mesangial cells and the mesangial matrix. **(b)** Diagram of the glomerular filtration barrier showing the basement membrane aligned between the endothelial cells and the podocytes[11].

d) Glomerulus

The glomerulus is a complex network of capillaries supplied by the afferent arteriole and drained by the efferent arteriole, responsible for the selective plasma ultrafiltration and the clearance of small solutes such as water, sodium, and urea while excluding the passage of cells and large proteins such as albumin.

The glomerular filtration barrier, located between the glomerular capillary lumen and the Bowman's space, consists of the endothelial glycocalyx, endothelial cells, the glomerular basement membrane (GBM) and podocytes, which are negatively charged and confer a net negative charge to the filtration barrier (Figure 3). As a result, proteins having negative charge such as albumin are preferentially excluding to pass through the filtration barrier. The interstitium in the glomerular capillaries is composed of mesangial cells and the mesangial matrix, which are also involved in glomerular filtration and provide with the podocytes a structural scaffold that supports the glomerular capillaries[1,8,12].

The endothelial glycocalyx is located on the surface of endothelial cells, it is important for the vascular physiology of the kidney and prevents protein leakage. The glomerular basement membrane (GBM) is aligned between the endothelial cells and the podocytes, it constrains the filtration of proteins in concert with the endothelium and podocytes. GBM functions as a selective barrier helping to restrict the macromolecules passage and has an important role in limiting the flux of solutes and fluids. The endothelial layer features 70–90 nm fenestrations. The GBM has pores with sizes of 2–8 nm and is mainly composed of type IV collagen, laminin and proteoglycans. Podocytes are arranged in a monolayer with gaps of 4–11 nm and reside on the other side of the GBM, facing the Bowman's space. Like endothelial cells, podocytes are covered by a glycocalyx with a thickness of ~200 nm. These four layers form the size-selective and charge-selective glomerular filtration membrane[1,11].

2. Podocytes

Podocytes are highly specialized cells of the kidney glomerulus that represent the essential component for the formation and maintenance of the glomerular filtration barrier. Podocytes play an active role in preventing the entry of plasma proteins into the urinary ultrafiltrate by providing a barrier comprising filtration slits between foot processes, which represent a dynamic network of cellular extensions. The podocytes structure is characterized by cytoplasmic projections localized and attached on the glomerular basement membrane surface known as "foot processes". Foot processes of adjacent podocytes interdigitate and form a network of narrow and rather uniform

gaps of 2–8 nm that envelop the glomerular capillaries[11,13,14]. These intercellular junctions act as a critical barrier to block the passage of high-molecular-weight proteins[1].

Podocytes are a main functional element for filtering blood in the glomerulus, they are influenced by different signals of the surrounding environment such as mechanical and chemical signal from GBM. These signals control the maintenance of slit diaphragm and thus the main podocytes activity which maintain the main function of the kidney glomerulus. A healthy renal GBM is characterized by specific mechanical characteristics with a modulus of elasticity of 2.5 kPa. An increase of GBM elasticity has shown loss of organ function due to the damage generated in the podocytes or the podocytes-GBM interaction[15].

3. Kidney Filtration

Kidney filtration pass through three primary steps: glomerular filtration, reabsorption of substances from the renal tubules into the blood, and secretion of substances from the blood into the renal tubules.

Glomerulus Filtration is the first step in the formation of urine. Most substances in the plasma, except for proteins, are freely filtered, through the glomerular filtration barrier into Bowman's capsule. The filtered fluid (called the glomerular filtrate) is protein free and devoid of cellular elements, including red blood cells. The glomerular filtrate leaves Bowman's capsule and passes through the tubules, where water and specific solutes are reabsorbed and back into the blood[1,8,12].

a) Glomerular Filtration

The glomerular capillary membrane is composed of three major layers: the *endothelium* of the capillary, a *basement membrane,* and a layer of *podocytes* (Figure 3). Together, these layers make up the filtration barrier, which normally prevents filtration of plasma proteins. The capillary endothelium filtration is perforated by thousands of small holes called fenestrae that are relatively large and negatively charged hindering the passage of plasma proteins. The basement membrane consists of collagen scaffold and proteoglycan fibrillae allow the passage of a large amount of

water and small solutes, and effectively prevents filtration of plasma proteins, in part because of strong negative electrical charges. The final part of the glomerular membrane is a layer of epithelial cells or podocytes that line the outer surface of the glomerulus. The foot processes of podocytes are separated by a slit pores of 4–11 nm, in addition to the negative charges of the podocytes provide additional restriction to filtration of plasma proteins. Thus, the glomerular capillary wall layers provide a barrier to filtration of plasma proteins.

The final concentrations of the constituents of the glomerular filtrate, including salts and organic molecules, are similar to the concentrations in the plasma. Except a few low molecular-weight substances, such as calcium and fatty acids, which are partially bound to the plasma proteins and cannot freely filtered through the glomerulus capillaries[1,8,12].

Table I. Filtration, Reabsorption, and Excretion Rates of Different Substances by the Kidneys per day[12].

	Filtered	**Reabsorbed**	**Excreated (Urine)**
Glomerular filtration rate ml/min	110	109.1	0.9
Water volume filtered per day	180 L	179 L	1 L
Ions (g/l of filtered water)			
Chloride Cl^-	630 g (3.5 g/l)	625 g (3.49 g/l)	5 g (g/l)
Soduim Na^+	540 g (3 g/l)	537 g (3 g/l)	3g (g/l)
Bicarbonate HCO_3^-	300 g (1.67 g/l)	299.7 g (1.67 g/l)	0.3 g (g/l)
Potassium K^+	28 g (0.16 g/l)	24 g (0.13 g/l)	4 g (g/l)
Phosphate PO_4^{2-}			
Proteins (mg/l of filtered water)	10-20 mg/l	10-20 mg/l	-
Fibrinogen (340 KDa)	0.4-0.8 mg/l	0.4-0.8 mg/l	0
Albumine (69 KDa)	6-12 mg/l	6-12 mg/l	0
Globulins (93 kDa)	3.5-7 mg/l	3.5-7 mg/l	0
Other	~0.1 mg/l	-	-
Other (g/l of filtered water)			
Urea (60 Da)	53 g	28 g	25 g
Glucose (180 Da)	180g	180g	0
Uric Acid (168 Da)	8.5 g	7.7 g	0.8 g
Creatinine (113 Da)	1.4 g	0	1.4 g

b) Reabsorption and Secretion

The volume and composition of the final urine are quite different from those of the glomerular filtrate. As the filtrate flows from Bowman's capsule through the different parts of the tubule, its composition is changed, mainly by removing material (tubular reabsorption) but also by adding material (tubular secretion)[8]. In general, reabsorption is quantitatively more important than secretion in the formation of urine, but secretion plays an important role in determining the amounts of potassium and hydrogen ions and a few other substances that are excreted in the urine. Most substances such as urea, creatinine, and uric acid that must be cleared from the blood are poorly reabsorbed and are therefore excreted in large amounts in the urine[1,8,12].

Conversely, electrolytes, such as sodium ions, chloride ions, and bicarbonate ions, are strongly reabsorbed, so only small amounts appear in the urine. Some nutritional substances, such as amino acids and glucose, are completely reabsorbed from the tubules and do not appear in the urine even though large amounts are filtered through the glomerular capillaries (Table I). Other foreign substances and drugs are secreted from the blood into the tubules.

Each of the processes - glomerular filtration, tubular reabsorption and tubular secretion - is regulated according to the needs of the body. For example, when there is excess sodium intake, the rate of sodium filtration increases and a smaller fraction is reabsorbed, resulting an increase of sodium concentration in the urine[2,12].

c) Effect of Solute Size and Charge on the Filtration

The glomerular filtration barrier is selective based on their size and electrical charge. All electrolytes and small organic compounds are freely filtered; as the molecular weight of the molecule approaches that of albumin (69 kDa), the filterability rapidly decreases[8,12].

Large molecules having negative charge are filtered less easily than those having positive charge of equal molecular size. Albumin that have a molecular diameter of 6 nanometers is restricted from filtration through the 8 nm pores of the glomerular membrane because of its negative charge and the electrostatic repulsion exerted by negative charges of the glomerular capillary. Studies are made on positive, negative and neutral Dextran, show that for a given molecular weight the neutral and

positively charged molecules are filtered more readily than negatively charged dextrans of equal molecular weight[12].

4. Chronic Kidney Disease

Chronic kidney disease (CKD) is defined by persistent abnormalities of kidney structure or function. CKD is a chronic condition, meaning kidney function continues to decline over time, it refers to a wide range of conditions that damage the kidneys and reduce their efficiency in purifying blood[2,6,7].

CKD is a progressive loss of kidney function where the nephrons are damaged and they stop working. It is due to old age and can be accelerated by diabetes, hypertension, obesity, genetics and primary renal disorders. In its turn, CKD can accelerate Cardiovascular Disease (CVD) and is considered an independent risk factor for CVD events. There is a graded inverse relationship between CVD risk and glomerular filtration rate (GFR) that is independent of age, sex and other risk factors[2,6,16].

Since Podocytes are influenced by mechanical and chemical signal from GBM. Once podocytes or podocytes-GBM interaction are damaged, the podocytes connectivity will be modified and the foot processes will become flattened and fused. This abnormal slit diaphragm structure between podocytes foot processes cause the waste of some protein. A change in the glomerular membranes charge a protein leak through the glomerular capillaries. The massive proteins leakage into the urine during the blood filtration is the sign of kidney disease caused by the glomerular filtration barrier dysfunction. In addition, the increase in blood pressure leads to an increase the rate of decline in kidney function by damaging nephrons and glomeruli[2,8,15].

Kidney have an essential role for a normal body function. Kidney filtration membrane (basement membrane, endothelium, and podocytes) is responsible of normal kidney filtration. Chronic kidney disease is a global public health problem, it reduces the efficiency of kidneys to filter the blood, and affects 10 to 15% of adults worldwide and more than half of adults older than 70 years. In addition, 48% of those with severely reduced kidney function are unaware of having CKD and do not receive any treatment[1–4,11].

The following section will present the actual treatments for patients suffering from kidney disease - organ transplantation and dialysis treatment - and the disadvantages of these treatments will be mentioned. The microfluidic bioartificial kidney will be presented in the following section as a promising approach to treat the patients in case of kidney failure. The application and the preparation methods of microfluidic devices will be detailed, explaining the preparation method of PDMS layers and their assembly using Plasma Oxygen treatment, forming a small device encapsulating a specific filtration membrane. Different types of membranes used in the literature as a filtration barrier bioartificial kidney devices will be mentioned.

III. Existing Treatment

Kidney failure is currently treated by either two methods: dialysis or kidney transplant. However, the future of kidney failure treatment is relying on artificial kidney-on-chip preparing by combining microfluidics and tissue engineering that has the potential to produce alternative therapies which can circumvent the obstacles posed by organ shortage and immune rejection and are worthy of further consideration.

In this section, the actual treatments in case of kidney disease are developed - organ transplantation and dialysis treatment - and the disadvantages of these treatment are mentioned. The microfluidic bioartificial kidney is presented as a promising approach to treat the patients in case of kidney failure. The applications of microfluidic devices are mentioned, and the preparation method of multilayers PDMS device are detailed, starting from the preparation of a PDMS layer, passing by their assembly using Plasma Oxygen treatment, in order to form a small device encapsulating a specific filtration membrane.

1. Transplantation

Kidney transplant involves surgically placing a healthy kidney from a donor into the patient body. Transplanted kidneys can come from deceased or living donors. Patients need to take medications for the rest of their life to keep their body from rejecting the new organ. However, a limited number

of patients benefit from organ transplant as there's a severe shortage of cadaveric organ. This shortage is a major obstacle preventing the full development of transplant services. Therefore, patients will resort to renal replacement therapy because organ supply falls drastically short of demand[17].

2. Dialysis Treatment

Patient suffering from CKD will definitely need to go through dialysis treatment. The concept of dialysis is the separate two fluid-containing compartments by a membrane (Figure 4). These fluids are the patient's blood, usually rich on urea, potassium and other waster products, and the dialysis solution composed of highly purified water to which sodium, potassium, calcium, magnesium, chloride, bicarbonate, and dextrose have been added[18].

Blood mixed with heparin is pumped through a dialyzer at flow rates of 300 to 500 mL/min, while dialysis solution or dialysate flows at 500 to 800 mL/min in order to remove waste products. A dialysis treatment requires a three to four hours' sessions every two days in a hospital and in each session, and the urea clearance rate in the blood drops 65 to 70% depending on the surface area of the dialyzer and the permeability of the membrane[19,20].

If the blood and dialysate were left in static contact with each other via the membrane, the concentration of permeable waste products in the dialysis solution would become equal to that in the blood, and no waste products removal would occur. In practice, during dialysis, concentration equilibrium between the blood and the dialysate is prevented at all cost and the concentration gradient between them is maximized, by continuously adding fresh dialysis solution to the dialysate compartment and also by adding undialyzed blood to replace dialyzed blood. Normally, the dialysis solution and the blood flow in opposite directions (Figure 4.B)) in order to maximize the concentration difference of waste products between blood and dialysate in all parts of the dialyzer[18].

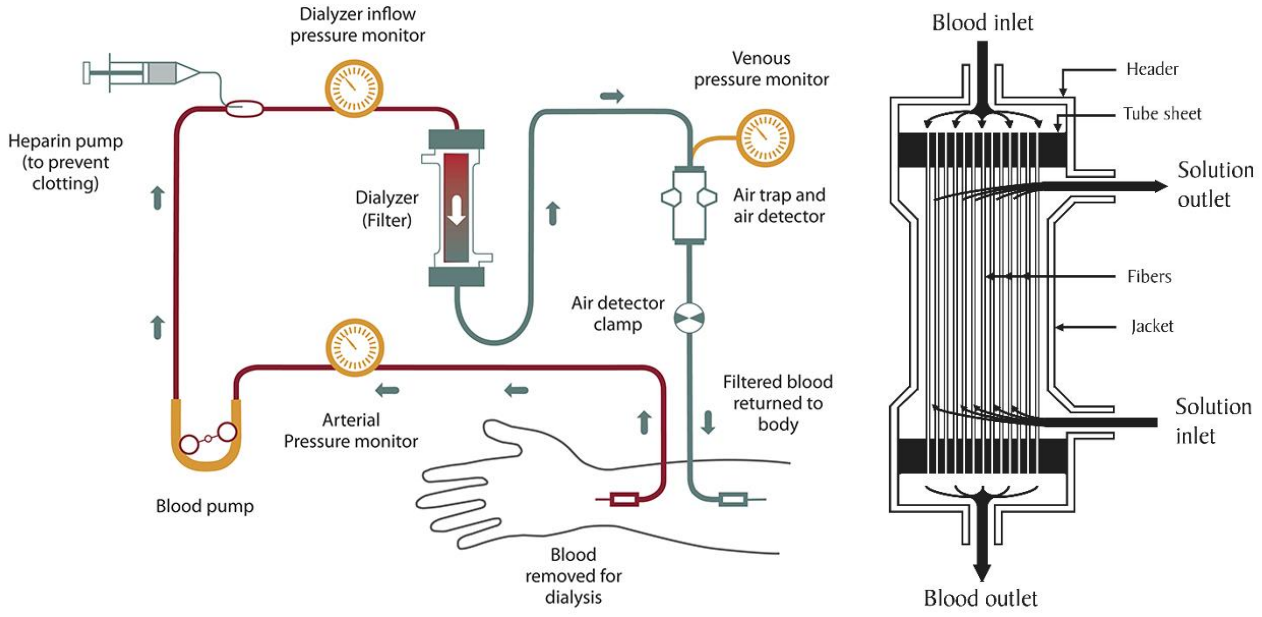

Figure 4. Schematic representation of **(a)** Hemodialysis treatment and **(b)** the Structure of a typical hollow fiber dialyzer. (Credit to: National Institute of Diabetes and Digestive and Kidney Diseases, National Institutes of Health).

However, a dialysis treatment is not an easy deal. As already mentioned before, patients are suggested to visit the hospital every two days and stay there for four hours for dialysis treatment. So, in addition to the fact that these visits will limit the patients' activities, having a dialysis treatment for twelve hours a week is rather intensive and tiring in comparison to the twenty-four hours a day dialysis conducted by a healthy kidney[21]. The financial cost of this treatment on the patients and on the hospitals should also be taken into consideration. Therefore, many studies are conducted on how to make dialysis easier on patients and hospitals[20].

Future of Dialysis: Minimizing the size of the dialyzer and transforming it into an implantable or portable biocompatible device is a prospect solution as the device costs way less than the dialysis treatment over the years and it does not bind the patient to hours of treatments in hospitals.

3. Microfluidic Bioartificial Kidney

Inspired by the dialysis system many studies are made to develop an implantable Microfluidic Bioartificial Kidney by miniaturizing the whole dialysis system[5,21–24].

A. Definition of Microfluidics

Microfluidics, is a promising technology for improving diagnostics and biology research, it is characterized by the engineering and the manipulation of fluids at the submillimeter scale. Microfluidic technologies are characterized by the rapid sample processing and the precise control of fluids in an assay, which made them important candidates to replace traditional experimental approaches[25].

A microfluidic device is based on principle of miniaturization, integration, automation and parallelization of (bio-)chemical processes[26]. Microfluidics offers advantages in terms of small volume, low cost, short reaction time and high-throughput. Microfluidics are largely used for biology and medicine research[27–31]. With the appropriate scale that matches the scales of cells, microfluidics is well positioned to contribute significantly to cell biology[32].

B. Polydimethylsiloxane Microfluidics

Currently, several robust and cost-effective polymeric materials, such as polydimethylsiloxane (PDMS), polymethyl methacrylate (PMMA), polycarbonate (PC), polystyrene (PS), polyvinyl chloride (PVC), and polyimide (PI) have been widely used for fabrication of microfluidic devices[27,33]. PDMS offers several advantages compared with other polymetric materials, silicon and glass due to the low cost, facile surface modification, and rubber-like elasticity which make it a very popular and the most used material for microfluidics-based systems[27,29,34,35]. In addition, PDMS is found to show excellent biocompatibility, high gas permeability, optical transparency and low autofluorescence, opening up a wide arena in the field of biotechnology and biomedical engineering[34].

PDMS is optically transparent from a 240–1100 nm wavelength and is therefore compatible with many optical detection methods and it enables the direct optical access into microchannels for real-time monitoring of the process[29,34,36]. Despite the optical transparency of PDMS, it has an intrinsic fluorescence, with smaller intensity values comparing to other polymers, that is considerably lower than the signals from fluorescence measurements performed on cells. So the reflected fluorescence

signal from the PDMS polymer will be weak on the background, in case of using an inverted microscope[33,34].

PDMS is gas permeable and therefore a perfect material for cell cultures, since it allows the control of the amount of O_2 and CO_2 gases through the exchange across the polymer matrix and keep it in the required range for good cell viability[33,34,36].

In medicine and biology, there had been a tendency to use natural polymers or modified natural polymers for scaffold fabrication in tissue engineering. PDMS is known by its excellent biocompatibility, which is the most important requirement for a material that interfaces with biological samples. Several studies have demonstrated the success of using the PDMS for the fabrication of microdevices for cell cultures, for organ-on-chip models, and for making implantable devices or parts of them. PDMS is also used in some cases as a covering film for non biocmpatible materials (i.e. metal) used for biological application[29,33,34].

All these intrinsic PDMS properties make it an appropriate choice of polymer for cell culture applications. In addition, the ease of prototyping of PDMS allows for the design, molding, and fabrication of microfluidic systems, and for the integration of active elements, such as sensors or continuous perfusion systems[33].

C. Preparation of Multilayer Polydimethylsiloxane

PDMS is a basic silicone polymer that has a unique combination of properties due to the presence of an inorganic siloxane $-Si-O-$ backbone and organic methyl groups attached to silicon $-R_2Si-O-$. The high flexibility of PDMS originates from the structural features of the $Si-O$ bonds; they have a longer bond length, larger bond angle, and significantly lower torsional potential than $C-C$ bonds. In addition, the strength of the $Si-O$ bond gives the polymer its thermal and chemical stability, which is important for its use in high-temperature applications[33,37–39].

PDMS is fluid at room temperature which makes it suitable for the fabrication of microfluidic devices using the soft lithography technique based on replication molding of micromachined molds[33–35].

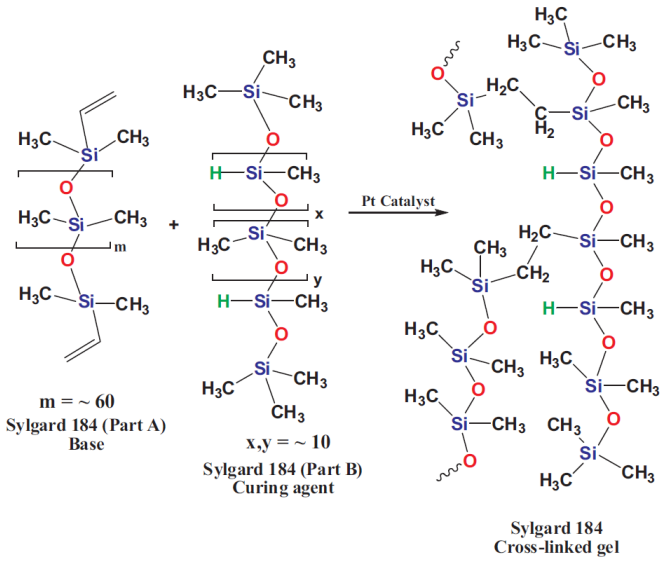

Figure 5. The chemical structure of Sylgard®184 elastometers[40].

The polymer is supplied as a two-part kit: a liquid silicon rubber base produced as linear macromolecules chains and a catalyst or curing agent. One of the most commonly used silicon-based polymers is Sylgard®184 polydimethylsiloxane (PDMS) elastomer. The base contains a linear chain of dimethylsiloxane oligomers with $Si-vinyl$ end groups (0.68 mol%), and a platinum catalyst. The curing agent contains dimethyl methylhydrogen siloxane, which is rich in $Si-H$ bonds and an inhibitor (tetramethyl tetravinyl cyclotetrasiloxane)[37,40,41]. By mixing the base with the curing agent, the cross-linking of the polymer chains is activated, and liquid material is converted into solid elastomer[33,38] (Figure 5). The time needed for ending the process is strongly dependent on the temperature. Indeed, at ambient thermal conditions (20–25 ˚C), the process can take 72 h. By putting the polymer in an oven or on a hot plate, the common range is 75–100 ˚C and the time is reduced to 1–2 h[33].

Another interesting point is the mechanical properties of PDMS, that are dependent on base polymer: curing agent mixing ratio. The high flexibility of PDMS originates from the structural features of the $Si-O$ bonds highly present in the base[38], while the curing agent is rich in rigid $Si-H$ bounds. So by increasing the curing agent, the hardness of the PDMS increases and consequently the elasticity decreases due to the increase of $Si-H$ bounds[42].

D. Plasma Oxygen Treatment

PDMS consists of repeating $-O-Si-(CH_3)_2$ units; the $-CH_3$ groups at the surface produce a hydrophobic surface with a very poor adhesion[36,39,43]. The bonding quality of the PDMS layer is critical in microfluidic applications which are typically designed to handle very small amounts of fluids, which can cause leakage due to a breakdown of the bonding between the two layers.

Oxygen plasma treatment has an important role in current research on surface modification and functionalization of polymers. Electrical discharges in low-pressure gases create cold plasmas in the chamber; the contact of polymer surface with the cold plasmas produce a mixture of highly reactive species such as ions, radicals, electrons, photons and excited molecules[39]. During oxygen plasma treatment, surface methyl groups are replaced by hydroxyl groups $(-Si-OH)$, and create an effective bonding between the first and the second layer PDMS or between a PDMS layer and glass[36,39,43]. Plasmas activate the surface and improve adhesiveness and hydrophilicity of PDMS surface and it will be maintained if it stays in contact with water. In air, the hydrophilicity is not permanent; hydrophobic groups reattach to the surface to lower the surface free energy within 30 min[36,39].

After O_2 Plasma activation of the surfaces to be bonded, the two exposed sides of PDMS layers are placed together creating irreversible bonding a due to the formation of strong $Si-O-Si$ covalent bonds between the surfaces, meaning that PDMS layers share electrons producing a very strong bond.

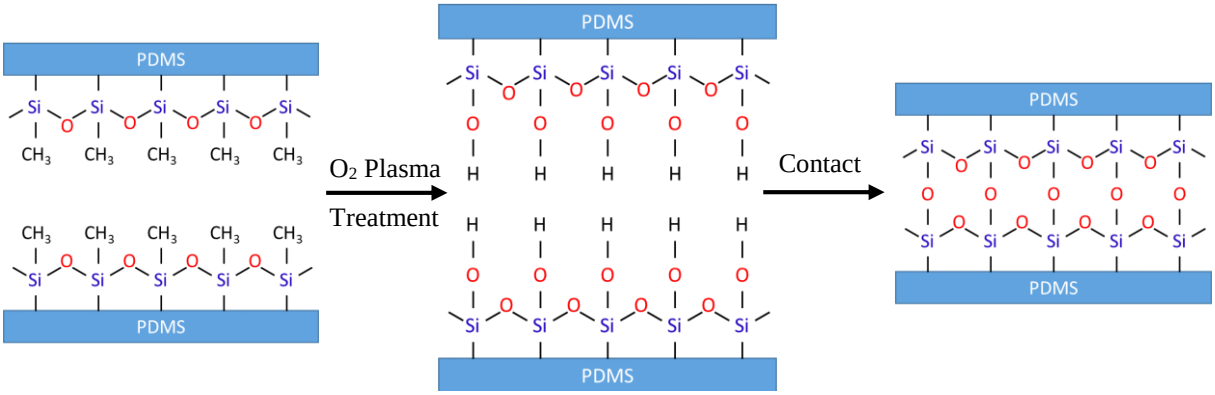

Figure 6. Schematic of the surface modification steps of PDMS by oxygen-plasma treatment.

The resulting device containing microfluidic channels can resist the liquid flow without any leakage or detachment. This device encapsulates a filtration membrane mimicking renal filtration. Lead to substantial benefits for patients by increasing life expectancy, mobility and quality of life; with less risk of infection and lower costs[47].

E. Benefits of Size Reduction of a Microfluidic System

Microfluidic systems are widely used in many research applications. Part of the attraction to microfluidics is based on its combination of small size and ability to process very small volumes of liquid, thus minimizing the use of potentially expensive reagents[45]. In addition, microfluidic system offers a precise control[27] of the operation conditions and fluid properties, an instantaneous control of temperature and flow[46], reproducibility, in situ reaction monitoring using sensor integration, rapid screening of parameters, fast heat and mass transfer and low reagent consumption during optimization. Additionally, such small, controlled reaction volumes enable reactions to be performed under more aggressive conditions[28].

For biological application, microfluidics provides new perspectives into cell biology and brings new protocols for precise control of cell growth. Additionally, the small size of a microfluidic system offers many advanced features such as low energy and reagents consumption, high throughput, tumor cells isolation, low risk of contamination and a fluid control for a better analysis of single cells to organs on fully automated chips[27,47,48].

F. Applications of Microfluidic Technology

Featured by handling small quantities of fluids at micrometer and nanometer scale, microfluidics has emerged as a powerful platform enhanced many fields, such as biomaterials fabrication, drug discovery, single cell analysis and electronics[27].

Due to the precise manipulation of multiphasic flows and highly controllable processes, microfluidics technology provides a strong tool for high throughput synthesis of nanoparticles[49], microfibers, and three dimensional (3D) structures[28], with specific narrow size, complex

morphologies and tunable composition, which are great innovations in electrochemical engineering, robotics, tissue soft and flexible electronics. In addition, microfluidics plays an important role in biomaterials manufacturing, it have provided exciting opportunities for efficient and controlled drug delivery[27].

Microfluidics brings new and improved protocols for precise control of cell growth, that make form it an ideal platform for clinical diagnosis, circulating tumor cells isolation, and single cell analysis[27,28]. More importantly, microfluidic organs-on-chips present a microengineered models of human organs, and it is mainly used in two applications: Organ replacement or improvement and drug discovery. Compared with conventional 2D culture and animal models, organs-on-chips can recapitulate 3D microenvironment and physiological fluid flow of human tissues and organs, and offer innovative new platforms for biologists in organ replacement, disease modeling, drug discovery, and toxicology research[27,29].

Organ-on-chip combine microfluidic and tissue engineering, in order to simulate the activities and the microenvironments of an organ. The aim of the researchers is to create an artificial organ that can replace function of the natural one in case of loss or failure. Kidney-on-chip is one of the example of artificial organs, it aims the replacement of kidney filtration function regulate metabolism, endocrine function, and homeostasis in case of kidney disease [21,50,51].

Organ-on-chip is also used for drug discovery after the high failure rate of drugs that enter clinical trials and have been tested using 2D in vitro models and animal models[29]. In addition to the high cost and the innumerable animal lives lost caused by the current drug test methods, organ-on-chip models provide the opportunity to fabricate a personalized device[52] for each patient to reflect the genetics, physiology and biometric parameters of specific individuals[53].

Currently, the microfluidics-based wearable electronics that incorporate microfluidic devices with flexible electronics have drawn attentions for diagnosis and healthcare. Flexible electronics, which can sustain functions under mechanical deformation, offer distinct advantages over existing rigid electronics; it offers a precise manipulation of conductive fluids, which connect electronics with flexible biological systems. Advances in flexible electronics have spurred tremendous potential for wearable sensors, electronic skin, implantable biomedical devices, and soft robotics[27].

G. Artificial and Bioartificial Kidney

Artificial kidney is a microfluidic device that replaces kidney filtration function by minimizing the whole dialysis system, consist of a filtration membrane placed inside a device prepared from biocompatible materials. Artificial kidney can replace the filtration function of kidney by removing fluids and wastes, but does not replace the kidneys' role in regulating metabolism, endocrine function, and homeostasis[21,50,51].

Ota *et al*. has developed an implantable multilayered dialysis device composed of nanoporous poly (ether sulfone) PES membranes and titanium microfluidic channels having Serpentine-shape. It consists of two dialysis membranes, two blood flow path layers, and one filtrate flow path layer. The device is designed to work under blood pressure and without the need of dialysate, which leads to the miniaturization of the dialysis system since a storage tank with a pump for the dialysate is not necessary. The filtration performance decreased by one third after 7 days before it stabilized. This decrease is caused by biofouling on the surface of the membrane, such as coagulation, and protein adhesion[5,21]. Perozziello *et al.* present in their work a microfluidic device fabricated by micromilling using poly (methyl methacrylate) PMMA encapsulating a regenerated cellulose dialysis membrane. The PMMA layer contain microchannels and a small fluid-membrane contact area allowed to reduce any deformation of the membrane. The device has successfully filtered the small and medium having a molecular weight less than 10 kDa, but albumin sticks on the membrane reducing its performance after each experiment[54].

On the other hand, bioartificial kidneys provide an extension to conventional artificial kidneys and dialysis systems, by incorporating tissue engineering with living cellular and tissue, in an order to better mimic normal kidneys. Bioartificial kidney involves the design, growth and maintenance of living tissues embedded in natural or synthetic scaffolds to enable them to perform complex biochemical functions and replace normal living tissues[55,56].

Jang *et al.* used human primary renal tubules epithelial cells exposed to fluidic flow in microfluidic device to mimics the human kidney proximal tubule for drug transport and nephrotoxicity assessment. The epithelial cells were culture on Porous polyester membrane pre-coated with collagen type IV. Contrary to previews studies, they showed that the presence of physiological flow is absolutely critical for maintaining many physiological functions of these cells, but still

having cell detachment from the membrane for high fluid flow[57]. Wang *et al.* built a glomerulus-on-a-chip for assessment of diabetic nephropathy. Endothelial cells and podocytes were cultured on a 3D Matrigel basement membrane forming a glomerular filtration barrier, that closely mimic the *in vivo* glomerular filtration membrane[58]. Qu *et al.* has developed a multilayer microfluidic device to simulate nephron. The microfluidic device consists of two connected chambers; each chamber is evenly divided into two compartments in the vertical direction by an endothelial-epithelial membrane interface. The nephron microdevice is based on primary rat glomerular endothelial cells, podocytes, tubular epithelial cells, peritubular endothelial cells, renal blood flow involving plasma proteins, and glomerular filtrate flow. The filtration flow was limited avoiding any additional pressure which might be generated in the cells membrane interface that is fragile and easily cracked by the pressure[59].

Shuvo *et al*. used the bio-hybrid approach to develop an implantable bio-artificial kidney, using silicon nanoporous membranes to build a biocompatible hemofilter and a renal tubule cell bioreactor, working together to selectively separate wastes and reabsorb salts and water. Despite the advanced step that this team could reach, but microscopic fractures in membranes were observed in animals implanted for 5 and 8 days[60–62].

In the case of artificial kidney, the filtration efficiency is maintained for 7 days before biofouling (coagulation and protein adhesion). In addition, it only replaces the filtration function of the kidney[5,21], hence the need to integrate tissue engineering to better mimic the whole kidney function. The use of cells in the bioartificial kidney have many advantages over the basic artificial kidney due to the resemblance to the human kidney composition and function, but they still facing many limitations such as the limited flow rate avoiding the detachment of cells cultured on the top of the filtration membrane[59]. Hence the importance of creating a 3D porous filtration membrane as an extracellular matrix for cell culture.

H. Membranes Used in Microfluidic Bioartificial Kidneys

Different types of membranes are used as a filtration barrier for kidney filtration application. First-generation hemodialysis membranes were commonly made out of cellulose membranes and regenerated cellulose (RC) membranes that had a good efficient clearance of small molecules and

limited clearance of medium molecules and macromolecules removal[63,64]. The second-generation of dialysis membranes are mainly polymers, such as Poly(ether sulfone) (PES), polyvinyl pyrrolidone (PVP), Coated-Polydimethylsiloxane (PDMS) and polyester[64]. In addition, the robust and cost-effective polymeric materials, such as polymethyl methacrylate (PMMA), polycarbonate (PC), and polystyrene[27] are considered among the second generation of dialysis membrane. These membranes are the most used in the filtration devices[65–67], they are characterized by their multifunctionality, including surface hydrophilicity, ion exchange and biofouling resistance to proteins and bacteria[68], but they are limited by their mirror-polished surface that can prevent protein adhesion[21].

Whole organ engineering and microfuildic bioartificial kidneys are different strategies to replace or regenerate kidney function. However, these approaches require scaffold that promote and maintain cellular organization and function. In this regard, hydrogels are interesting biomaterials capable to mimic cells micro- and macro-environments. Hydrogels resemble natural soft tissue due to their high water content contributing to biocompatible properties. The high porosity of the polymer network is beneficial for a continuous exchange of nutrients, gasses, waste products and signaling molecules with cells embedded in or grown on the hydrogel. Due to their polymeric nature, hydrogels are highly tunable in terms of mechanical properties. By changing preparation condition like crosslinking density or monomer concentration, the mechanical properties can be adjusted to better represent a specific type of tissue. In addition, preparation methods of hydrogels allow formation into different geometries, i.e. microporous hydrogel, microspheres, tubes or fibers[69]. The filtration efficiency of hydrogel depends on the mesh and pore size of each hydrogel that can be controlled by changing the hydrogel composition and the preparation method.

Kidney failure is currently treated by either two methods: dialysis or kidney transplant. However, the future of kidney failure treatment is relying on artificial kidney-on-chip preparing by combining microfluidics and tissue engineering that has the potential to produce alternative therapies which can circumvent the obstacles posed by organ shortage and immune rejection and are worthy of further consideration.

Microfluidics, is a promising technology for organ replacement in case a loss or failure. The resulting microfluidic device consist of multilayers of PDMS a containing microfluidic channels

that can resist the liquid flow without any leakage or detachment. Microfluidic kidney encapsulates a filtration membrane based usually on hydrogel seeded with podocytes in order to closely mimic the kidney filtration function.

The following section presents basic notions about biomaterials and biocompatibility, a review on gels in general and on hydrogels in particular. After the definition of polymer gels, the reasons for choosing polyacrylamide hydrogel as a natural tissue replacement will be explained and a study about the free radical polymerization, gelation mechanism, hydrolysis and the swelling thermodynamics will be developed.

Macroporous polymeric materials are widely used to mimic the extracellular matrix (ECM) environment for applications such as three dimensional (3D) cell culturing and tissue engineering[70]. Porous bulks prepared using emulsion technique will be used to form macroporous PAAM hydrogel scaffold for spheroids formation.

Hydrolyzed Polyacrylamide hydrogel will be presented as a functional membrane that have many advantages over other type of membranes, which can mix the filtration function of a membrane and the properties of a scaffolding materials suitable for cell culture. In addition, structural and mechanical properties of PAAM hydrogel can be easily controlled making it a good scaffold for cell, that can be affected by the stiffness and the porosity of scaffold.

IV. Hydrolyzed Polyacrylamide Hydrogels

Hydrolyzed Polyacrylamide hydrogel is a biocompatible, non-biodegradable material that offers a suitable substrate for cell culture[71], and holds many advantages over the non-swollen Polyacrylamide and other matrices, including its high fluid content, the possibility of cells adhesion without the need of protein and the absence of toxic unpolymerized Acrylamide in matrices.

The aim of our work is to develop PAAM hydrogel scaffolds with tunable stiffness and porosity by controlling the pre-gel composition and the polymerization conditions. This will help studying the interaction of cells with different substrates[72] aiming in the future to control their fate and function.

This section presents basic notions about biomaterials and biocompatibility, a review on gels in general and on hydrogels in particular. After the definition of polymer gels, the reasons for choosing polyacrylamide hydrogel as a natural tissue replacement is explained and a study about the free radical polymerization, gelation mechanism, hydrolysis and the swelling thermodynamics are developed. Porous bulks are prepared using emulsion technique forming a 3D macroporous PAAM hydrogel scaffold for spheroids formation.

The hydrolyzed form of Polyacrylamide hydrogel as a functional membrane that have many advantages over other type of membranes, that can mix the filtration function of a membrane and the properties of a scaffolding materials suitable for cell culture. In addition, the control of structural and mechanical properties of PAAM hydrogel that make it a good scaffold for cell culture.

1. Definition and Different Types of Hydrogels

A gel is a conventionally defined on the macroscopic scale as a state of matter with a connected network of structural elements (polymers) formed by physical or chemical linking, and leading to a solid state with a solid-like mechanical properties while retaining a large part of the solvent within its deformable structure[73].

There are several classifications of gels: according to their origin (such as natural or synthetic gels), according to the material contained in the polymer matrix (such as hydrogels, aerogels or organogels) according to the type of binding of the polymer matrix (such than chemical or physical gels)[74].

Hydrogels are three-dimensional, hydrophilic, polymeric networks capable of absorbing large amounts of water or biological fluids. Due to their high water content, porosity and soft consistency, they closely simulate natural living tissue, more than any other class of synthetic biomaterials. Hydrogels may be chemically stable or they may degrade and eventually disintegrate and dissolve[75]. Hydrogels are water-swollen polymeric networks, usually consisting of crosslinked hydrophilic polymers that can swell without dissolving in water. This ability to swell under biological conditions makes them an ideal class of materials for biomedical applications. Hydrogels

possess a 3D network structure, crosslinked together either physically or chemically. This insoluble cross-linked structure allows effective immobilization and release of active agents and biomolecules. Owing to their high water content, hydrogels resemble natural soft tissue.

Hydrogels can be classified into physical and chemical hydrogels based on their crosslinking mechanism. Physical crosslinks include entangled chains, hydrogen bonding, Van der Waals interaction, hydrophobic interaction and crystallite formation. While these physical crosslinks may not be permanent junctions, they are sufficient to keep the hydrogel from dissolving in an aqueous media. On the other hand, Chemical (or covalent) crosslinks, are permanent junctions formed by covalent bonds. One common way to create a covalently crosslinked network is to polymerize end-functionalized macromers. Hydrogel networks may include both permanent junctions and semipermanent junctions like chain entanglements. The type and degree of crosslinking influences many of the network properties, like swelling properties, elastic modulus and transport of molecules[76].

2. Hydrogels as Scaffolding Materials

Millions of patients are suffering from the loss or failure of an organ or a tissue caused by an accident or a disease every year[75]. The structure of 3 dimensional porous hydrogels make it capable to absorb a considerable amount of water, and serve as a suitable candidate to mimic the natural tissues[77].

Tissue engineering aimed primarily to mimic the extracellular matrix (ECM) which is the one of the most significant guides in the design of scaffolds for tissue engineering. Hydrogels are stretchable, transparent, ionic conductors that can transmit electrical signals of high frequency over long distance, enabling ionotronic devices such as artificial muscles, skins and axons[78]. In addition, hydrogels in tissue engineering must meet a number of design criteria including classical mechanical and physicochemical parameters (such as biodegradation, stiffness and porosity), and biological performance parameters (such as biocompatibility and cell adhesion), as well as demonstrating enhanced vascularization[79].

a) Biocompatibility

Biocompatibility refers to the ability of a biomaterial to perform its desired function with respect to a medical therapy, without eliciting any undesirable local or systemic effects in the recipient or beneficiary of that therapy, but generating the most appropriate beneficial cellular or tissue response in that specific situation, and optimising the clinically relevant performance of that therapy[80].

b) Stiffness and Strength

Extracellular matrix (ECM) provides mechanical support as well as biological and biophysical signals to the cells incorporated into it. One of the most important characteristics of ECM is its mechanical stiffness, in other words the hardness of the adhesion matrix, that can be controlled by varying the concentration of monomer and or cross-linker, method of preparation and the degree of ionization, to mimic the stiffness of the natural tissue[77,81]. The strength of the gel is usually measured by the term of the elastic modulus and yield stress. Mechanical stiffnesses of human tissues vary from very soft brain and fat (E = 1 kPa), to intermediate kidney (E= 20 kPa), muscles and heart (E = 10 - 20 kPa) to very hard decalcified bone (E = 50 - 60 kPa)[72,81].

c) Porosity

Porosity of hydrogels is another important parameter helping cell migration and nutrient supply[77]. In gels, the interconnected porous network aid in the more efficient movement of solutes and nutrients throughout the gel, thus leading to faster cell growth and proliferation, enables the removal of waste from the cells, and also allows the neovascularization of the matrix. Porosity can be tuned by using different pre and post fabrication techniques[79].

Hydrolyzed PAAM hydrogel has been shown to be a good candidate in tissue engineering, because it meets all criteria needed to build a suitable environment for cell culture. In previous study, PAAM was demonstrated to be a biocompatible, non-toxic material[74,82–85] and non-biodegradable

except under the influence of microbial interaction[86,87]. Porosity, stiffness and hydrophilicity properties of PAAM hydrogel will be studied in chapter 2.

3. Free Radical Polymerization of Polyacrylamide

The polyacrylamide gels are formed by free radical polymerization in aqueous solution from the acrylamide monomer (AAM) and a crosslinking agent, N, N'-methylenebisacrylamide (BIS) (Figure 7), in presence of an initiator and an accelerator. However, linear polyacrylamide gels are formed only by AAM.

BIS is a bifunctional reagent, equivalent to two acrylamide monomers linked by a methylene group. It is used as binding agent bridging polyacrylamide chains by covalent bonds to form the three dimensional structure of the gel.

Use of the bisacrylamide like crosslinker structure will avoid problems associated with differential reactivity of co-monomers (many structural units), and bridging groups which endow the gel with specific properties may be used to form the cross-linkages[88].

In the chemical way, the polymerization initiated by a system for generating free radicals from the Ammonium Persulfate (APS) and N,N'-tetramethylenediamine (TEMED) used as chemical initiator/accelerator. Physical crosslinking occurs using riboflavin under ultraviolet light.

This polymerization is formed by three fundamental steps: initiation, propagation and termination.

(a) **(b)**

Figure 7. Chemical Structure of **(a)** Acrylamide **(b)** N,N'-methylenebisacrylamide

a) Initiation

Initiation involves the generation of active species "monomers", which can be through free-radical, ionic, or coordination mechanism. This may occur spontaneously by the absorption of heat, light (ultraviolet), or high-energy irradiation. Most frequently, initiation of free radical polymerization is brought about by the addition of small quantities of compounds called initiators[89].

The initiation of polymerization occurs in two successive steps: Production of free radicals and the addition of radicals to the first monomer molecule[90].

i. Production of free radicals

The decomposition of an initiator molecule leads to $R^{\bullet}$ radicals. This reaction is slow and continues throughout the polymerization:

$$I \rightarrow 2R^{\bullet}$$

In the case of APS the reaction leading to radical production is shown in Figure 8, with Ammonium persulfate (i) and TEMED (tetramethyl ethylene diamine) (ii). The radicals are (iii) and (iv). Ammonium bisulfate (v) is the inert by-product.

(i) (ii)

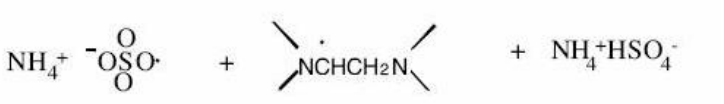

(iii) (iv) (v)

(a)

(b)

Figure 8. Formation of free radicals **(a)** Chemical way **(b)** Thermal way[74].

The rate of formation of the radicals R• is twice as fast as the decomposition rate of the initiator since there is a formation of two radicals R• by decomposition of a molecule I.

ii. Addition of radicals:

This reaction leads to the formation of the active center $RM_1^{\bullet}$

$$R^{\bullet} + M \xrightarrow{k_a} RM_1^{\bullet}$$

Where M represents a monomer molecule and k_a is the constant rate for the initiation step.

The rate of this reaction is governed by that of the slowest reaction which is the step of formation of the primary radicals (Figure 9).

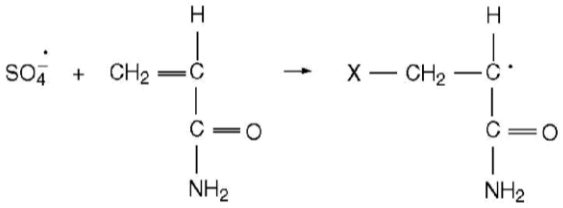

Figure 9. Addition of the initiator radical to the acrylamide monomer[74].

b) Propagation

The propagation is the sequence of additional reactions of acrylamide monomer M on an active center $RM_1^{\bullet}$ thus leading to the growth of the macromolecular chain. Each addition creates a new radical that has the same identity as the one previously, except that it is larger by one monomer unit. The successive additions may be represented generally by:

$$RM_1^{\bullet} + M \xrightarrow{k_p} M_2^{\bullet}$$
$$M_2^{\bullet} + M \xrightarrow{k_p} M_3^{\bullet}$$
$$M_x^{\bullet} + M \xrightarrow{k_p} M_{x+1}^{\bullet}$$

Figure 10. Sequence of polymerization reactions.

Where k_p is the rate constant for propagation

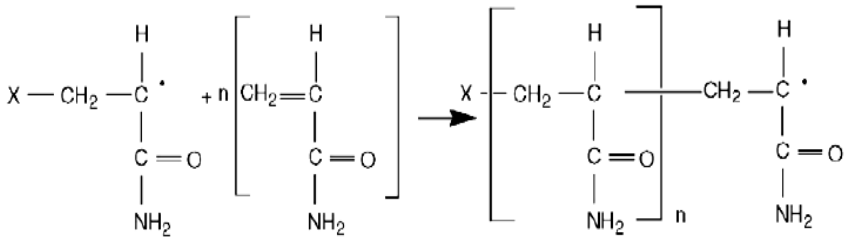

Figure 11. Polymerization propagation of the PAAM[74].

When one of the carbons of the acrylamide involved in the double bond takes on a radical form under the influence of the initiator, it can attack the C = C double bond of another molecule. Then each monomer will be incorporated in covalent bonds to form a single chain, while the crosslinking agent may be incorporated into none or in one or two chains to form a crosslinked network.

The crosslinking agent is formed by two identical poles, each, similar to the monomer[91].

c) Termination

The termination reactions lead to the destruction of the active centers and the end of the chains growth. They can be carried out by:

- Recombination of radicals: formation of macromolecules.

$$M_n^{\bullet} + M_m^{\bullet} \xrightarrow{k_{td}} M_n + M_m$$

- Dismutation: formation of a non-saturated macromolecule and a saturated molecule.

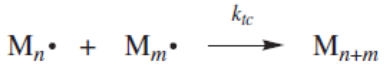

Recombination will lead to cross-linking, whereas dismutation will lead to the appearance of unsaturation[91].

d) Polymerization Velocity

The polymerization velocity V_{pol}, is equal to the global velocity of monomer consumption M; this is also the propagation velocity v_p when the velocity of the initiation reaction is neglected. The velocities of these various steps are represented in Table II. With f the fraction of the radicals effectively initiates the polymerization

Table II. The rates of the various steps of polymerization.

Steps	Reaction	Polymerization Velocity
Initiation	$I \xrightarrow{k_d} 2R^{\bullet}$ $R^{\bullet} + M \xrightarrow{k_a} M_1^{\bullet}$	$v_p = \frac{d[M^{\bullet}]}{dt} = 2fk_d[I]$ (1.1)
Propagation	$M_1^{\bullet} + M \xrightarrow{k_p} M_2^{\bullet}$ $M_2^{\bullet} + M \xrightarrow{k_p} M_3^{\bullet}$ $M_x^{\bullet} + M \xrightarrow{k_p} M_{x+1}^{\bullet}$	Propagation rate= polymerization rate
Termination	$M_x^{\bullet} + M_y^{\bullet} \xrightarrow{k_{tc}} M_{x+y}$ $M_x^{\bullet} + M_y^{\bullet} \xrightarrow{k_{td}} M_x + M_y$	$v_t = -\frac{d[M^{\bullet}]}{dt} = 2k_t[M^{\bullet}]^2$ (1.2)

e) Length of Kinetic Chain

The length of the kinetic chain $\bar{\lambda}$ is inversely proportional to the polymerization velocity, it measures the average number of elementary reactions by active center.

$$\bar{\lambda} = \frac{v_{pol}}{v_p} = \frac{v_{pol}}{v_t} = k_p \frac{\left[M^\bullet\right][M]}{2k_t\left[M^\bullet\right]^2} = k_p \frac{[M]}{2k_t\left[M^\bullet\right]} \tag{1.3}$$

$$\left[M^\bullet\right] = \frac{v_{pol}}{k_p[M]} \tag{1.4}$$

With

$$\bar{\lambda} = \frac{{k_p}^2[M]^2}{2k_t v_{pol}} \tag{1.5}$$

f) Inhibition of Polymerization

Inhibitors are substances which react with radicals and convert them to either non-radical species or radicals that the reactivity is too low to let them participate in the propagation.

Oxygen plays a key role during the polymerization of vinyl compound. The presence of oxygen significantly decreases the rate of the reaction and increases the induction period, so a longer duration is needed to consume inhibitors and thus start polymerization reaction. In addition, the polymerization rate decreases due to the consumption of initiators during the inhibition phase.

g) Gelation Mechanism

The polymerization is represented in a simple scheme of random paths (Figure 12). Each path begins with the initiator and constructed randomly by bringing monomers and crosslinking agents. The final result is a three dimensional network of the PAAM gel.

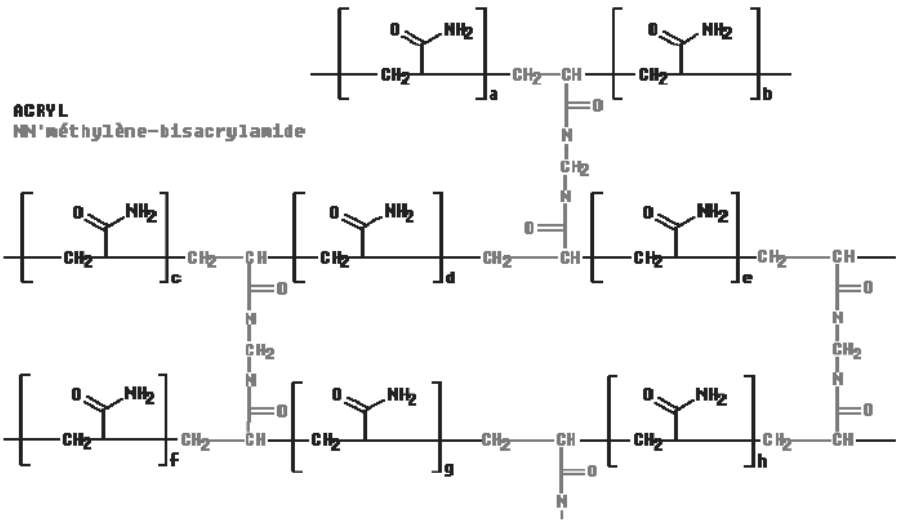

Figure 12. Three dimensional network of PAAM cross-linked[74].

Gelation is defined by the formation of an infinite three-dimensional network, characterized by the passage from a liquid state to a viscoelastic gel.

The polymerization of PAAM is an exothermic reaction, its thermal profile is composed of three distinct phases represented in Figure 13:

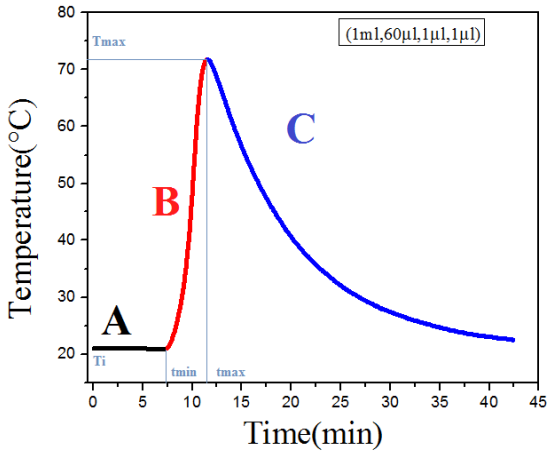

Figure 13. Temperature profile of the AAM polymerization[74].

Part A ($t < t_i$ et $T = T_i$), part B ($t_i < t < t_{max}$ et $T_i < T < T_{max}$) and part C ($t > t_{max}$ et $T<T_{max}$).

-Part A did not present any variation in temperature; it is the induction phase which corresponds to the consumption of the inhibitors in the reaction medium.

-Part B presents an increasing in temperature from the initial value T_i indicating the beginning of the polymerization. The temperature continues to increase reaching a maximum T_{max} indicating the polymerization of monomers which predominate this phase of micro-gels formation.

-Part C shows a decrease of temperature from its maximum indicating that the concentration of monomers became low and the concentration of chains predominate in the reactional medium. The polymerization continues even after reinstallation of Ti, but with a very slow velocity, leading to low heat loss that can be dissipated before its detection.

Since it is a chemical gel, then the templating of its network should be done in phases A and B before reaching the gel point.

4. Hydrolyzed Polyacrylamide

When the PAAM gel is hydrolyzed in a basic solution, a part of the group amide of the polymer chain will be transformed to a carboxylic group. After hydrolysis, the obtained charged macromolecule networks will form a polyelectrolyte gel.

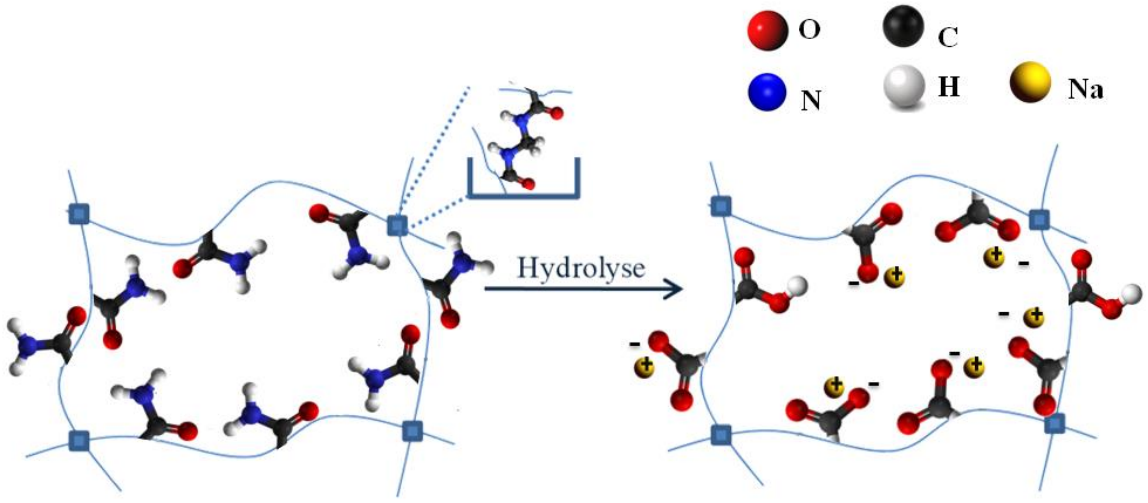

Figure 14. Hydrolysis of the PAAM network in basic solution.

a) Hydration of Hydrolyzed Polyacrylamide Gel

After hydrolysis, when the gel becomes in contact with water, they diffuse into each other. The gel swells in water due to the hydrophilic nature of the carboxyl groups and the polymer system swells under the effect of the osmotic pressure of the counter ions until the osmotic and the elastic forces of the polymer chains are balanced[92,93].

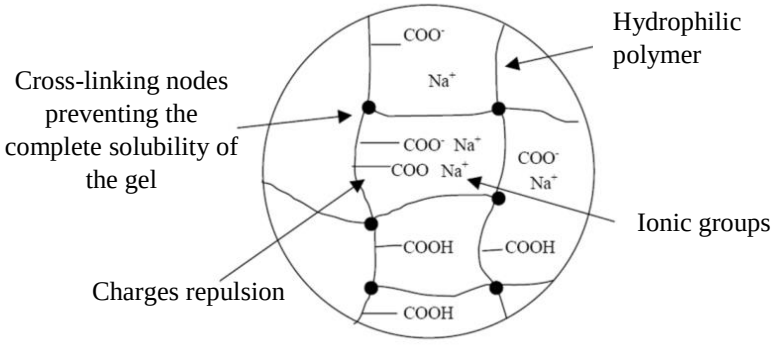

Figure 15. Schematic representation of the polymer chain functional groups.

The resistance to the flow of the swollen gel is ensured by the crosslinking nodes which are chemical junctions between the macromolecules[94].

b) Equilibrium Swelling of Polyelectrolyte Gels

The swelling rate of hydrogel depends strongly on the architecture of the macromolecular network and is often analyzed from a thermodynamic point of view by Flory-Huggins' theory. We present the case of an ionic gel.

The swelling of polyelectrolyte gels is not well understood because of its complexity. We will present below the Flory approach for a polyelectrolyte gel swelled in distilled water.

The gel swelling is controlled by the osmotic and the elastic forces.

Osmotic force π is expressed as following:

$$\boldsymbol{\pi = \pi_{mix} + \pi_{el}} \tag{1.6}$$

The expressions of π_{mix} et π_{el} can be written as:

$$\pi_{mix} = -\frac{RT}{v_s}[\ln(1-\phi_n) + \phi_n + \chi_{sn}\phi_n^2] \tag{1.7}$$

$$\pi_{el} = -\frac{RTv_e}{v_0}\left[\left(\frac{\phi_n}{\phi_0}\right)^{1/3} - \frac{1}{2}\left[\frac{\phi_n}{\phi_0}\right]\right] \tag{1.8}$$

R is the gas constant, T is the absolute temperature, v_s molar volume of the solvent molecules, v_e is the number of active network chains, v_0 is the volume of the unswollen polymer, χ_{sn} is the Flory-Huggins interaction parameter between the solvent and the polymer matrix, and φ_n is the volumetric fraction of the network.

In addition to the two osmotic forces in a polyelectrolyte gel, we should take into consideration the ionic osmotic term π_{ion}, due to the pressure caused by the motion of ions in the polymer network.

$$\pi_{ion} = -RT\frac{v\frac{N}{A}\phi_n}{N_{Av}v_0\phi_0} \tag{1.9}$$

According to Flory's theory, the rate of swelling at equilibrium is given by:

$$S_{equ}^{\frac{2}{3}} = \frac{N}{A}\frac{M_C}{V_C\rho}\left(1-2\frac{M_C}{M}\right)^{-1} \tag{1.10}$$

With A number of monomer between two charges, N number of monomers, V_c molar volume, ρ monomer density, M_c mean molar weight of a segment between two nodes and M is the initial molar weight of the chains.

The equation above indicates that the rate of swelling S increases with the augmentation of the ionization rate of gel.

The hydrogel can be assimilated as an elastomer[95],which its elastic modulus is given by the theory of rubber elasticity:

$$E = \frac{3\rho RT}{M_c} \tag{1.11}$$

We can conclude that when the rate of swelling increases, the Young modulus decreases, indicating a lower capacity of deformation.

5. Polyacrylamide Hydrogels Properties

Polyacrylamide hydrogel is a biocompatible, non-biodegradable material that offers a suitable substrate for cell culture[71], because it can be easily tailored to optimize cells growth rate, and it can be made to closely mimic the mechanical properties of natural tissues. It can be prepared by the free radical polymerization method.

This hydrogel is composed from 90% of water making it close to the internal environment of the body composition.

Polyacrylamide hydrogel have been the material of choice in tissue engineering due to its mechanical characteristics (stiffness, swelling ratio…)[81] and its visco-elasticity. The shape of this hydrogel can be tailored by different methods of fabrication, in addition to its stiffness that can be controlled by changing the monomer and/or the cross-linker concentration[96]. Furthermore, polyacrylamide has all criteria for tissue engineering mentioned previously such as biodegradation, stiffness, porosity, biocompatibility and cell adhesion.

Hydrogel swelling is induced by osmotic forces generated by hydrophilic COO^- and Na^+ ions entrapped inside the hydrogel matrix, while the 3D structure is maintained by the mechanical forces of the crosslinked network.

6. Templating 3D Porous Polyacrylamide Hydrogels

Macroporous polymeric materials are widely used to mimic the extracellular matrix (ECM) environment for applications such as three dimensional (3D) cell culturing and tissue engineering[70]. Porous bulks can be prepared using many different techniques of fabrication, but in this work the emulsion technique will be used to prepare macroporous hydrogel scaffold for spheroids formation.

- **Emulsion: Oil-in-Water**

Briefly, an emulsion is a dispersion of small droplets of one liquid in another liquid, it can be formed by any two immiscible liquids, but in most emulsions one of the phases is water. Oil-in-water (O/W) emulsions are those in which oil droplets are dispersed in the continuous phase of water. Water-in-oil (W/O) "inverted" emulsions are those in which the continuous phase is an oil and the disperse phase is water. Emulsions can have more complex structures (multiple emulsions) when the disperse phase contains another phase which may not have the same composition as the continuous phase, e.g. oil-in-water-in-oil (O/W/O), water-in-oil-in-water (W/O/W). In O/W emulsion, water molecules at the interface between the two liquids have higher energy than those in bulk water. The production of emulsion involves the minimize of the interfacial energy and the creation of a large interfacial area between the oil and water[97–99]. Surfactants are compounds which lowers the interfacial tension between two phases to reduce the energy of emulsification, prevents coalescence during emulsification, and stabilizes the final emulsion by preventing flocculation, and coalescence. The surfactant consisting of two parts of different polarity (Figure 16 (a,b)): lipophilic and apolar, hydropilic and polar[100].

In aqueous solutions, the hydrophobic groups of these surfactants can associate to minimize their exposure to the hydraulic solvent, to form an aggregate called micelles[101]. These micelles lead to the stability of the oil in the water (Figure 16 (c)).

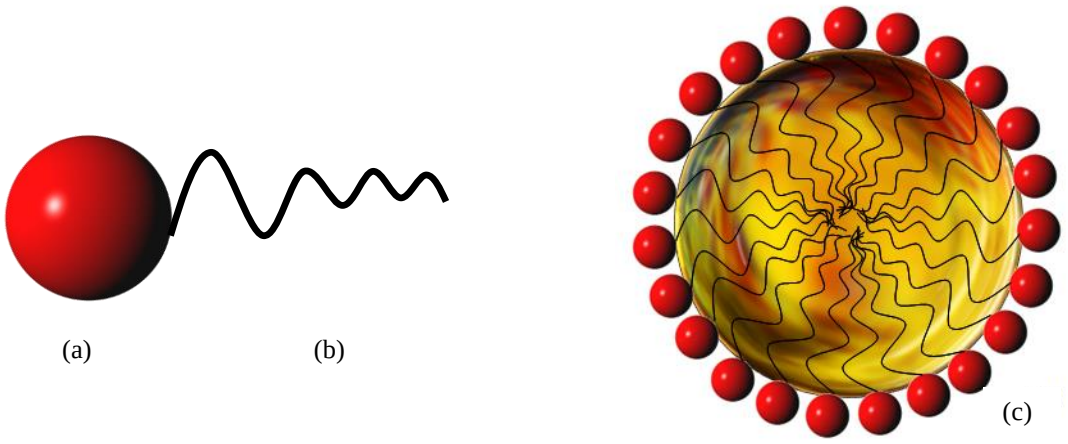

Figure 16. Schematic representation showing the surfactant having **(a)** hydrophilic head and **(b)** lipophilic tail **(c)** oil droplet inside the hydrophobic cores of the micelle dissolved in water solution.

Hydrophile–lipophile balance (HLB) is one of the most important properties of surface-active agents, it represents the relative proportion of hydrophilic to lipophilic components of the surfactant molecule. O/W emulsions require a high HLB number in the range of 8–18, whereas a W/O emulsion requires a low HLB number in the range 3–6[102–105]. In addition to the HLB, the surfactant concentration, the O/W ratio and the energy given for the emulsion formation are the most important parameters affecting the droplet size.

In this thesis, the water is replaced by water based polymer, which is polymerized after the emulsion formation. After polymerization, the oil droplets are leached out the polymer creating a macroporous structure used as scaffolding material for spheroids formation.

Hydrogels are three-dimensional, hydrophilic, polymeric networks capable of absorbing large amounts of water or biological fluids. Due to their high water content, porosity and soft consistency, they closely simulate natural living tissue, more than any other class of synthetic biomaterials. The polyacrylamide gels are formed by free radical polymerization, hydrolyzed in a basic solution, then swelled in water due to the hydrophilic nature of the carboxyl groups.

Polyacrylamide hydrogel is a biocompatible, non-biodegradable material that offers a suitable substrate for cell culture[71], because it can be easily tailored to optimize cells growth rate, and it can be made to closely mimic the mechanical properties of natural tissues. The properties of this hydrogel such as swelling, porosity and stiffness can be controlled to mimic cell environment for better conditions for cell growth.

In the following section, the hydrogel will be presented as an extracellular matrix suitable for cell culture, as well as the interaction between cell and the ECM depending on its topography and rigidity. The effect of the mechanical properties of ECM on tissue function will be briefly shown.

V. Hydrogels for Tissue Engineering Applications

Millions of patients worldwide are suffering from the loss or failure of an organ or a tissue[75]. Tissue or organ transplantation is a standard therapy to treat these patients but this is limited by the lack of organ donors, possible rejection, and other complications. In addition, Clinical studies for the development of new drugs take years to complete and testing a compound can cost more than $2 billion. Meanwhile, innumerable animal lives are lost, and the process often fails to predict human responses.

Tissue engineering has emerged as a promising approach to treat the loss or malfunction of a tissue or organ and allow a rapid and low cost drug testing.

Tissue engineering is an emerging field that aims to regenerate natural tissues and create new tissues using biological cells, biomaterials and biotechnology, by combining living cells with scaffold to build a three-dimensional living tissue that will restore, maintain, and improve tissue functions. Most of the traditional models for the development of a bioartificial kidney have been mainly applied in classical 2D cell culture systems and have limited proximal tubular functions. Therefore, for high throughput bioartificial kidney applications, more vigorous cell models that ensure consistent availability and a stable phenotype are needed[66]. Many researches have been conducted in order to explore new methods and approaches that allow the development of a 3D artificial organs. Coupling the cells culture with microfluidic known or “microfluidic-based cell cultures” is the most promising approach where the dynamic physiological conditions of the cells can be reproduced.

Hydrogels are a biocompatible, non-biodegradable materials[71]. Due to their high fluid content, porosity and soft consistency, they closely simulate natural living tissue, more than any other class of synthetic biomaterials[77], and offer a suitable substrate for cell culture, because it can be easily

tailored to closely mimic the mechanical properties of natural tissues and to optimize cells growth rate.

In this section, the hydrogel is presented as an extracellular matrix suitable for cell culture, as well as the interaction between cell and ECM that depend in the topography and the rigidity of the matrix. The effect of the mechanical properties of ECM on tissue function is briefly shown.

1. Hydrogel as Extracellular Matrix for Organ on Chip Application

The development of 3D hydrogel scaffolds for such as ECM, enables cell structures to be organized as in native tissues, which led to significant advances of *in vitro* culture systems. Despite the great potential of 3D hydrogel culture models, they have several important limitations including complex sample handling, difficulty in forming a complex vascular network and challenges with transporter studies in organs such as the intestine or kidneys. These systems are also missing important elements of the in vivo, dynamic microenvironment such as mechanical forces and fluid flow[106,107]. Therefore, cells and specially organoids are unable to survive, due to the lack of oxygen and nutrients, as well as the accumulation of metabolic waste[107].

The limitations associated with 3D hydrogel cultures led to the development of engineered microfluidic systems, called Organs-on-Chips. These microengineered systems consist of two or more microfluidic channels, separated by a porous matrix able to accommodate different types of cells in structures resembling the tissues of origin. Organ-on-chip systems are emerging as a versatile tool in biomedical applications allowed researchers to design a controllable complex tissue microenvironment by introducing cells into a microfluidic device, which reproduce organ-level functions[106,107]. This microfluidic device acts as a bioreactor, where cells can be engineered by reproducing the biomimetic stimuli such as chemical cues and dynamic mechanical cues[108] (Stress/Strain, Flow/Shear, Stiffness, Topography)[109] creating a micro-environment similar to natural tissue, that provide oxygen and nutrients, and handle the discharge of metabolic waste[107,110].

In the past decade, microfluidic technologies and organ-on-chip devices became popular as *in vitro* models able to replicate *in vivo* environment. However, in conventional microfluidic devices, cell

barriers are primarily grown on hard polymeric membranes within polydimethylsiloxane (PDMS) matrix that do not mimic the cell–ECM interactions[110].

The use of porous hydrogel in Organ-on-Chip provides a soft and controllable mechanical properties of the ECM, improve the cell-cell and cell-ECM interaction and enables the embedding of cells, as oxygen and nutrients are able to diffuse through their structure and provide the proper environment for cell culture. Combining hydrogels with microfluidics technology provides unique opportunities to better recreate *in vitro* the functionality of the *in vivo* tissues[110].

Currently, hydrogels in Organ-on-Chips are the most advanced *in vitro* platforms for disease modeling, drug screening, and lead to design parameters for larger scale functional tissue replacements[110,111].

2. Cell-ECM Interaction

Chemical, mechanical, and topographic extracellular matrix signals have an important role on cell behaviour[110]. Cells sense, integrate and interpret the topography and the rigidity of ECM and therefore produce appropriate physiological responses regulating the cellular activities such as proliferation, migration, differentiation and apoptosis. Consequently, each living tissue is determined by a specific elasticity.

Previous studies have shown the significant role of ECM mechanical properties in the growth rate of cells, and the progression of a healthy tissue function and tumors. They have proved that the stiffness of healthy mammary glands is around 150 Pa, while the tumor exhibits a stiffness higher than 4 kPa, a difference in stiffness easily probed by physical palpation, a common diagnostic for breast tumors[112]. Regarding the liver tissue, the stiffness of healthy liver is around 6 kPa while the stiffness of liver diseases such as fibrosis and cirrhosis increases over 10 kPa[51,113].

Cellular adhesion machinery is composed of specialized transmembrane receptors associated with the actin cytoskeleton via cytoplasmic domains. These domains of diverse group of adhesion molecules enhance the ECM – cells and cells - cells interactions in a way to maintain the specific form and mechanical properties of tissues[114].

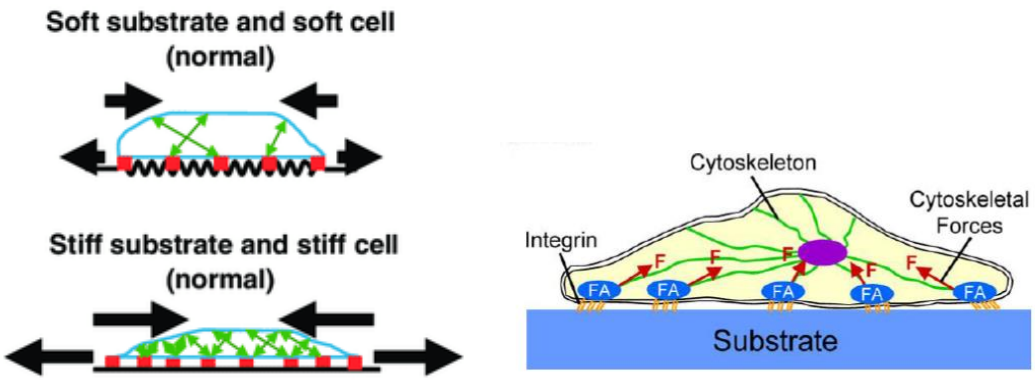

Figure 17. Cell-matrix mechanical signals[115].

Through these active sites, cells recognize the physical cues which are defined by the mechanical forces applied to cellular membrane.

Several studies have investigated the importance of microenvironment mechanical properties in the regulation of cellular behaviors[116–119]. In fact, cells sense and respond to the mechanical properties generated by ECM through integrin. Integrin is a transmembrane cell adhesion protein characterized by the presence of two domains: an intracellular domain in interaction with the cell cytoskeleton and an extracellular domain binding to the substrate. ECM mechanical signals will be transduced into intracellular signals and affect the cells properties as cells morphology, migration, cytoskeleton organization, differentiation and cells stiffness[120].

3. Effect of Mechanical Properties on Tissue Functions

A prime function of the ECM is to provide tissues with shape, strength, and elasticity. Actually, cells feel the variation of ECM stiffness and react in a different process. For instance, cells sense the ECM high stiffness which contributes to the loss of cells ability to respond and to contract against the matrix. Thus, cells produce additional forces and the number of focal adhesion and so the number of actin fibers connected to non-muscle myosin will be increased leading to an increase in cell stiffness in order to go with matrix stiffness. Contrariwise, the cells on a matrix with low stiffness generate a small force and show a few number of focal adhesion complex and thus actin fibers. In conclusion, cell responds and reacts to the variation of substrate stiffness which contributes to regulate the organization of actin cytoskeleton[120].

VI. Conclusion and Thesis Objectives

Kidney have an essential role for a normal body function. Kidney filtration membrane (basement membrane, endothelium, and podocytes) is responsible of normal kidney filtration. Chronic Kidney Disease (CKD) reduce their efficiency to filter the blood of 10% to 15% of the population worldwide and few of them receive treatment (Dialysis, transplantation and Microfluidic Bioartificial Kidney).

Microfluidics, is a promising technology for organ replacement in case a loss or failure. Microfluidic kidney device consists of multilayers of PDMS encapsulating a filtration membrane based usually on hydrogel seeded with podocytes in order to closely mimic the kidney filtration function. The use of cells in the bioartificial kidney have many advantages over the basic artificial kidney due to the resemblance to the human kidney composition and function, but they still facing many limitations such as the limited flow rate avoiding the detachment of cells cultured on the top of the filtration membrane[59]. Hence the importance of creating a 3D porous filtration membrane as an extracellular matrix for cell culture. PAAM hydrogel is an ionic gel used in cell culture, because its high fluid contents, its possibility of cells adhesion without the need of protein. The properties of this hydrogel such as swelling, porosity and stiffness can be controlled to mimic cell environment for better conditions for cell growth. In the next chapters, many parameters will be changed to study these gel properties, as well as the possibility to control the gel behavior, to ensure the best condition for cell growth. Porous bulks are prepared using emulsion technique forming a 3D macroporous PAAM hydrogel scaffold for spheroids formation.

The ultimate goal of this work is to develop a biocompatible implantable bioartificial kidney that mimic the work of a natural kidney. In this project, we aim to develop several “filtration units” each having a specific filtration function and serving as building blocks of the future bioartificial kidney.

This thesis work lies in the bioinspired design of a single microchip “filtration unit” that replicate the *in vivo* model and works as a miniaturized dialysis machine. The “filtration unit” consist of PDMS layers encapsulating a hydrogel membrane or a hydrogel extracellular matrix seeded with podocyte and endothelial cells. The filtration ability of the membrane will be tested to ensure the

maintenance of essential proteins and nutrition, and the cleaning of internal wastes, by testing composition of the resulting fluids after filtration.

Controlling the hydrogel membrane physicochemical properties will help monitoring the filtration ability and efficiency of the "filtration unit". (As an example: controlling the pore size of the hydrogel matrix will allow monitoring the size selectivity or the molecular weight cutoff).

In addition, the usage of the 3D macroporous hydrolyzed PAAM hydrogel as an extracellular matrix allows the formation of podocyte cells spheroids, and serves as a membrane in some "filtration units" that will work as bioreactors and avoid cell detachment in case of a high flow rate of filtrate.

Then the encapsulated hydrogel seeded with cells or not will determine the "filtration unit" selectivity. Using hydrogels having different properties will lead to the generation of different filtration units each having a specific function and imitating a specific renal activity.

Finally, the future bioartificial kidney could be an assembly of several filtration units working in parallel, each unit having a specific filtration function. Developing such device would be an epic advance in medicine and could address a chronic shortage of donor kidneys needed.

During this thesis, the design, the conception and the fabrication of a single filtration unit encapsulating 2D hydrogel membrane, and the ability of podocytes to form spheroids inside 3D hydrogel was realized. This content is divided into 2 chapters.

The chapter 2 will describe the design and the conception of bioarticial kidney, which is composed of several filtration units. The fabrication of filtration unit is detailed after, from the mold design, to the PDMS preparation, to the assembly of several PDMS layers.

The preparation of 2D hydrogel that will be encapsulated inside the device will be detailed. The hydrogel having different Crosslinker concentration were characterized by measuring the swelling degree and Young's Modulus.

The filtration ability of the device is tested under different experimental condition, using different flow rate, hydrogels having different crosslinker density. The ability of the hydrogel to mimic the

kidney filtration is tested using different compounds, ions and molecules having different molecular weight.

In chapter 3, the ability of PAAM hydrogel to encapsulate cell spheroids was tested. The fabrication of a macroporous Hydrolyzed Polyacrylamide Hydrogel was detailed. Different hydrogel was prepared having different experiment parameters (volume of the mixture, oil/water ratio of the emulsion, the surfactant content, the crosslinker density, hydrolysis rate) and the effect of each parameter on the 3D PAAM Hydrogels properties is evaluated (swelling, Young's Modulus, Porosity, morphology).

The formation of podocyte spheroids is tested on different hydrogel prepared in order to investigate their effect on the spheroid formation, stability, proliferation and death.

The filtration effect of marcoporous hydrogel seeded with Podocytes spheroids and encapsulated inside the "filtration unit" designed in chapter 2, will be studied in future work. To finish by assembling different filtration units encapsulating hydrogels seeded with podocytes cells or not, working in parallel forming the bioartificial kidney that replace the normal kidney function.

VII.References

1. Bomback, A. S. *et al. National Kidney Foundation's primer on kidney diseases*. (2018).
2. N, R. *et al.* Improvements in Glomerular Filtration Rate (GFR) in Chronic Kidney Disease (CKD) Patients Using a Commercial Patented and Proprietary ProbioticPrebiotic Formulation* -3rd Biennial Survey. *International Journal of Nephrology and Kidney Failure* **4**, (2018).
3. Levey, A. S., Inker, L. A. & Coresh, J. Chronic Kidney Disease in Older People. *JAMA* **314**, 557 (2015).
4. Ising, C. & Brinkkoetter, P. T. Prohibitin Signaling at the Kidney Filtration Barrier. in *Mitochondrial Dynamics in Cardiovascular Medicine* (ed. Santulli, G.) vol. 982 563–575 (Springer International Publishing, 2017).
5. Ota, T., Nakayama, M., Kanno, Y., Suzuki, T. & Miki, N. In vitro and in vivo tests of nanoporous membrane coated with biocompatible fluorine-doped diamond-like carbon for hemofiltration treatment. in 412–414 (IEEE, 2018). doi:10.1109/MEMSYS.2018.8346575.
6. Webster, A. C., Nagler, E. V., Morton, R. L. & Masson, P. Chronic Kidney Disease. *The Lancet* **389**, 1238–1252 (2017).
7. Romagnani, P. *et al.* Chronic kidney disease. *Nature Reviews Disease Primers* **3**, (2017).
8. Eaton, D. C., Pooler, J. & Vander, A. J. *Vander's renal physiology*. (McGraw-Hill Medical, 2009).
9. Koeppen, B. M. & Stanton, B. A. *Renal physiology*. (Elsevier Mosby, 2013).

10. Dalal, R., Bruss, Z. S. & Sehdev, J. S. Physiology, Renal Blood Flow and Filtration. in *StatPearls* (StatPearls Publishing, 2020).
11. Du, B., Yu, M. & Zheng, J. Transport and interactions of nanoparticles in the kidneys. *Nature Reviews Materials* **3**, 358–374 (2018).
12. Hall, J. E. *Guyton and hall textbook of medical physiology*. (Elsevier, 2020).
13. Reiser, J. & Altintas, M. M. Podocytes. *F1000Research* **5**, 114 (2016).
14. Greka, A. & Mundel, P. Cell Biology and Pathology of Podocytes. *Annual Review of Physiology* **74**, 299–323 (2012).
15. Abdallah, M. *et al.* Influence of Hydrolyzed Polyacrylamide Hydrogel Stiffness on Podocyte Morphology, Phenotype, and Mechanical Properties. *ACS Applied Materials & Interfaces* **11**, 32623–32632 (2019).
16. Hill, N. R. *et al.* Global Prevalence of Chronic Kidney Disease – A Systematic Review and Meta-Analysis. *PLOS ONE* **11**, e0158765 (2016).
17. Organ shortage: Current status and strategies for improvement of organ donation - A European Consensus Document. (2013).
18. Daugirdas, J. T., Blake, P. G. & Ing, T. S. *Handbook of dialysis*. (2012).
19. Pastan, S. & Bailey, J. Dialysis Therapy. *New England Journal of Medicine* **338**, 1428–1437 (1998).
20. Breyer, M. D. & Susztak, K. Developing Treatments for Chronic Kidney Disease in the 21st Century. *Seminars in Nephrology* **36**, 436–447 (2016).
21. Ota, T., To, N., Kanno, Y. & Miki, N. Evaluation of biofouling in stainless microfluidic channels for implantable multilayered dialysis device. *Japanese Journal of Applied Physics* **56**, (2017).
22. Pinger, C. W., Heller, A. A. & Spence, D. M. A Printed Equilibrium Dialysis Device with Integrated Membranes for Improved Binding Affinity Measurements. *Analytical Chemistry* **89**, 7302–7306 (2017).
23. Conlisk, A. T., Datta, S., Fissell, W. H. & Roy, S. Biomolecular Transport Through Hemofiltration Membranes. *Annals of Biomedical Engineering* **37**, 722–736 (2009).
24. Dang, B. V., Taylor, R. A., Charlton, A. J., Le-Clech, P. & Barber, T. J. Toward Portable Artificial Kidneys: The Role of Advanced Microfluidics and Membrane Technologies in Implantable Systems. *IEEE Reviews in Biomedical Engineering* **13**, 261–279 (2020).
25. Sackmann, E. K., Fulton, A. L. & Beebe, D. J. The present and future role of microfluidics in biomedical research. *Nature* **507**, 181–189 (2014).
26. Zengerle, R., Mark, D., Kosse, D., Roth, G. & von Stetten, F. Microfluidic solutions for miniaturization, integration, automation and parallelization of tests on commercially available instruments. in 12–15 (IEEE, 2011). doi:10.1109/TRANSDUCERS.2011.5969897.
27. Dong, R., Liu, Y., Mou, L., Deng, J. & Jiang, X. Microfluidics-Based Biomaterials and Biodevices. *Advanced Materials* **31**, 1805033 (2019).
28. Marre, S., Roig, Y. & Aymonier, C. Supercritical microfluidics: Opportunities in flow-through chemistry and materials science. *The Journal of Supercritical Fluids* **66**, 251–264 (2012).
29. Mittal, R. *et al.* Organ-on-chip models: Implications in drug discovery and clinical applications. *Journal of Cellular Physiology* **234**, 8352–8380 (2019).
30. Fang, X. Microfluidic Chip. in *Clinical Molecular Diagnostics* (eds. Pan, S. & Tang, J.) 357–375 (Springer Singapore, 2021). doi:10.1007/978-981-16-1037-0_26.
31. Jammes, F. C. & Maerkl, S. J. How single-cell immunology is benefiting from microfluidic technologies. *Microsystems & Nanoengineering* **6**, (2020).
32. Chen, J., Chen, D., Xie, Y., Yuan, T. & Chen, X. Progress of Microfluidics for Biology and Medicine. *Nano-Micro Letters* **5**, 66–80 (2013).

33. Torino, S., Corrado, B., Iodice, M. & Coppola, G. PDMS-Based Microfluidic Devices for Cell Culture. *Inventions* **3**, 65 (2018).
34. Raj M, K. & Chakraborty, S. PDMS microfluidics: A mini review. *Journal of Applied Polymer Science* **137**, 48958 (2020).
35. Haeberle, S. & Zengerle, R. Microfluidic platforms for lab-on-a-chip applications. *Lab on a Chip* **7**, 1094 (2007).
36. Sia, S. K. & Whitesides, G. M. Microfluidic devices fabricated in Poly(dimethylsiloxane) for biological studies. *ELECTROPHORESIS* **24**, 3563–3576 (2003).
37. Wolf, M. P., Salieb-Beugelaar, G. B. & Hunziker, P. PDMS with designer functionalities—Properties, modifications strategies, and applications. *Progress in Polymer Science* **83**, 97–134 (2018).
38. Mani, S. Fundamentals aspects of crosslinking control of PDMS rubber at high temperatures using TEMPO nitroxide. (UNIVERSITÉ LAVAL QUÉBEC and UNIVERSITÉ CLAUDE BERNARD LYON 1, 2011).
39. Juárez-Moreno, J. A., Ávila-Ortega, A., Oliva, A. I., Avilés, F. & Cauich-Rodríguez, J. V. Effect of wettability and surface roughness on the adhesion properties of collagen on PDMS films treated by capacitively coupled oxygen plasma. *Applied Surface Science* **349**, 763–773 (2015).
40. Venkatachalam, S. & Hourlier, D. Heat treatment of commercial Polydimethylsiloxane PDMS precursors: Part I. Towards conversion of patternable soft gels into hard ceramics. *Ceramics International* **45**, 6255–6262 (2019).
41. Eduok, U., Faye, O. & Szpunar, J. Recent developments and applications of protective silicone coatings: A review of PDMS functional materials. *Progress in Organic Coatings* **111**, 124–163 (2017).
42. Kim, T. K., Kim, J. K. & Jeong, O. C. Measurement of nonlinear mechanical properties of PDMS elastomer. *Microelectronic Engineering* **88**, 1982–1985 (2011).
43. Tang, K. C. *et al.* Evaluation of bonding between oxygen plasma treated polydimethyl siloxane and passivated silicon. *Journal of Physics: Conference Series* **34**, 155–161 (2006).
44. Humes, H. D., Buffington, D., Westover, A. J., Roy, S. & Fissell, W. H. The bioartificial kidney: current status and future promise. *Pediatric Nephrology* **29**, 343–351 (2014).
45. Mariella, R. Sample preparation: the weak link in microfluidics-based biodetection. *Biomedical Microdevices* **10**, (2008).
46. Hasani-Sadrabadi, M. M. *et al.* Enhanced osteogenic differentiation of stem cells via microfluidics synthesized nanoparticles. *Nanomedicine: Nanotechnology, Biology and Medicine* **11**, 1809–1819 (2015).
47. Aziz, A. *et al.* The Role of Microfluidics for Organ on Chip Simulations. *Bioengineering* **4**, 39 (2017).
48. Paiè, P., Martínez Vázquez, R., Osellame, R., Bragheri, F. & Bassi, A. Microfluidic Based Optical Microscopes on Chip: Microscopes on Chip. *Cytometry Part A* **93**, 987–996 (2018).
49. Khan, I. U., Serra, C. A., Anton, N. & Vandamme, T. F. Production of nanoparticle drug delivery systems with microfluidics tools. *Expert Opinion on Drug Delivery* **12**, 547–562 (2015).
50. Ndegwa, S. *CADTH Issues in Emerging Health Technologies*. (Canadian Agency for Drugs and Technologies in Health, 2016).
51. Wang, X. Bioartificial Organ Manufacturing Technologies. *Cell Transplantation* **28**, 5–17 (2019).
52. Hojs, N., Fissell, W. H. & Roy, S. Ambulatory Hemodialysis-Technology Landscape and Potential for Patient-Centered Treatment. *Clinical Journal of the American Society of Nephrology* **15**, 152–159 (2020).
53. van den Berg, A., Mummery, C. L., Passier, R. & van der Meer, A. D. Personalised organs-on-chips: functional testing for precision medicine. *Lab on a Chip* **19**, 198–205 (2019).

54. Perozziello, G. *et al.* A microfluidic dialysis device for complex biological mixture SERS analysis. *Microelectronic Engineering* **144**, 37–41 (2015).
55. De Bartolo, L. Membrane Bioartificial Organs. in *Encyclopedia of Membranes* (eds. Drioli, E. & Giorno, L.) 1–2 (Springer Berlin Heidelberg, 2015). doi:10.1007/978-3-642-40872-4_355-3.
56. Corridon, P. R., Ko, I. K., Yoo, J. J. & Atala, A. Bioartificial Kidneys. *Current Stem Cell Reports* **3**, 68–76 (2017).
57. Jang, K.-J. *et al.* Human kidney proximal tubule-on-a-chip for drug transport and nephrotoxicity assessment. *Integrative Biology* **5**, 1119–1129 (2013).
58. Wang, L. *et al.* A disease model of diabetic nephropathy in a glomerulus-on-a-chip microdevice. *Lab on a Chip* **17**, 1749–1760 (2017).
59. Qu, Y. *et al.* A nephron model for study of drug-induced acute kidney injury and assessment of drug-induced nephrotoxicity. *Biomaterials* **155**, 41–53 (2018).
60. Chui, B. W. *et al.* A Scalable, Hierarchical Rib Design for Larger-Area, Higher-Porosity Nanoporous Membranes for the Implantable Bio-Artificial Kidney. *Journal of Microelectromechanical Systems* **29**, 762–768 (2020).
61. Fissell, W. H. & Roy, S. The Implantable Artificial Kidney. *Seminars in Dialysis* **22**, 665–670 (2009).
62. Salani, M., Roy, S. & Fissell, W. H. Innovations in Wearable and Implantable Artificial Kidneys. *American Journal of Kidney Diseases* **72**, 745–751 (2018).
63. Luo, J., Fan, J. & Wang, S. Recent Progress of Microfluidic Devices for Hemodialysis. *Small* **16**, 1904076 (2020).
64. Mollahosseini, A., Abdelrasoul, A. & Shoker, A. Challenges and advances in hemodialysis membranes. in *Advances in Membrane Technologies* (IntechOpen, 2020).
65. Ota, T., Nakayama, M., Kanno, Y., Suzuki, T. & Miki, N. In vitro and in vivo tests of nanoporous membrane coated with biocompatible fluorine-doped diamond-like carbon for hemofiltration treatment. in 412–414 (IEEE, 2018). doi:10.1109/MEMSYS.2018.8346575.
66. Wilmer, M. J. *et al.* Kidney-on-a-Chip Technology for Drug-Induced Nephrotoxicity Screening. *Trends in Biotechnology* **34**, 156–170 (2016).
67. Jang, K.-J. *et al.* Human kidney proximal tubule-on-a-chip for drug transport and nephrotoxicity assessment. *Integrative Biology* **5**, 1119–1129 (2013).
68. Yi, Z., Liu, C.-J., Zhu, L.-P. & Xu, Y.-Y. Ion Exchange and Antibiofouling Properties of Poly(ether sulfone) Membranes Prepared by the Surface Immobilization of Brønsted Acidic Ionic Liquids via Double-Click Reactions. *Langmuir* **31**, 7970–7979 (2015).
69. Jansen, K., Schuurmans, C. C. L., Jansen, J., Masereeuw, R. & Vermonden, T. Hydrogel-Based Cell Therapies for Kidney Regeneration: Current Trends in Biofabrication and In Vivo Repair. *Current Pharmaceutical Design* **23**, (2017).
70. Ma, L., Zhou, C., Lin, B. & Li, W. A porous 3D cell culture micro device for cell migration study. *Biomedical Microdevices* **12**, 753–760 (2010).
71. Haque, Md. A., Kurokawa, T. & Gong, J. P. Super tough double network hydrogels and their application as biomaterials. *Polymer* **53**, 1805–1822 (2012).
72. Sunyer, R., Jin, A. J., Nossal, R. & Sackett, D. L. Fabrication of Hydrogels with Steep Stiffness Gradients for Studying Cell Mechanical Response. *PLoS ONE* **7**, e46107 (2012).
73. Dickinson, E. Microgels — An alternative colloidal ingredient for stabilization of food emulsions. *Trends in Food Science & Technology* **43**, 178–188 (2015).
74. Bassil, M. Muscles artificiels à base d'hydrogel électroactif. (Université Claude Bernard-Lyon I, 2009).
75. Caló, E. & Khutoryanskiy, V. V. Biomedical applications of hydrogels: A review of patents and commercial products. *European Polymer Journal* **65**, 252–267 (2015).

76. Zhu, J. & Marchant, R. E. Design properties of hydrogel tissue-engineering scaffolds. *Expert Review of Medical Devices* **8**, 607–626 (2011).
77. Sivashanmugam, A., Arun Kumar, R., Vishnu Priya, M., Nair, S. V. & Jayakumar, R. An overview of injectable polymeric hydrogels for tissue engineering. *European Polymer Journal* **72**, 543–565 (2015).
78. Yang, C. & Suo, Z. Hydrogel ionotronics. *Nature Reviews Materials* **3**, 125–142 (2018).
79. El-Sherbiny, I. M. & Yacoub, M. H. Hydrogel scaffolds for tissue engineering: Progress and challenges. *Global Cardiology Science and Practice* **2013**, 38 (2013).
80. Williams, D. F. On the mechanisms of biocompatibility. *Biomaterials* **29**, 2941–2953 (2008).
81. Shkumatov, A. A. *Extracellular matrix stiffness and geometry: the impact on static and dynamic cellular systems in vitro and the treatment of tissue ischemia*. (University of Illinois at Urbana-Champaign, 2014).
82. Xu, C. *et al.* Mussel-Inspired Biocompatible PAADOPA/PAAm Hydrogel Adhesive for Amoxicillin Delivery. *Industrial & Engineering Chemistry Research* **59**, 13556–13563 (2020).
83. Zhang, X.-Q. *et al.* Multiresponsive Reversible Deformation of Patterned Polyacrylamide Hydrogel Constructed by a Computer-Assisted Dispenser. *ACS Applied Polymer Materials* **1**, 1187–1194 (2019).
84. Koushki, N. *et al.* A new injectable biphasic hydrogel based on partially hydrolyzed polyacrylamide and nanohydroxyapatite as scaffold for osteochondral regeneration. *RSC Advances* **5**, 9089–9096 (2015).
85. Ding, H. *et al.* Hydrolyzed Hydrogels with Super Stretchability, High Strength, and Fast Self-Recovery for Flexible Sensors. *ACS Applied Materials & Interfaces* **13**, 22774–22784 (2021).
86. Caulfield, M. J., Qiao, G. G. & Solomon, D. H. Some Aspects of the Properties and Degradation of Polyacrylamides. *Chem. Rev.* **102**, 3067–3084 (2002).
87. Zhang, C., Zhao, L., Bao, M. & Lu, J. Potential of hydrolyzed polyacrylamide biodegradation to final products through regulating its own nitrogen transformation in different dissolved oxygen systems. *Bioresource Technology* **256**, 61–68 (2018).
88. O'Connell, P. B. H. & Brady, C. J. Polyacrylamide gels with modified cross-linkages. *Analytical Biochemistry* **76**, 63–73 (1976).
89. Ebewele, R. O. *Polymer Science and Technology*. (CRC Press, 2000). doi:10.1201/9781420057805.
90. Odian, G. G. *Principles of polymerization*. (Wiley-Interscience, 2004).
91. Chassanieux, C., Lefebvre, H. & Pascual, S. *L'indispensable en polymères*. (Bréal, 2008).
92. Osada, Y., Ping Gong, J. & Tanaka, Y. Polymer Gels. *Journal of Macromolecular Science, Part C: Polymer Reviews* **44**, 87–112 (2004).
93. De Gennes, P.-G. & Gennes, P.-G. *Scaling concepts in polymer physics*. (Cornell university press, 1979).
94. Li, Y. & Tanaka, T. Phase Transitions of Gels. *Annual Review of Materials Science* **22**, 243–277 (1992).
95. Anseth, K. S., Bowman, C. N. & Brannon-Peppas, L. Mechanical properties of hydrogels and their experimental determination. *Biomaterials* **17**, 1647–1657 (1996).
96. Tse, J. R. & Engler, A. J. Preparation of Hydrogel Substrates with Tunable Mechanical Properties. *Current Protocols in Cell Biology* **47**, (2010).
97. James, A. Overview of asphalt emulsion. *Transportation Research Circular E-C102: Asphalt Emulsion Technology* 1–15 (2006).
98. Tang, J., Lin, N., Zhang, Z., Pan, C. & Yu, G. Nanopolysaccharides in Emulsion Stabilization. in *Advanced Functional Materials from Nanopolysaccharides* (eds. Lin, N., Tang, J., Dufresne, A. & Tam, M. K. C.) vol. 15 221–254 (Springer Singapore, 2019).

99. *Advanced functional materials from nanopolysaccharides*. (Springer, 2019).
100. Binks, B. P. Particles as surfactants—similarities and differences. *Current Opinion in Colloid & Interface Science* **7**, 21–41 (2002).
101. Taylor, K. C. & Nasr-El-Din, H. A. Water-soluble hydrophobically associating polymers for improved oil recovery: A literature review. *Journal of Petroleum Science and Engineering* **19**, 265–280 (1998).
102. Friberg, S. E. & Friberg, S. H. Emulsion Formation. in *Encyclopedia of Colloid and Interface Science* (ed. Tadros, T.) 366–414 (Springer Berlin Heidelberg, 2013). doi:10.1007/978-3-642-20665-8_16.
103. Sjöblom, J., Stenius, P., Simon, S. & Grimes, B. A. Emulsion Stabilization. in *Encyclopedia of Colloid and Interface Science* (ed. Tadros, T.) 415–454 (Springer Berlin Heidelberg, 2013). doi:10.1007/978-3-642-20665-8_83.
104. Tadros, T. Polymeric Surfactant. in *Encyclopedia of Colloid and Interface Science* (ed. Tadros, T.) 964–995 (Springer Berlin Heidelberg, 2013). doi:10.1007/978-3-642-20665-8_35.
105. Tadros, T. Surfactants. in *Encyclopedia of Colloid and Interface Science* (ed. Tadros, T.) 1242–1290 (Springer Berlin Heidelberg, 2013). doi:10.1007/978-3-642-20665-8_40.
106. Varone, A. *et al.* A novel organ-chip system emulates three-dimensional architecture of the human epithelia and the mechanical forces acting on it. *Biomaterials* **275**, 120957 (2021).
107. Zhao, X. *et al.* Review on the Vascularization of Organoids and Organoids-on-a-Chip. *Frontiers in Bioengineering and Biotechnology* **9**, (2021).
108. Unagolla, J. M. & Jayasuriya, A. C. Hydrogel-based 3D bioprinting: A comprehensive review on cell-laden hydrogels, bioink formulations, and future perspectives. *Applied Materials Today* **18**, 100479 (2020).
109. Urbanczyk, M., Layland, S. L. & Schenke-Layland, K. The role of extracellular matrix in biomechanics and its impact on bioengineering of cells and 3D tissues. *Matrix Biology* **85–86**, 1–14 (2020).
110. Vera, D. *et al.* Engineering Tissue Barrier Models on Hydrogel Microfluidic Platforms. *ACS Applied Materials & Interfaces* **13**, 13920–13933 (2021).
111. Stowers, R. S. Advances in Extracellular Matrix-Mimetic Hydrogels to Guide Stem Cell Fate. *Cells Tissues Organs* 1–18 (2021) doi:10.1159/000514851.
112. Levental, I., Georges, P. C. & Janmey, P. A. Soft biological materials and their impact on cell function. *Soft Matter* **3**, 299–306 (2007).
113. Mueller, S. Liver stiffness: a novel parameter for the diagnosis of liver disease. *Hepatic Medicine: Evidence and Research* 49 (2010) doi:10.2147/HMER.S7394.
114. Cell Adhesion and the Extracellular Matrix. in *Goodman's Medical Cell Biology* 203–247 (Elsevier, 2021). doi:10.1016/B978-0-12-817927-7.00007-7.
115. Janmey, P. A. & Miller, R. T. Mechanisms of mechanical signaling in development and disease. *Journal of Cell Science* **124**, 9–18 (2011).
116. Orr, A. W., Helmke, B. P., Blackman, B. R. & Schwartz, M. A. Mechanisms of Mechanotransduction. *Developmental Cell* **10**, 11–20 (2006).
117. Janmey, P. A. & Weitz, D. A. Dealing with mechanics: mechanisms of force transduction in cells. *Trends in Biochemical Sciences* **29**, 364–370 (2004).
118. Bershadsky, A. D., Balaban, N. Q. & Geiger, B. Adhesion-Dependent Cell Mechanosensitivity. *Annual Review of Cell and Developmental Biology* **19**, 677–695 (2003).
119. Bershadsky, A., Kozlov, M. & Geiger, B. Adhesion-mediated mechanosensitivity: a time to experiment, and a time to theorize. *Current Opinion in Cell Biology* **18**, 472–481 (2006).
120. Abdallah, M. Développer des hydrogels et étudier les effets des propriétés mécaniques sur les activités biologiques des podocytes. (Université de Montpellier, 2019).

Chapter II: Development of a microfluidics hydrogel-based device for selective filtration of proteins and ions as a bioactive model of artificial kidney

I. Introduction

The kidney plays an important role for a normal body function; it maintains the normal body fluid composition for a normal cellular size and function, retains plasma volume and excretes toxic compounds in the urine[1]. Chronic Kidney Disease refers to a wide range of conditions which damage the kidneys, and reduce their efficiency to filter the blood[1,2]. Haemodialysis is a treatment method that purifies blood using a dialyzer machine by diffusion of molecules through a porous hollow fiber membrane. Big equipment are required for dialysis treatment, hence the necessity for the patients to receive treatments at the hospitals 3-4 times a week, lead to low quality of life of the patients and rising socio-economical burdens on the societies[3,4].

Many studies are made to develop an implantable or portable dialysis device, in order to alleviate the burden of dialysis treatment, by miniaturizing the whole dialysis system[3]. A dialysis device is composed generally of a filtration membrane sandwiched between two hydrophobic flexible polymer layers that contain micro to macroscale channels for fluid circulation. Currently, the robust and cost-effective polymeric materials, such as polydimethylsiloxane (PDMS), polymethyl methacrylate (PMMA), polycarbonate (PC), and polystyrene[5] are the most used for in the fabrication of such devices. Blood and filtrate flow are introduced into the device on both sides of the membrane. Small molecules, toxins and ions can diffuse through the porous membrane from blood (highly concentrated in ions, toxins and proteins) to filtrate (low concentrated in ions, toxins-free). The blood clearance rate depends on the contact surface area between fluids and the membrane[6,7]. Increasing the contact surface will increase the possibility of the molecules diffusion from the blood to the filtrate. The specific pore size of the membrane allows the maintenance of essential proteins and nutrition. After the filtration process, cleaned blood flows into the veins and the filtrate is brought to the bladder and discarded as urine.

First-generation haemodialysis membranes were commonly made out of cellulose membranes and regenerated cellulose (RC) membranes that had a good efficient clearance of small molecules and limited clearance of medium molecules and macromolecules removal[8,9]. The second generation of dialysis membranes are mainly polymers, such as Poly(ether sulfone) (PES), polyvinyl pyrrolidone (PVP), Coated-Polydimethylsiloxane (PDMS) and polyester[9]. These membranes are the most used in the filtration devices[3,10,11], they are characterized by

their multifunctionality, including surface hydrophilicity, ion exchange and biofouling resistance to proteins and bacteria[12], but they are limited by their mirror-polished surface that can prevent protein adhesion[13].

The microfluidic dialysis device or "artificial kidney" can replace the filtration function of kidney by removing fluids and wastes, but does not replace the kidneys' role in regulating metabolism, endocrine function, and homeostasis[13–15].

On the other side, bioartificial kidneys provide an extension to conventional artificial kidneys and dialysis systems, by incorporating tissue engineering with living cellular and tissue, in order to better mimic normal kidneys. The bioartificial kidney involves the design, growth and maintenance of living tissues embedded in natural or synthetic scaffolds to enable them to perform complex biochemical functions and replace normal living tissue[16,17]. Many studies are made to develop an implantable or portable bioartificial kidneys, but they still facing many limitations, such as the limited flow rate used (1 ml/min ≈ 1.44 L per day) in order to avoid additional pressure at the cells membrane interface, that is fragile, and thus inducing cracks in the membrane[18]. In addition to the loss of blood pressure in the in vivo application, the short lifetime of the membrane and the decrease of filtration efficiency after 7 days[3,12] .

Hydrogels could be advantageous over other types of dialysis membrane for a bioartificial kidney. Firstly, hydrogels could be an ECM-mimetic providing additional mechanical and biochemical cues as described earlier, possibly leading to enhanced cell differentiation and functionality. The second advantage of hydrogels in bioartificial kidney device is their potential for implantation. Hydrolyzed Polyacrylamide is a hydrogel material with a high absorption capacity of a liquid, and have many advantages over other types of membranes, since it can combine the filtration function of a membrane and the properties of scaffolding materials suitable for cell culture. PAAM hydrogel is a biocompatible, non-biodegradable material that offers a suitable substrate for cell culture[20]. In addition, the structural and mechanical properties of PAAM hydrogels can be easily controlled by controlling the pre-gel composition and the polymerization conditions, which affect the stiffness and the porosity of the scaffold. Current research focus to design an implantable construct, which allows a continuous blood clearance and more independence for the patient. So the device would be a wearable or implantable bioartificial kidney that supersedes conventional dialysis treatment[21].

This chapter aims to develop a "filtration unit" encapsulating a hydrolyzed polyacrylamide hydrogel having a specific filtration function and serving as building blocks of the future bioartificial kidney, that will replace the kidney function in case of a lost or a failure.

In this chapter, the design and fabrication of a single microfluidic "filtration unit" is detailed. Starting from the conception of different layers of the device, moving to the drawing and the printing of molds for PDMS preparation, ending with the preparation and the characterization of PAAM membrane that is encapsulated between the PDMS layers. Finally, a preliminary evaluation of the filtration ability of the fabricated unit is performed using different Hydrolyzed PAAM hydrogels samples and different experimental conditions.

II. Bioartificial Kidney Design

The ultimate goal of this work is to develop a biocompatible artificial kidney, composed of several "filtration units".

The "filtration unit" can encapsulate a hydrogel membrane or a hydrogel extracellular matrix seeded with podocytes. Controlling the hydrogel physicochemical properties will help to monitor the filtration ability and efficiency of the "filtration unit", i.e., the size selectivity or the molecular weight cutoff can be controlled by changing the hydrogel matrix pores size.

Using hydrogels having different properties will lead to the generation of different filtration units each having a specific selectivity and imitating a specific renal filtration function. The future bioartificial kidney could be an assembly of several filtration units working together, each unit having a specific filtration function.

The objectives in this thesis chapter are to design and fabricate a new design of a single "filtration unit", optimize the processing parameters of the device, and gather preliminary filtration results to evaluate the future potential of the "filtration unit" by means of controlling the hydrogel physicochemical properties, in order to mimic a specific filtration ability of the kidney, such as the ion selectivity, the molecular weight cut off and the clearance of solutes.

Different designs of microfluidic device and microchannel geometries have been studied for bioartificial kidney applications. The device channels can be simply designed in a simple tubular shape, where fluids flow through two tubes on both sides of a membrane[11,22–25]. In the linear tubular shape channel, the small fluid-membrane contact area reduces the possibility of membrane deformation. The reduction in the fluid-membrane contact surface causes a decrease in molecules diffusion, hence the importance of creating a model increasing the contact surface. The microfluidic channels having serpentine shape are designed to increase the fluid-membrane contact area and therefore the molecule diffusion[13,26–28]. The serpentine-shape channel consists of a rectangular cross-section multichannels connected by two semicircular subsections, forming a repeating S-shaped[29].

Hydrogels are widely used as basement membranes in microfluidic devices for kidney replacement. The microfluidic devices encapsulating hydrogels cultured with podocytes and endothelial cells are designed in a way to increase the culture surface area and therefore the active diffusion area. Due to the hydrogel thickness (more than 500 µm), the fluid-membrane contact area can be increased while reducing the stress on the membrane avoiding any membrane deformation. A three-layer compartmentalized microfluidic kidney chip is designed, consist of an upper, middle, and lower PDMS layers. A circular shape chamber connected to microchannels is created in both upper and lower layers sandwiched with a middle layer holding a porous membrane cultured with epithelial and endothelial cells[18,30–32].

In this section, the design of a microfluidic device is detailed, and the dimension of each layer of the resulting "filtration unit" are mentioned.

Filtration Unit Conception

The "filtration unit" (Fig. 1) consist of 5 layers:

- The first PDMS layer square shape (side = 44 mm and thickness = 1 mm) contains a cubic reaction chamber (side = 10 mm and thickness = 1 mm) connected through 2 channels (wide = 1 mm length = 12 mm and depth = 0.8 mm) to an inlet and an outlet. In this layer the fluid representing the urine (or the fluid to be filtrate) will flow.

- The second PDMS layer square shape (side = 44 mm and thickness = 1 mm) contains a cubic reaction chamber (side = 10 mm and thickness = 1 mm) connected through 2 channels (wide = 1 mm length = 12 mm and depth = 0.8 mm) to an inlet and an outlet. In this layer the fluid representing the blood (or the fluid to be filtered) will flow.

- The middle PDMS layer holds the hydrogel based filtration membrane (diameter = 16 mm and thickness = 2 mm) in place to be sandwiched between the 2 reactions chambers.

- The device is encapsulated between 2 PDMS layers (side = 44 mm and thickness = 2 mm) holed to insert the needles.

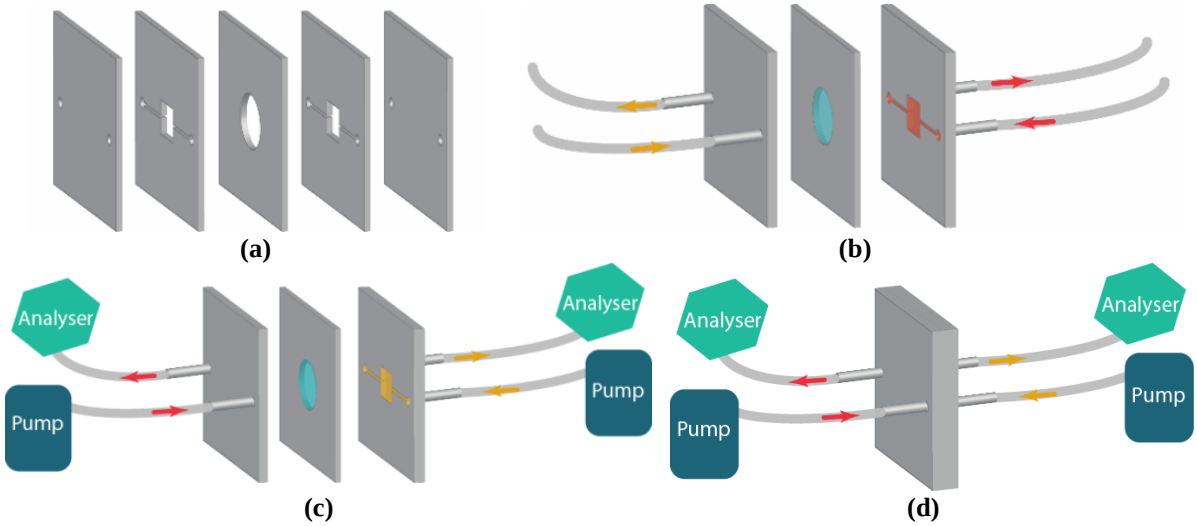

Figure 1. Schematic representation of the "filtration unit" showing **(a)** different layers of the microfluidic system **(b, c)** the microfluidic system encapsulating the hydrogel in the middle layer and connected through the first inlet to the "blood flow" (represented in red) and through the second inlet to the "urine flow" (represented in yellow) and **(d)** setup to be used to test the properties of the "filtration unit".

In this work, the "filtration unit" encapsulates a PAAM hydrogel membrane. The filtration ability of the membrane is tested to ensure the maintenance of essential proteins and nutrition, and the cleaning of internal wastes, by testing the composition of the resulting fluids after filtration.

Controlling the hydrogel physicochemical properties, help to monitor the filtration ability and efficiency of the "filtration unit". (As an example: controlling the pore size of the hydrogel matrix will allow monitoring the size selectivity or the molecular weight cutoff).

In addition, the “filtration unit” can encapsulate a hydrogel extracellular matrix seeded with podocyte and endothelial cells. The usage of the hydrolyzed PAAM hydrogel as a semipermeable membrane allows the attachment of podocyte and endothelial cells in some “filtration units” that will work as bioreactors for future studies. Then, the encapsulated hydrogel seeded with cells or not will determine the “filtration unit” selectivity.

Using hydrogels having different properties will lead the generation of different filtration units each having a specific function and imitating a specific renal activity. Finally, the future bioartificial kidney could be an assembly of several filtration units working in parallel, each unit having a specific filtration function.

III. Materials and Methods

The fabrication of the “filtration unit” passes through different steps. At first, we will present the PDMS layer fabrication and the device assembly. Then the characterization of different active PAAM hydrogel membranes having different properties will be detailed. Finally, the experimental setup used for the filtration tests and the sample analysis will be presented. We will evaluate the ions and waste diffusion, and the block of proteins having a molecular weight above 69 kDa through the PAAM membranes.

1. Chemicals

Polylactic acid (PLA) filament (Prusa Research, FLM-PLA-175-SLV) was used for 3D printing. Polydimethylsiloxane (PDMS) (Sylgard 184, Silicone Elastomer Kit, Dow Corning) was used to form PDMS polymer layers, by mixing the base Part A and the crosslinker Part B.

Acrylamide ≥ 99% (AAM, Sigma Aldrich, A8887), was used as monomer, N,N-methylenebisacrylamide ≥ 99.5% (BIS, Sigma Aldrich, M7279) as a cross-linker, N,N,tertramethylethylenediamine 99% (TEMED, Sigma Aldrich, T9281) as accelerator and ammonium persulfate ≥98% (APS, Sigma Aldrich, 248614) as initiator. Sodium Hydroxide 98-100.5% (NaOH, Sigma Aldrich, S8045) was used for gel hydrolysis. Dulbecco’s Phosphate Buffered Saline (PBS, Sigma Aldrich, D8537) was used for the swelling. Deionized water

(DW) was used for all the dilutions, the polymerization reactions, as well as for the swelling. AAM:BIS (30:x w/w) and APS (25% w/w) were used in aqueous solution. Ammonium persulfate was freshly prepared before each preparation.

Optimal Cutting temperature (O.C.T., Scigen^{TM}, 4586) compound is a water-soluble blend of glycols and resins, used as embedding medium that provides a convenient specimen matrix for cryostat sectioning at temperatures of -10^{o}C and below. Ethanol 96% (Sigma Aldrich, 1.59010) was used for samples storage.

Fluorescein isothiocyanate–dextran (FITC-Dextran, Sigma Aldrich, FD10S- FD40S- FD70S-69658), having respectively 10, 40, 70, 150 kDa molecular weight, were used to test the diffusion of different molecular weight through the filtration membrane. Bovine Serum Albumin (BSA) ≥98% (Sigma-Aldrich, A2153, 9048−46−8) with a molecular weight of 66 kDa was also used for filtration tests.

2. Fabrication of the Filtration Unit

a) 3D Printing of the Molds

The first attempt for the fabrication of the PDMS layers was the adoption of the molding technique. Different molds were prepared using the 3D printing technique.

Two 3D printing techniques, Fused Deposition Modeling **(**FDM**)** and Stereolithography **(**SLA**),** were used to print the molds for the PDMS layers fabrication. The 3D printing process passed through different steps. First the blueprint model was created using the "DesignSpark 3D" design software and saved as STereoLithography file format ".stl".

Then, for FDM printing, the model was digitally sliced using "PrusaSlicer' software. The printing parameters were adjusted to have a 100% infill then saved as ".G-code", exported to the printer and printed via FDM printer "Prusa i3 MK3S+" (Prusa Research, PRI-MK3S-COM-ORG-PEI) using PLA filaments. The mold is printed at a temperature of 55°C for the bed and 215°C for the nozzle.

For SLA, the file is imported into “PreForm” software and printed after generating support scaffold using clear resin. The SLA 3D Printer “Form 2” (Formlabs, PKG-F2-REFURB) use UV laser (violet 405nm-120mW) to cure isotropic solids pieces from liquid photopolymer resin. After printing, the molds were rinsing and post-curing to obtain the best results and mechanical properties. Both, sample and holder were soaked in "Form Wash" (Formlabs, FH-WA-01) that contains isopropanol to clear all non-polymerized resin, and then treated in "Form Cure" UV chamber (Formlabs, FH-CU-01) at 405 nm for 60 minutes at 60°C.

b) Polydimethylsiloxane

Polydimethylsiloxane (PDMS) (Sylgard 184, Dow Corning) was mixed at 10:1 ratio (base to crosslinker) and degassed in a vacuum oven (France ETUVES, XF020) for 30 minutes under a -0.08 MPa at room temperature. After, the mixture was poured carefully in the mold and degassed a second time for 15 minutes, then cured for 3 hours at 50°C avoiding the deformation of mold polymers starting from 60°C.

c) Fabrication of the Polydimethylsiloxane Layers

Different molds were tested. In a first attempt a “complete mold” was 3D printed and the PDMS was poured inside it (Fig. 2 (a)). The resulting PDMS layers were hard removed from resin mold and were not flat, they presented a meniscus on the edges due to the capillarity action of the mold (Fig. 2 (b)).

To facilitate the de-molding, avoid breakage of the PDMS and cancel the capillarity action a complex combinable mold with cover was fabricated (Fig. 2 (c)) and placed in a glass Petri dish to avoid the leakage of liquid PDMS during the procedure. PDMS is poured in the mold, degassed for 1 hour. Then, covered slowly starting from one side to the end. This mold presented several drawbacks like the PDMS leakage between the assembled parts and the uncontrolled formation of air bubbles (Fig. 2 (d)).

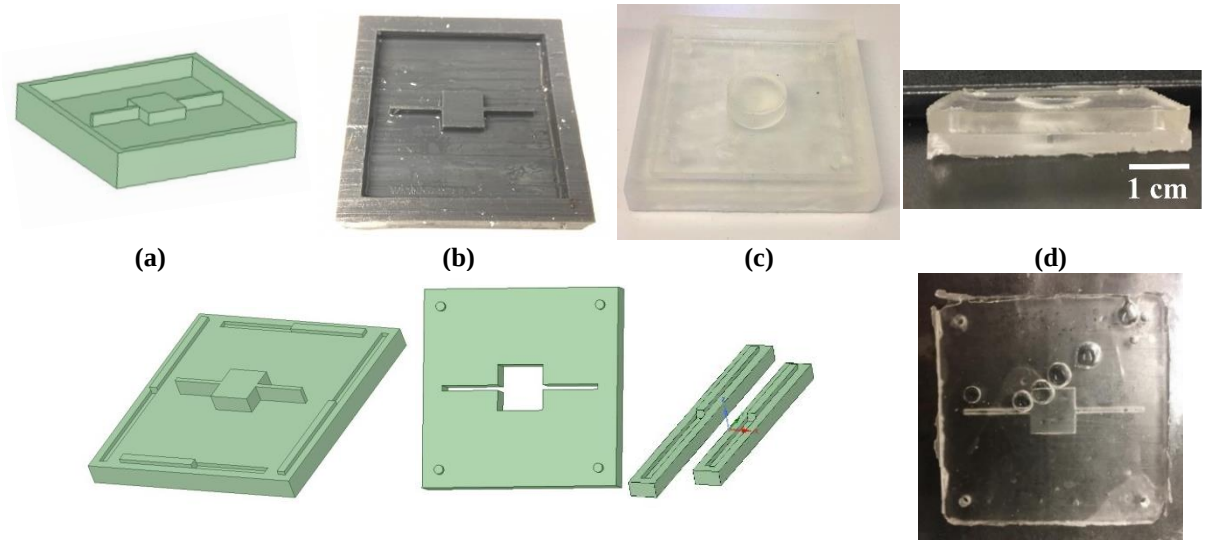

Figure 2. The 3D printed mold for PDMS layers fabrication **(a)** blueprint model, the mold printed with **(b)** FDM, **(c)** SLA and **(d)** the resulting PDMS layer of the latter one.
(e) The design of the complex combinable mold and **(f)** the resulting PDMS layer.

To overcome these problems, the "complete mold" was replaced by a second mold having the form of the reaction chamber. The PLA 3D chamber is printed using FDM printers (Fig. 3 (a)), and fixed on the glass substrate.

PDMS was degassed for 30 minutes, poured carefully on the glass, and degassed a second time for 15 minutes. Then, the PDMS was cured for 3 hours at 50°C to avoid the deformation of the PLA mold that occurs at 60°C.

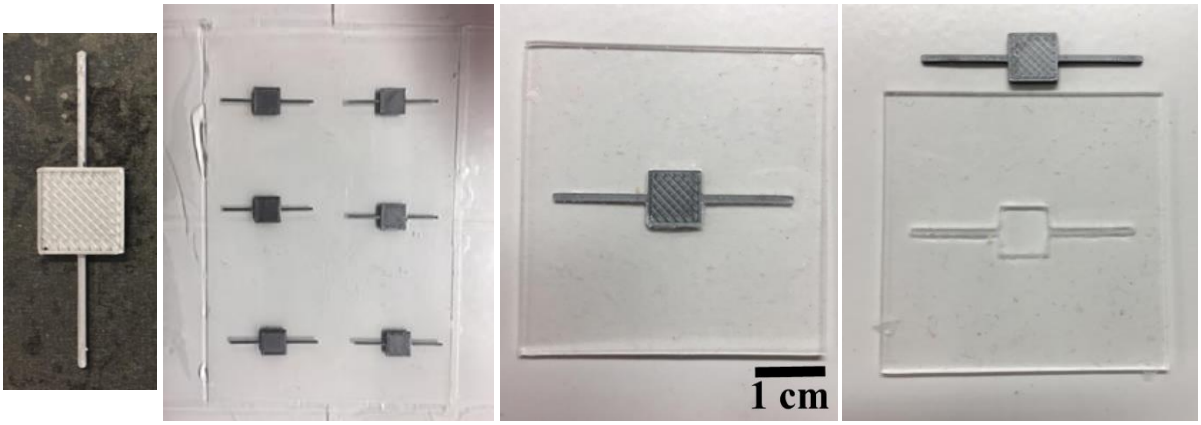

Figure 3. (a) PLA chamber mold. PDMS on glass molded with PLA **(b)** before cutting, **(c)** before and **(d)** after removing PLA

The PDMS samples are left covered for one hour to cool before cutting them into squares and de-molding. Finally, PDMS layers of 1 mm thickness were gently removed avoiding any stain or dust on the surface.

The middle and the cover layers were prepared by pouring PDMS carefully on the glass, then degassed and cured for 3 hours at 50°C. The PDMS layers of 2 mm thickness are left to cool, cut to square of 44 mm side. A 16 mm circle was removed from the center of the square middle layer by cutting the layers using a sharp stainless steel cylinder mold, in order to replace it by a PAAM hydrogel membrane on 2 mm thickness. The cover layers were holed to introduce needles for fluid circulation.

d) Plasma Treatment of the Polydimethylsiloxane Layers

The fabricated PDMS layers were subjected to oxygen plasma treatment (Henniker plasma HPT-100). The samples were washed with isopropanol then in distilled water and dried using compressed air then placed on the metal plate of the Plasma cleaner. After the PDMS surfaces of the bottom and top layers were activated by O_2 plasma treatment. To increase the PDMS-PDMS bonding strength, the layer was compressed between two heavy metal plates and heated at 80 °C for 1 h, which led to an irreversible bonding between PDMS layers[33,34].

The experimental conditions mentioned in the protocols working on PDMS-PDMS bonding (Power: 30 W, Time: 15s, and O_2 Flow Rate: 50 sccm)[33,34] did not lead to an irreversible adhesion between different PDMS layers. So, the power, the O_2 flow and the treatment time were optimized in order to obtain a strong adhesion and an irreversible bonding between PDMS layers (Table I and II).

Table I. The results of PDMS-PDMS bonding with different powers and time, using 50 sccm O_2 flow.

Power (W) / Time (s)	30	60	100
15	FAIL	FAIL	PASS
30	PASS	PASS	PASS
45	PASS	PASS	PASS

Table II. The results of PDMS-PDMS bonding with different O_2 flow, at 60 W, 30 s.

O_2 flow (sccm)	5	10	20	30	50
	PASS	PASS	PASS	PASS	PASS

The results show that for a short treatment time (15 second), the plasma treatment need a higher power (100 W) to obtain an irreversible PDMS-PDMS bonding. By increasing the treatment time, the bounding between PDMS layers start at low power.

The change of O_2 flow did not affect the PDMS-PDMS bonding for a certain time and power. So for Plasma treatment, the parameters are fixed at 30 s, 60 W power and 20 sccm O_2 flow.

e) Device Assembly

After the fabrication and treatment of the 5 PDMS layers, the hydrogel membrane was dried for 5 minutes at 50°C and then inserted in the hole of the mid layer. The 5 layers are compressed together to form the final "filtration unit".

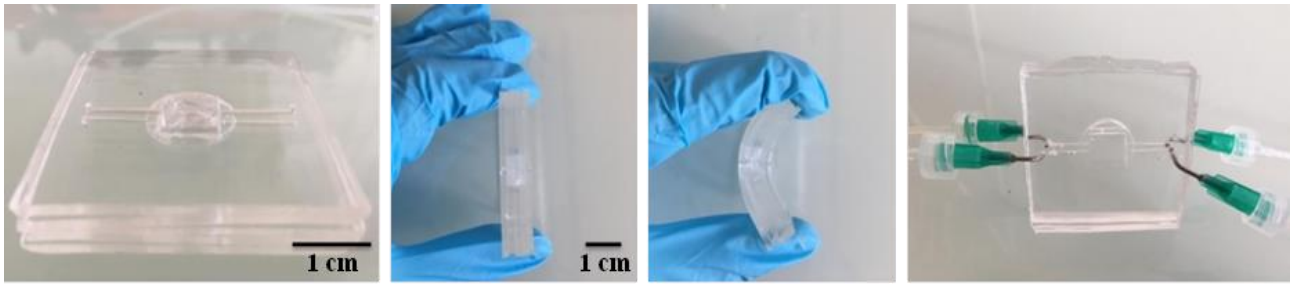

Figure 4. The resulting device after Plasma O_2 treatment showing **(a)** the different layers **(b)** their resulting thickness and **(c)** the flexibility of the PDMS device. **(d)** The device connected to the inputs/output needles.

The bounding between the PDMS layers were irreversible. The resulting device is flexible, has 8 mm thickness and it was connected to an input and an output from each side. The inputs/outputs consist of a stainless steel 18 G needle (18 gauge: 0.84 mm Inner diameter; 1.26 mm Outer diameter) connected via Luer hose connectors ROTILABO® (inner-diameter 2.4 mm) to an Adtech Polymer Engineering™ PTFE Microtubing (BIOBLOCK/01: 1.32 mm ID; 1.93 mm OD), allowing the circulation of fluids inside the device. The device is supplied by two 50 ml syringes with a regulated flow rate.

3. Fabrication of Hydrolyzed Polyacrylamide Hydrogels

This section presents the preparation methods and the characterization of the PAAM hydrogel 2D filtration membranes.

a) Hydrogel Layers Preparation

PAAM gels were synthesized via the free radical polymerization described in Chapter 1 by mixing 1 ml of "30:x AAM:BIS", 10 µl of "APS" and 2 µl of "TEMED" in a pre-gel solution. The AAM:BIS mixture was degassed for 10 minutes prior its usage to remove the O_2 that inhibits the polymerization. Seven gels samples having variable crosslinking densities were prepared. The different crosslinker compositions used are shown in the Table III.

Table III. PAAM gels with different concentrations of BIS in the pregel solution (1 ml "30:x AAM:BIS", 10 µl "APS", 2 µl "TEMED")

Gels	AAM : BIS
A1	30 : 0.002
A2	30 : 0.004
A3	30 : 0.01
A4	30 : 0.02
A5	30 : 0.06
A6	30 : 0.12
A7	30 : 0.18
A8	30 : 0.24

The pre-gel solution was transferred to 10 ml pipette and left to polymerize. After 15 minutes the gel was extracted from the pipette and cut into 2 cm thick samples along its length. The samples were then frozen at 80°C in an O.C.T. compound bath for 30 min. The resulting blocks were sliced into 300 to 500 µm layers using a Cryostat (Leica CM3050).

Each 10 gel layers were hydrolyzed in 1 ml NaOH 1M overnight. After hydrolysis, the gel layers were soaked in 100 ml of Deionized water (DW). Water was changed every 12 hours until reaching full swelling. After full swelling in DW the resulting hydrogels were soaked in

50 ml of PBS 1X. PBS was changed every 24 hours for 3 days. The resulting hydrogel layers are fully swelled in PBS and ready to be used for the filtration tests.

(a) **(b)** **(c)** **(d)**

Figure 5. **(a)** Schematic representation of PAAM hydrogel cylinder sliced into thin layers. PAAM hydrogel cylinder **(b)** soaked in liquid OCT **(c)** freeze at -80°C and **(d)** cut into 500 µm layers.

The swelling degree and the Young's Modulus of the samples were evaluated. For the characterization tests the samples were cut into 3 mm thickness and the same procedure was followed.

For storage, the non-used cut layers were stored in ethanol 70 % at -20 °C in order to avoid the O.C.T. diffusion into the gel.

b) Swelling

The swelling ratio determine the capacity of the hydrogels to absorb and retain aqueous medium. The swelling and deswelling capabilities of gels are defined as the weight of fluid uptake per unit weight of dried polymers and is expressed as:

$$S = D = \frac{W_S - W_d}{W_d} \qquad (1)$$

where W_s and W_d are the weight of the swollen hydrogel at equilibrium and the weight of dry hydrogel, respectively.

The swelling degree was measured for PAAM Hydrogels fully swollen in PBS. The weight of dry hydrogel W_d was measured after drying the sample for 24 hours at 75℃, then for 2 hours at 105℃ over a Teflon paper to assure the complete evaporation of water.

4. Rheology of PAAM Hydrogel

The mechanical properties of the hydrogel layers having increased Bis-acrylamide crosslinker concentrations were evaluated. An electromechanical material testing machine (zwickiLine Z5.0) was used to test samples in compression mode. The analyses are performed on four cylindrical samples from each composition after full swelling in PBS. The samples were inserted between two horizontal plates and compressed with a rate of 2 $mm.min^{-1}$. Measurement time is of 3 min and within this short period of time the humidity of the sample is considered constant. Young's modulus is the stiffness (the ratio between stress and strain) of a material at the elastic stage. It is determined as the slope of the linear part of the stress-strain curve.

5. Filtration Tests

The filtration ability of the prepared hydrogel layers is tested after being encapsulated in the middle layer of the device. The filtration unit was connected to an inlet and an outlet from each side; the inputs/outputs consist of a 90° angle 18 G stainless steel needle (0.84 mm ID; 1.26 mm OD) connected via Luer hose connectors ROTILABO® (ID 2.4 mm) to an Adtech Polymer Engineering™ PTFE Microtubing (BIOBLOCK/01: 1.32 mm ID; 1.93 mm OD) allowing the circulation of fluids inside the device. Both liquid inputs were introduced to a 50 ml syringes, supplied by a syringe pump with a controllable flow rate, and the outputs were collected to be analyzed. All these parameters, in addition to the PDMS treatment and the gel size were optimized separately in order to avoid any leak in the device.

The filtration capacity of the PAAM hydrogels is tested for different compounds. In each experiment one compound is diluted in DPBS solution and tested. The concentrations are presented in Table IV.

The prepared solution is drawn into a 50 ml syringe (input 1), and DPBS solution is also drawn in a syringe (input 2). These syringes are supplied by a New Era Pump Systems (WPI, NE-4000), connected each to a side of the device through PTFE microtubes of 2 mm inner diameter and the outlets are collected into microtubes of 1 ml to be analyzed later (Fig. 6 B).

Table IV. Blood composition before filtration, the waste extracted in the urine, and the component used to test the filtration efficiency of PAAM hydrogels.

	Filtered	Excreted (Urine)	Replacement
Ions			PBS
Chloride Cl^-	630 g (3.5 g/l)	5 g (g/l)	4.96 g/l
Soduim Na^+	540 g (3 g/l)	3g (g/l)	3.61 g/l
Bicarbonate HCO_3^-	300 g (1.67 g/l)	0.3 g (g/l)	
Potassium K^+	28 g (0.16 g/l)	4 g (g/l)	0.17g/l
Phosphate PO_4^{2-}			1.12 g/l
Proteins	10-20 mg/l	-	FITC Dextran
Albumine (69 KDa)	6-12 mg/l	0	70 kDa
Fibrinogen (340 KDa)	0.4-0.8 mg/l	0	150 kDa
Globulins (93 kDa)	3.5-7 mg/l	0	
Other			Methyl Orange/ FITC Dextran
Urea (60 Da)	53 g/day	25 g/day	327 Da 10 kDa 40 kDa
Glucose (180 Da)	180 g/day	0	
Uric Acid (168 Da)	8.5 g/day	0.8 g/day	
Creatinine (113 Da)	1.4 g/day	1.4 g/day	

The microfluidic device encapsulating the membrane is washed before each experiment by flowing a PBS solution for 12 hours before each filtration experiment to eliminate the contamination particles.

Figure 6 A. shows a schematic representation of the device cross section, it presents the input and the output of the device and the exchange area between the fluids through the hydrogel membrane.

The zoomed section of the exchange area shows the size selectivity of the PAAM hydrogel depending from the mesh size of the polymeric matrices after swelling. So controlling the crosslinker concentration, leads to manage the mesh size and then the passage of molecules having certain molecular weight.

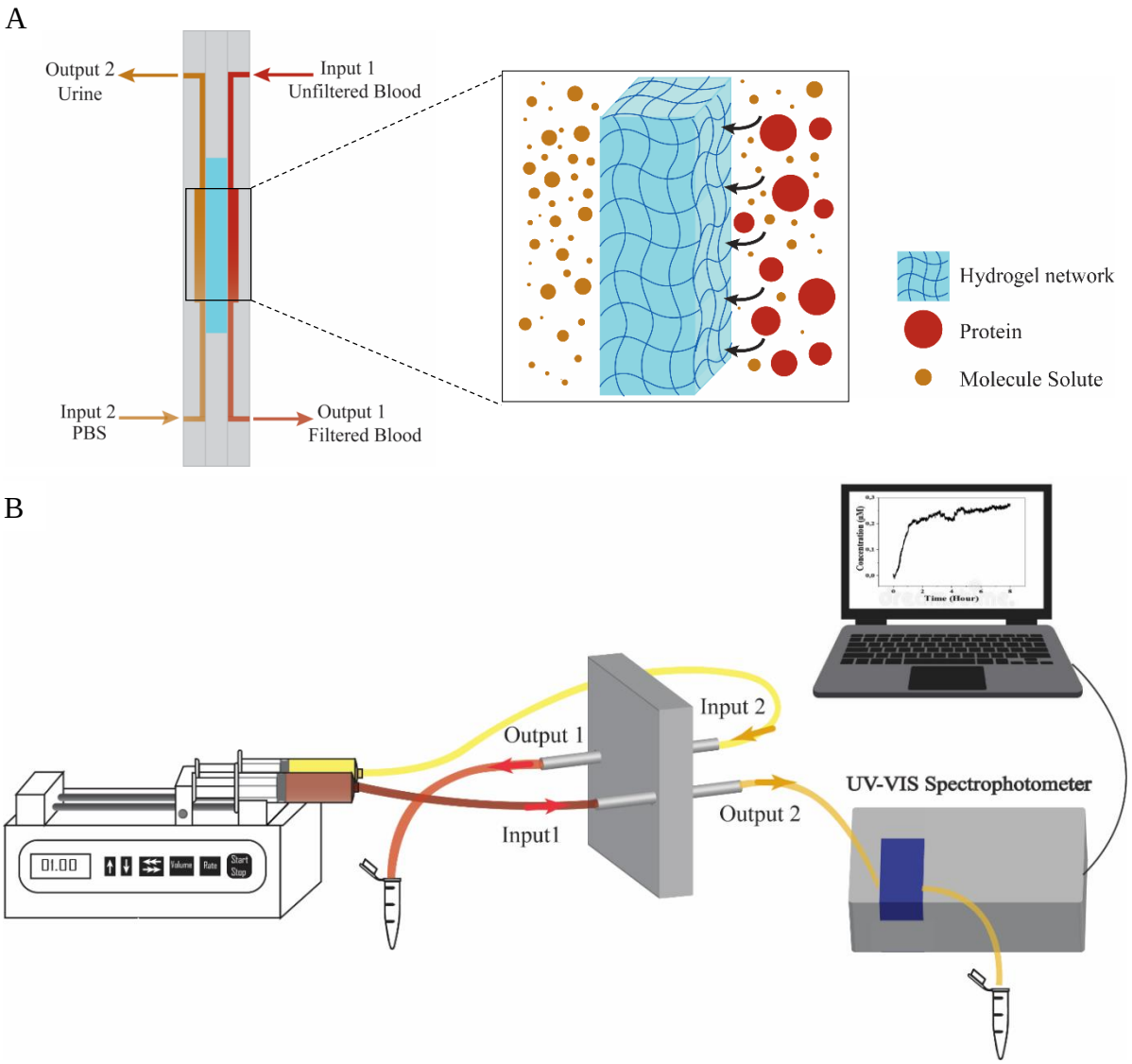

Figure 6. **A.** Representative scheme of the filtration unit and the diffusion process through the membrane. **B.** Schematic representation of the filtration setup: the "filtration unit" encapsulating the hydrogel and connected to two inlets supplied by a syringe pump, and two outlets collected to be analyzed. The "outlet 2" is analyzed by UV-VIS Spectrophotometer to detect the instantaneous passage of molecules through the membrane.

In a first set of experiments, Methyl Orange (MO) (40 mg/L in DPBS) is used to test the filtration device (avoiding leakage, determining the best way for collecting the samples and making sure the results are reproducible) and optimize the experimental parameters like the flow rate to be used and the flow direction. MO can mimic molecules having small molecular weight and it is easily detectable. Then it is used to test the filtration ability of the hydrogel samples with variable mesh size.

The diffusion ability of MO through the PAAM hydrogel is compared to a Spectrum™ Spectra/Por™ 3 Regenerated Cellulose Dialysis Membrane Tubing (3.5 kDa MWCO), since

the regenerated cellulose membranes show a good filtration efficiency for small solute removal but negligible middle molecule removal[35].

The diffusion of ions through the membrane is analyzed by ion chromatography (DIONEX ICS-900 and ICS-1000) while the live diffusion of FITC Dextran and Methyl Orange is evaluated using UV-Visible Spectrophotometer (JASCO, V-570). All experiments were repeated 3 times, in order to increase the accuracy of the results.

a) Ion Diffusion Experiment

The ion selectivity of the PAAM membrane was tested using (Na^+, K^+, Cl^-, PO_4^{3-}) in order to test the hydrogel capacity to stabilize and maintain the normal body fluid composition.

The input solutions are prepared in the following concentration (Table V). For the "input 1" DPBS solution were used because it has an ion composition close to that filtered by the kidney. Chloride and sodium concentration were doubled in the "input 2", in order to evaluate the diffusion of both positively and negatively charged ions.

Table V. Ion composition before filtration of the two inputs

	Input 1	Input 2
Ions	PBS	PBS
Chloride Cl^-	**4.96 g/l**	**8.43 g/l**
Soduim Na^+	**3.61 g/l**	**5.77 g/l**
Potassium K^+	0.17g/l	0.17g/l
Phosphate PO_4^{2-}	1.12 g/l	1.12 g/l

The ion diffusion through the PAAM membrane is tested in a static and cross-flow condition with three different flow rates (1, 2 and 5 ml/h). In static conditions the feed is applied perpendicularly to the surface of the membrane (i.e., feed stream flows through the pore of the membrane). This flow method enables rapid separation, because the feed is forced against the membrane surface. In this case, the fluid stays static and the fluid volume remain constant. In the tangential flow filtration, the feed stream is applied tangentially, crossing the surface of the porous membrane, which minimizes membrane fouling[36].

b) Molecular weight cut off

Bovine serum albumin 66 kDa and fluorescein isothiocyanate–dextran (FITC-Dextran, MW: 10, 40, 70, 150 kDa) were used to test the molecular weight cut-off of PAAM membrane as they mimic the blood proteins.

The prepared solutions have a concentration of 40 mg/L in a PBS. UV-visible spectroscopy is used in live-time to detect the instant diffusion of molecules through the hydrogel. In live-time, the fluid coming out of the chip circulates inside the spectrophotometer in order to measure the absorbance every 5 seconds during fluid circulation.

IV. Results and Discussion

Porosity and the mesh size of the hydrogels matrix are the most important factor influencing the filtration capacity of the hydrogel. An increase the crosslinker density reduces the polymer mesh size and consequently the size of the molecules that can pass across the hydrogel membrane.

The effect of crosslinker density on the hydrogel properties is studied for 2D PAAM membranes. Afterwards, the filtration ability of these hydrogels is tested in order to evaluate if they closely mimic the kidney filtration performance.

1. PAAM Hydrogel Properties

The effect of BIS density on the hydrogel properties is evaluated by polymerizing different solutions of pre-gels (1 ml "30:x AAM:BIS", 10 µl "APS", 2 µl "TEMED"). The swelling degree, the Young's Modulus and the mesh size are measured for different samples having different BIS concentration (Table III).

The A1 sample has a very loose structure, which prevents it from being characterized. An exponential decrease of swelling ratio from 73 to 27 with increasing crosslinker concentration from 0.004 to 0.24 % is determined in PBS (Fig. 7a). Thus, while increasing the concentration of bis-acrylamide crosslinking, the polymer network becomes more compact and therefore less able to absorb water[37–39].

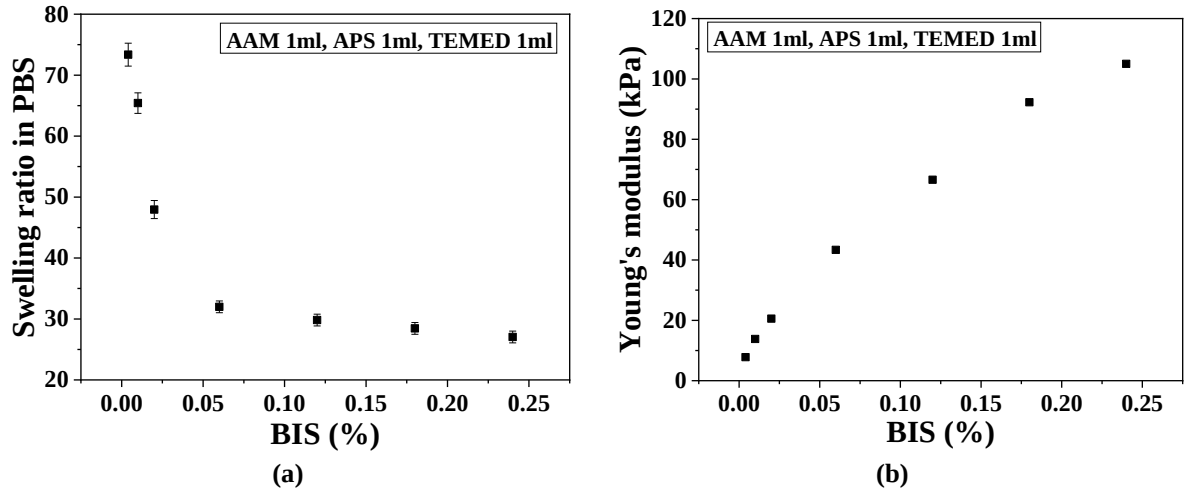

Figure 7. (a) Swelling ratio, and **(b)** Young's modulus as a function of BIS concentration after full swelling.

This is due to the fact that the movement of the network chains is limited by the crosslinking nodes. When the network swells, the chains are extended between the nodes. More the nodes are close to each other less the chains can extend and less the gel can swell[40]. This explains the influence of crosslinking density of polymer chains on the swelling capacity of the gel. Comparing to non-hydrolyzed PAAM, the swelling ratio is 10 times more important in hydrolyzed PAAM hydrogel[41].

The mechanical properties of the gels are evaluated by measuring the Young modulus. Figure 7 B. shows that by controlling the crosslinker density, the mechanical properties can be tuned[42].

For low crosslinker concentration (A2: 0.004 %), the Young modulus is about 2.74 kPa and it increase to 110 kPa for higher crosslinker concentrations (A8: 0.25 %) (Fig. 7b). A higher degree of crosslinker reduce the average molecular weight between crosslinked points and thus, induce a rise of the gel stiffness. Hydrolyzed PAAM hydrogels have a Young modulus 3 times smaller than non-hydrolyzed ones[43].

Only few studies have worked this composition on hydrogels and on the determination of viscoelastic properties of PAAM hydrogels having different crosslinker density. Abdallah, M. ***et al***. have already analyzed the viscoelasity of PAAM hydrogels having the same composition as in our case, by applying an oscillatory force on the surface of the samples. A frequency of 1 Hz, strain amplitude of 1 % and a fixed force of 0.5 N were applied. The rheology measurements were recorded at a temperature of 37˚C.

The elastic and viscous properties are represented by the storage modulus and the loss modulus respectively. The storage modulus (G′), describe elastic deformation and it is defined by the membrane capacity to store a recoverable energy, while the loss modulus (G″) attributes to the energy dissipation by viscous flow. It was noted that for all the samples the storage modulus was greater than the loss modulus, i.e., G′ > G″ representing the elastic behavior predominates over the viscous nature.

The storage modulus values show an increase with the concentration of crosslinker agent. This indicates that a densely connected network requires more energy to be deformed[37].

We can therefore conclude that when the crosslinker density increase, the gel swelling rate decreases, i.e., shorter macromolecular chains between crosslinked point, the Young's modulus and storage modulus increases, resulting in a lower deformation ability.

Hydrolyzed PAAM hydrogel samples showed a high fluid content, which is 10 times more than the non-hydrolyzed PAAM, 2 times hydroxypropyl cellulose synthesized with methacrylate anhydride (HPC-MA)[44] and 50 times Poly (N-isopropyl acrylamide)[45].

The PAAM characterized samples covers a wide range of Young's modulus that will be used as a filtration membrane. The filtration efficiency of different samples will be compared and their efficiency on controlling the toxins diffusion and proteins cut-off will be tested, in order to be employed in the future to build the bioartificial kidney that is composed of several "filtration units" each having different filtration role.

2. Filtration Tests

In a first set of experiments, the filtration ability of the prepared PAAM hydrogels is tested by measuring the diffusion of Methyl Orange through the hydrogel membrane under different conditions. First, the effect of the mesh size of the hydrogel membrane is tested by measuring the instantaneous diffusion of Methyl Orange for different samples having different BIS concentration. Then, the effect of the inlet flow rate is evaluated using 3 different speeds. Finally, a comparison between the diffusion of MO through the PAAM hydrogel membrane and regenerated cellulose dialysis membrane is measured.

In a second set of experiments, the ion diffusion through a selected PAAM membrane is tested using (Na^+, K^+, Cl^-, PO_4^{3-}) in static and cross-flow filtration modes using 0.5 ml/h for the flow rate.

In the third set of experiments, the molecular weight cutoff of PAAM membrane is evaluated using bovine serum albumin 66 kDa and fluorescein isothiocyanate–dextran (FITC-Dextran, MW: 10, 40, 70, 150 kDa) as they mimic the blood proteins.

a) Mesh Size

The porosity or the mesh size has an effect not only on the molecular weight cut off, but also on the toxins concentration that can diffuse through the membrane. The effect of the mesh size

of the prepared hydrogel scaffold samples is tested by measuring the instantaneous diffusion of Methyl Orange for 6 different samples having different BIS concentration.

Both A1 and A2 samples have a weak structure, so it was impossible to place and compress them between the PDMS layers in order to test their filtration capability.

Figure 8 shows that the diffusion of MO is the highest for A3 hydrogels, it stabilizes around 0.8 µm in the output. After 4 hours of filtration, the concentration of MO in output 2 changed suddenly because of cracking in the membrane. A4 hydrogel also shows a high diffusion, it stabilizes around 0.7 µm in the output, on the other hand, it stabilizes at 0.58 and 0.4 µm for A5 and A6 respectively.

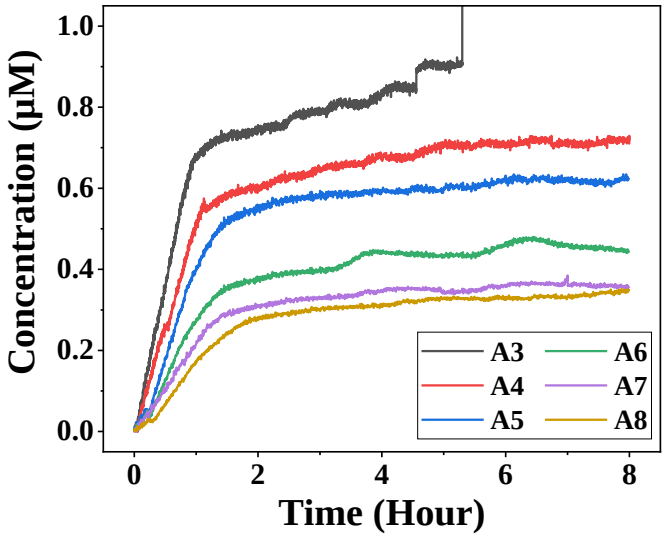

Figure 8. Methyl Orange concentration as a function of time measured from the outlet 2, diffused through A3, A4, A5, A6, A7 and A8 hydrogels for 1 ml/h flow rate

A7 and A8 hydrogels have both a close stability value around 0.3 µM of MO. So more the concentration of the crosslinker is important, more the mesh size is lower and the molecules diffusion through the gel is harder and slower.

As mentioned in the review "haemodialysis membranes" of *C. Ronco and W. Clark*, the mass transfer which expresses the diffusive permeability, is a function of fluids flow rate, and influenced by the pores density and size[46].

In the case of 2D hydrogels, the mesh between the scaffold nodes represent the porosity of the membrane. With a constant flow rate, the mass transfer change depending on the mesh size of the PAAM membrane. Increasing the crosslinker density leads to the formation of small mesh and slow down the diffusion through the membrane.

A5 samples were selected to be used in the following tests because they show good diffusion capacity and have a good mechanical resistance against fluid flow (Young's Modulus 40 kPa).

b) Effect of Flow Rate

The speed of the liquid flow along the two sides of the hydrogel membrane has shown in previous studies an effect on the toxins diffusion through the membrane from the high concentrated to the low concentrated side. The effect of the inlet flow rate is evaluated using 3 different speeds.

Figure 9 shows an increase in the concentration of Methyl orange in the outlet 2 and a concentration stability after around 2 hours.

The concentration of MO increase as the flow rate decreases from 5 to 1 ml/h. For a flow rate of 5 ml/h, the diffusion curve increases with a slope of 0.22 and stabilized around 0.25 µM. For 1 and 2 ml/h flow rate, the curves increase with a slope of 0.35 and 0.45 respectively, and stabilized around 0.45 and 0.6 µM.

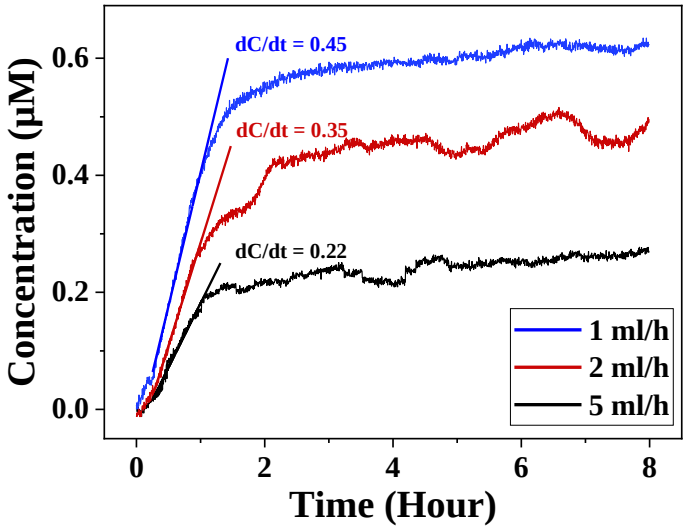

Figure 9. Methyl Orange concentration as a function of time measured from the outlet 2, diffused through A5 hydrogel for different flow rate.

More the flow is low more the molecules have time to diffuse through the membrane[46,47], so by decreasing the flow rate, the diffusion time of the molecules across the matrix increases and insures a more important equilibrium between the two sides of the hydrogel membrane. The flow rate can be controlled depending on the concentration of toxins that should be eliminated, while taking into account the high quantity of blood that should be filtrated.

c) Polyacrylamide versus Regenerated Cellulose Dialysis Membrane

Different types of membranes have been tested to be used for filtration, but most of them are tested in static condition[48,49] (without a fluid circulation and with a constant fluid volume). While in the case of the device designed in this chapter, the flow is tangential (cross flow filtration).

In order to test the filtration efficiency of PAAM hydrogels, regenerated cellulose dialysis membrane (MWCO 3.5 kDa) having a high filtration efficiency for small solute removal[8,35] was compared to A5 hydrogel by measuring the diffusion of MO through the membranes. Both membranes have been encapsulated in the device and tested in the same cross-flow of 1 ml/h.

The results show that the concentration of MO diffused through the dialysis membrane stabilize between 0.8 and 0.9 µM after 30 minutes, while for A5 hydrogels it stabilizes between 0.5 and 0.6 µM after 1.5 hours.

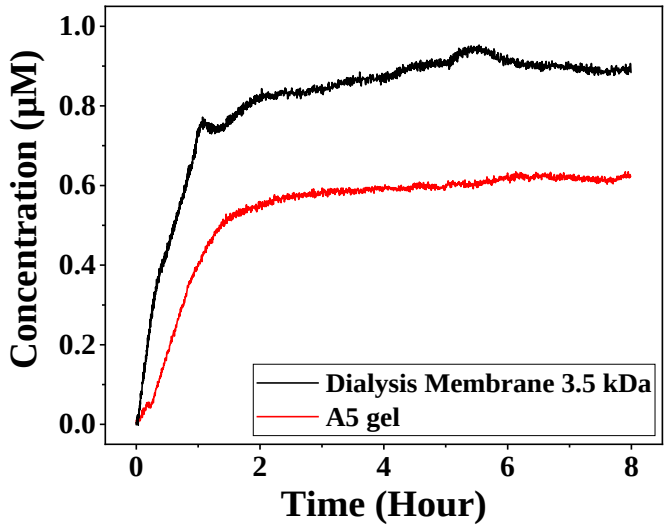

Figure 10. Methyl Orange concentration as a function of time measured from the outlet 2, diffused through the dialysis membrane (MWCO 3.5 kDa) and A5 hydrogel for a flow rate of 1 ml/h

The diffusion of MO is faster and more important through the dialysis membrane in comparison with the A5 hydrogel, this is due to the well-defined porosity and the thinness of the membrane (~ 30 µm). While the hydrogel thickness slow down the diffusion of the MO.

The filtration through the hydrogel represents approximately 70% of the filtration rate through the regenerated cellulose (RC) dialysis membrane, which shows a good filtration efficiency for small solute removal[8,35]. Decreasing the Crosslinker concentration will lead to increase the mesh size and therefore the diffusion through the membrane (85% for A4 compared to RC membrane), but it is limited by the mechanical properties of the hydrogel.

Although the regenerated cellulose dialysis membranes have a high filtration capacity for small solute, but the PAAM hydrogels still have the advantage over the RC dialysis membrane in terms of his potential future usage as an extracellular matrix[21].

d) Ion Diffusion Experiment

The ion diffusion through the PAAM membrane is tested using (Na^+, K^+, Cl^-, PO_4^{3-}) in a static and cross-flow filtration with 0.5 ml/h flow rate. The variation of ion concentration in both outputs is followed for 24 hours.

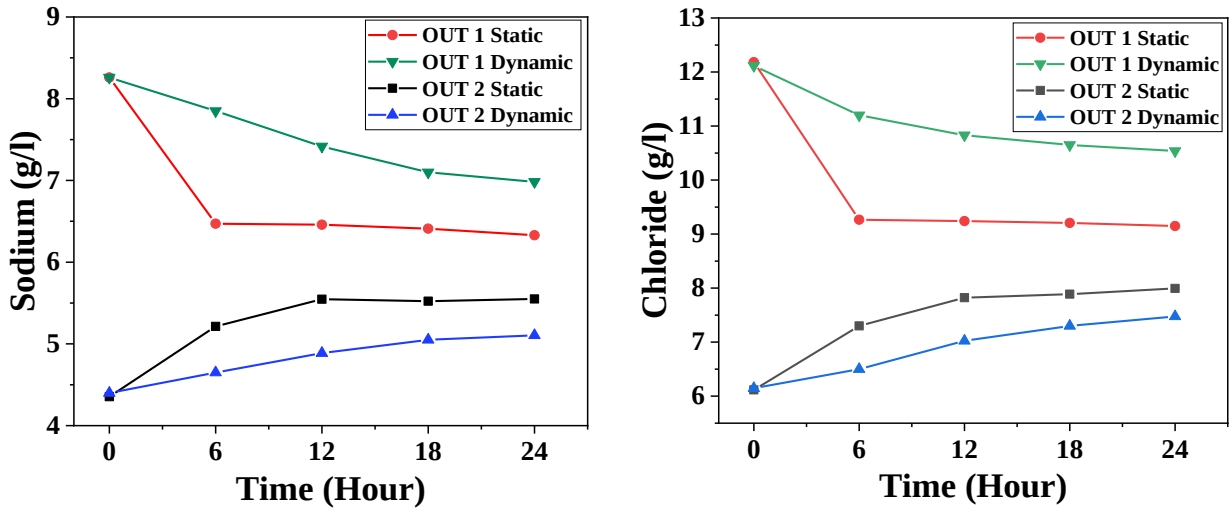

(a) (b)

Figure 11. Ion concentration of **(a)** Sodium Na^+ and **(b)** Chloride Cl^- as a function of time measured from the outlets 1 and 2, diffused through A5 hydrogels in a dynamic flow of 0.5 ml/h and static condition.

The results show that both anions and cations can diffuse through the neutral PAAM membrane to ensure the equilibrium between the two sides of the gel. It can be noticed that the decrease of the ion concentration in the "outlet 1" is more important than the increase in the "outlet 2", this is because the membrane is soaked in PBS of the same composition as the "input 2". So the equilibrium starts between the "input 1" and the hydrogel, then between the hydrogel and the "input 2" until having a balance between the gel and the 2 sides.

The gap between the sum of ions the outputs at 24 hours is less than the sum of the inputs, caused by the ions absorbed by the hydrogel.

In the case of dynamic diffusion, the ions diffuse through the hydrogel and circulate out of the device at a flow of 0.5 ml/h, so the detected values are the number of ions diffused at t=6, 12, 18 and 24 hours. While in the static state, the detected values are the accumulation of ions diffusion from t_0=0 to t=6, 12, 18 and 24 hours, which explain the gap between static and dynamic measurements.

For a specific ion selection, PAAM hydrogel can be doped positively or negatively after preparation, in order to block the ions having an opposite charge.

e) Molecular Weight Cut Off

Bovine serum albumin 66 kDa and fluorescein isothiocyanate–dextran (FITC-Dextran, MW: 10, 40, 70, 150 kDa) are used to test the molecular weight cutoff of PAAM membrane as they mimic the blood proteins. Figure 12 shows a comparison between the diffusion of MO and FITC-Dextran 10 kDa.

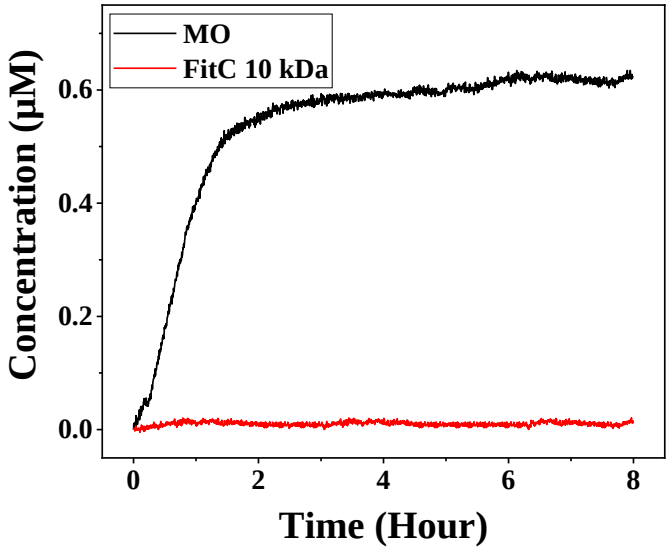

Figure 12. Methyl Orange and FITC-Dextran 10 kDa concentration as a function of time measured from the outlet 2, diffused through A5 hydrogel for a flow rate of 1 ml/h

The results show a restriction of the passage of FITC-Dextran 10 kDa through A5 membrane. The diffusion of FitC was also tested on A4 hydrogel obtaining the same results as in A5.

2D hydrolyzed PAAM hydrogels have presented a good diffusion for small molecules compared to regenerated cellulose membrane. With a constant flow rate, the mass transfer depends on the mesh size of the PAAM membrane. Increasing the crosslinker density leads to the formation of small mesh and slow down the diffusion through the membrane. The fluid flow rate also affects diffusion of molecules; more the flow is low, more the molecules have time to diffuse through the membrane[46,47], and that ensures a more important equilibrium between the two sides of the hydrogel. Ions are also diffused through the hydrogel unlike proteins that have a molecular size bigger than hydrogel mesh size.

A5 hydrogel has the best criteria to be used as a filtration membrane, due to its stiffness and its mesh size appropriate for a good diffusion of small molecules. So the first “filtration unit” of the bioartificial kidney will encapsulate A5 hydrogels that filters small molecules, which facilitates the next step of medium molecular weight filtration (between 1 and 69 kDa).

V. Conclusion

The PAAM hydrogel properties can be controlled by changing the gel composition or the fabrication method of the hydrogel. The swelling and the mesh size decrease by increasing the crosslinker density, and this is due to the small distance between the network nodes.

As the network density increases, the average molecular weight between crosslinked points decreases and leads to a rise of the gel stiffness. Hydrogels have potentially not just as filtration membrane but also they can be used as an extracellular membrane for kidney regeneration. Hence the importance to study the filtration ability of PAAM hydrogel as a new candidate to be used as a basement membrane for kidney replacement.

2D PAAM hydrogels have a good efficiency in small molecules clearance (< 500 Da) compared to regenerated cellulose membrane, but it blocks the passage of medium and large molecules. With a constant flow rate, the mass transfer change depends on the mesh size of the PAAM membrane. Increasing the crosslinker density leads to the formation of small mesh and slow down the diffusion through the membrane, which is also depending on the fluid flow rate. More the flow is low, more the molecules have time to diffuse through the membrane, so by decreasing the flow rate, the diffusion time of the molecules across the matrix increases and insures a more important equilibrium between the two sides of the gel. Ions are also diffused through the hydrogel unlike proteins that have a molecular size bigger than hydrogels mesh size. So the diffusion of small molecules can be controlled by changing the hydrogel composition or the experimental parameters. Increasing the flow rate as well as the crosslinker density, slow down the diffusion of molecules through the membrane.

A5 hydrogel has the best criteria to be used as a filtration membrane, due to its stiffness and its mesh size appropriate for a good diffusion of small molecules. So the first “filtration unit” of the bioartificial kidney will encapsulate A5 hydrogels that filters small molecules, which facilitates the next step of medium molecular weight filtration (between 1 and 69 kDa).

The fabrication of a second “filtration unit” encapsulating a nanoporous hydrogel having a pore size around 5 nm is required to eliminate molecules having a molecular weight between 1 and 69 kDa, and therefore to build the ultimate bioartificial kidney that will be the assembly of several “filtration units” having each different filtration role.

VI. References

1. Gilbert, S. J., Weiner, D. E., Bomback, A. S., Perazella, M. A. & Tonelli, M. *National Kidney Foundation's primer on kidney diseases*. (2018).
2. N, R. *et al.* Improvements in Glomerular Filtration Rate (GFR) in Chronic Kidney Disease (CKD) Patients Using a Commercial Patented and Proprietary ProbioticPrebiotic Formulation* -3rd Biennial Survey. *International Journal of Nephrology and Kidney Failure* **4**, (2018).
3. Ota, T., Nakayama, M., Kanno, Y., Suzuki, T. & Miki, N. In vitro and in vivo tests of nanoporous membrane coated with biocompatible fluorine-doped diamond-like carbon for hemofiltration treatment. in 412–414 (IEEE, 2018). doi:10.1109/MEMSYS.2018.8346575.
4. Ising, C. & Brinkkoetter, P. T. Prohibitin Signaling at the Kidney Filtration Barrier. in *Mitochondrial Dynamics in Cardiovascular Medicine* (ed. Santulli, G.) vol. 982 563–575 (Springer International Publishing, 2017).
5. Dong, R., Liu, Y., Mou, L., Deng, J. & Jiang, X. Microfluidics-Based Biomaterials and Biodevices. *Advanced Materials* **31**, 1805033 (2019).
6. Pastan, S. & Bailey, J. Dialysis Therapy. *New England Journal of Medicine* **338**, 1428–1437 (1998).
7. Breyer, M. D. & Susztak, K. Developing Treatments for Chronic Kidney Disease in the 21st Century. *Seminars in Nephrology* **36**, 436–447 (2016).
8. Luo, J., Fan, J. & Wang, S. Recent Progress of Microfluidic Devices for Hemodialysis. *Small* **16**, 1904076 (2020).
9. Mollahosseini, A., Abdelrasoul, A. & Shoker, A. Challenges and advances in hemodialysis membranes. in *Advances in Membrane Technologies* (IntechOpen, 2020).
10. Wilmer, M. J. *et al.* Kidney-on-a-Chip Technology for Drug-Induced Nephrotoxicity Screening. *Trends in Biotechnology* **34**, 156–170 (2016).
11. Jang, K.-J. *et al.* Human kidney proximal tubule-on-a-chip for drug transport and nephrotoxicity assessment. *Integrative Biology* **5**, 1119–1129 (2013).
12. Yi, Z., Liu, C.-J., Zhu, L.-P. & Xu, Y.-Y. Ion Exchange and Antibiofouling Properties of Poly(ether sulfone) Membranes Prepared by the Surface Immobilization of Brønsted Acidic Ionic Liquids via Double-Click Reactions. *Langmuir* **31**, 7970–7979 (2015).
13. Ota, T., To, N., Kanno, Y. & Miki, N. Evaluation of biofouling in stainless microfluidic channels for implantable multilayered dialysis device. *Japanese Journal of Applied Physics* **56**, (2017).
14. Ndegwa, S. *CADTH Issues in Emerging Health Technologies*. (Canadian Agency for Drugs and Technologies in Health, 2016).
15. Wang, X. Bioartificial Organ Manufacturing Technologies. *Cell Transplantation* **28**, 5–17 (2019).
16. De Bartolo, L. Membrane Bioartificial Organs. in *Encyclopedia of Membranes* (eds. Drioli, E. & Giorno, L.) 1–2 (Springer Berlin Heidelberg, 2015). doi:10.1007/978-3-642-40872-4_355-3.
17. Corridon, P. R., Ko, I. K., Yoo, J. J. & Atala, A. Bioartificial Kidneys. *Current Stem Cell Reports* **3**, 68–76 (2017).
18. Qu, Y. *et al.* A nephron model for study of drug-induced acute kidney injury and assessment of drug-induced nephrotoxicity. *Biomaterials* **155**, 41–53 (2018).

19. Ota, T., To, N., Kanno, Y. & Miki, N. Evaluation of biofouling in stainless microfluidic channels for implantable multilayered dialysis device. *Japanese Journal of Applied Physics* **56**, 06GN10 (2017).

20. Haque, Md. A., Kurokawa, T. & Gong, J. P. Super tough double network hydrogels and their application as biomaterials. *Polymer* **53**, 1805–1822 (2012).

21. Jansen, K., Schuurmans, C. C. L., Jansen, J., Masereeuw, R. & Vermonden, T. Hydrogel-Based Cell Therapies for Kidney Regeneration: Current Trends in Biofabrication and In Vivo Repair. *Current Pharmaceutical Design* **23**, (2017).

22. Caplin, J. D., Granados, N. G., James, M. R., Montazami, R. & Hashemi, N. Microfluidic Organ-on-a-Chip Technology for Advancement of Drug Development and Toxicology. *Advanced Healthcare Materials* **4**, 1426–1450 (2015).

23. Smith, A. F., Zhao, B., You, M. & Jiménez, J. M. Microfluidic DNA-based potassium nanosensors for improved dialysis treatment. *BioMedical Engineering OnLine* **18**, (2019).

24. Paoli, R. & Samitier, J. Mimicking the Kidney: A Key Role in Organ-on-Chip Development. *Micromachines* **7**, 126 (2016).

25. Vera, D. *et al.* Engineering Tissue Barrier Models on Hydrogel Microfluidic Platforms. *ACS Applied Materials & Interfaces* **13**, 13920–13933 (2021).

26. Lee, S.-B., Lee, H.-Y., Jung, M.-S., Park, Y.-B. & Joo, Y.-C. Effect of the composition of Sn-Pb alloys on the microstructure of filaments and the electrochemical migration characteristics. *Metals and Materials International* **17**, 617–621 (2011).

27. Kang-Yi Lien *et al.* Microfluidic Systems Integrated With a Sample Pretreatment Device for Fast Nucleic-Acid Amplification. *Journal of Microelectromechanical Systems* **17**, 288–301 (2008).

28. Fan, J.-B. *et al.* Bioinspired Microfluidic Device by Integrating a Porous Membrane and Heterostructured Nanoporous Particles for Biomolecule Cleaning. *ACS Nano* **13**, 8374–8381 (2019).

29. Rhoades, T., Kothapalli, C. R. & Fodor, P. S. Mixing Optimization in Grooved Serpentine Microchannels. *Micromachines* **11**, 61 (2020).

30. Yin, L., Yang, S.-M. & Zhang, W. A Three-Layer Microfluidic Kidney Chip for Drug Nephrotoxicity Test. *IJBBB* **9**, 237–247 (2019).

31. Perozziello, G. *et al.* A microfluidic dialysis device for complex biological mixture SERS analysis. *Microelectronic Engineering* **144**, 37–41 (2015).

32. Yin, L. *et al.* Efficient Drug Screening and Nephrotoxicity Assessment on Co-culture Microfluidic Kidney Chip. *Scientific Reports* **10**, (2020).

33. Ha, Y., Yoo, H.-J., Shin, S. & Jun, S. Hemispherical Microelectrode Array for Ex Vivo Retinal Neural Recording. *Micromachines* **11**, 538 (2020).

34. Wen, J. *PDMS-PDMS Bonding Protocol—Anatech*. 1–4 (2015).

35. *Advances in Membrane Technologies*. (IntechOpen, 2020). doi:10.5772/intechopen.82587.

36. A., S. & Duc, N. Organic–Inorganic Mesoporous Silica Nanotube Hybrid Anodic Alumina Membranes for Ultrafine Filtration of Noble Metal Nanoparticles. in *Noble Metals* (ed. Su, Y.-H.) (InTech, 2012). doi:10.5772/33768.

37. Abdallah, M. *et al.* Influence of Hydrolyzed Polyacrylamide Hydrogel Stiffness on Podocyte Morphology, Phenotype, and Mechanical Properties. *ACS Applied Materials & Interfaces* **11**, 32623–32632 (2019).

38. Avais, Mohd. & Chattopadhyay, S. Waterborne pH responsive hydrogels: Synthesis, characterization and selective pH responsive behavior around physiological pH. *Polymer* **180**, 121701 (2019).

39. Suekama, T. C., Hu, J., Kurokawa, T., Gong, J. P. & Gehrke, S. H. Tuning Mechanical Properties of Chondroitin Sulfate-Based Double-Network Hydrogels. *Macromolecular Symposia* **329**, 9–18 (2013).

40. Rumyantsev, A. M., Pan, A., Ghosh Roy, S., De, P. & Kramarenko, E. Yu. Polyelectrolyte Gel Swelling and Conductivity vs Counterion Type, Cross-Linking Density, and Solvent Polarity. *Macromolecules* **49**, 6630–6643 (2016).

41. Sokker, H. H., El-Sawy, N. M., Hassan, M. A. & El-Anadouli, B. E. Adsorption of crude oil from aqueous solution by hydrogel of chitosan based polyacrylamide prepared by radiation induced graft polymerization. *Journal of Hazardous Materials* **190**, 359–365 (2011).

42. Zaragoza, J., Fukuoka, S., Kraus, M., Thomin, J. & Asuri, P. Exploring the Role of Nanoparticles in Enhancing Mechanical Properties of Hydrogel Nanocomposites. *Nanomaterials* **8**, 882 (2018).

43. Schramm-Baxter, J., Katrencik, J. & Mitragotri, S. Jet injection into polyacrylamide gels: investigation of jet injection mechanics. *Journal of Biomechanics* **37**, 1181–1188 (2004).

44. Hoo, S. P. Development of a novel 3D hydrogel for tissue engineering and microfluidics applications. (2013).

45. Harada, I., Yanagisawa, S., Iwasaki, K., Cho, C.-S. & Akaike, T. Local Mechanical Stimulation of Mardin-Darby Canine Kidney Cell Sheets on Temperature-Responsive Hydrogel. *International Journal of Molecular Sciences* **13**, 1095–1108 (2012).

46. Ronco, C. & Clark, W. R. Haemodialysis membranes. *Nature Reviews Nephrology* **14**, 394–410 (2018).

47. Xiao, H.-F. *et al.* Selective removal of halides from spent zinc sulfate electrolyte by diffusion dialysis. *Journal of Membrane Science* **537**, 111–118 (2017).

48. Bruggeman, L. A., Doan, R. P., Loftis, J., Darr, A. & Calabro, A. A Cell Culture System for the Structure and Hydrogel Properties of Basement Membranes: Application to Capillary Walls. *Cellular and Molecular Bioengineering* **5**, 194–204 (2012).

49. Nguyen, H.-T., Massino, M., Keita, C. & Salmon, J.-B. Microfluidic dialysis using photo-patterned hydrogel membranes in PDMS chips. *Lab on a Chip* **20**, 2383–2393 (2020).

50. Dang, H. T., Narbaitz, R. M., Matsuura, T. & Khulbe, K. C. A Comparison of Commercial and Experimental Ultrafiltration Membranes via Surface Property Analysis and Fouling Tests. *Water Quality Research Journal* **41**, 84–93 (2006).

Chapter III: Engineering of 3D Hydrogel Scaffold for Spheroid Formation

I. Introduction

Extracellular matrix (ECM) is a complex and organized network composed of an array of macromolecules that provides mechanical and chemical signals that organize cellular, tissue and its functions[1,2]. To mimic the ECM in which cells reside, a wide variety of biocompatible polymers have been used in the manufacture of scaffolds[3]. Among them, Hydrogels have been progressed as biomaterials that closely simulate natural living tissue due to their unique properties such as high water content, softness, flexibility and biocompatibility[3,4]. Firstly, hydrogels could be an ECM-mimetic providing additional mechanical and biochemical cues, possibly leading to enhanced cell differentiation and functionality. The second advantage of hydrogels in bioartificial kidney device is their potential for implantation. Collagen, gelatin, chitosan, fibrin and alginate are natural hydrogels and they represent the most essential components of the extracellular matrix *in vivo*. The reproducibility of the structure and the mechanical properties of this category remains a problem poorly understood. These drawbacks can be limited and controlled by using hydrogels based on synthetic polymers. The synthetic hydrogels including polyethylene glycol (PEG), polyacrylamide (PAAM) and polyvinyl Alcohol (PVA) are more reproducible and can be controlled and modified for tuning the desired mechanical properties[5].

PAAM hydrogels are scaffolding materials used for cell growth. Hydrolyzed Polyacrylamide is a hydrogel material with a high absorption capacity of liquids, and have many advantages over other type of membranes, since it can combine the filtration function of a membrane and the properties of scaffolding materials suitable for cell culture. PAAM hydrogel is a biocompatible, non-biodegradable material that offers a suitable substrate for cell culture[6]. In addition, structural and mechanical properties of PAAM hydrogels can be easily controlled by controlling the pre-gel composition and the polymerization conditions, which affects the stiffness and the porosity of the scaffold[6].

The most important thing about hydrogels, and especially the PAAM, is the ability to form a 3D structure that simulates *in vivo* microenvironments to support spatial activities of the cells, instead of 2D planar structure[3]. 3D porous hydrogels are usually formed using particle suspension[7] and emulsion templating technique[3]. In this work, the 3D structure of PAAM hydrogels is formed using emulsion technique by encapsulating oil droplets inside the pregel mixture that is composed of monomer, crosslinker, initiator and catalyst. After polymerization,

the droplets are subsequently leached out of the hydrogel in presence of methanol, to create a macroporous structure.

Podocytes are highly specialized cells of the kidney glomerulus that represent the essential component for the formation and maintenance of the glomerular filtration barrier, and play an active role in preventing the entry of plasma proteins into the urine[8–10]. Podocytes cells are used in Renal Assist Devices, due to their high importance in the kidney filtration. But the use of cells in the filtration devices still limited by the cell detachment caused by the flow rate of blood and filtrate[11].

This chapter aims to build a 3D scaffold with a specific tissue architecture and mechanical signals, adapted to podocytes spheroid formation, in order to enhance cell–cell / cell–matrix interactions and bio-mimic *in vivo* microenvironment. The developed 3D hydrolyzed PAAM hydrogel scaffold cultured with podocytes spheroids is intended used in future as a membrane in a "filtration unit" of the bioartificial kidney.

In this chapter, 3D macroporous PAAM hydrogels are fabricated and used as a scaffold for the formation of podocytes spheroids, that will be encapsulated inside the hydrogel pores having an average pore size between 100 and 250 µm[12] avoiding the cell detachment in the filtration application.

The mechanical and structural properties of different 3D PAAM prepared under different conditions are studied. In addition, the effect of the hydrogel properties on the podocytes spheroids formation.

II. Materials and Methods

1. Chemicals

Acrylamide ≥ 99% (AAM, Sigma Aldrich, A8887), is used as monomer, N,N-methylenebisacrylamide ≥ 99.5% (BIS, Sigma Aldrich, M7279) as a cross-linker, N,N,tertramethylethylenediamine 99% (TEMED, Sigma Aldrich, T9281) as the accelerator and

ammonium persulfate ≥98% (APS, Sigma Aldrich, 248614) as the initiator for the free radical polymerization reaction. Triton™ X-100 (Sigma Aldrich, X100) having an Hydrophilic-lipophilic balance (HLB) of 13.5, and Sesame oil (Sigma Aldrich, S3547) are used respectively as surfactant and oil for O/W emulsion formation.

Sodium Hydroxide 98-100.5% (NaOH, Sigma Aldrich, S8045) is used for gel hydrolysis. Sodium chloride ≥ 99% (NaCl, Sigma Aldrich, S9625), Potassium chloride ≥ 99% (KCl, Sigma Aldrich, P9333), Sodium phosphate dibasic ≥ 99% (Na_2HPO_4, Sigma Aldrich, 71640) and Potassium phosphate monobasic (KH_2PO_4, Sigma Aldrich, P5655) is used to prepare PBS. Deionized water (DW, Milli-Q, conductivity >18 MΩ) is used for all the dilutions, the polymerization reactions, as well as for the swelling. AAM:BIS (30%:0.06% w/w) and APS (25% w/w) are used in aqueous solution. Ammonium persulfate is freshly prepared before each preparation.

Optimal Cutting temperature (O.C.T., ScigenTM, 4586) is used to embed samples prior to frozen sectioning on a cryostat. Methanol BioReagent, ≥99.93% (Sigma Aldrich, 494437) is used to remove oil from the porous structure after cutting.

RPMI−1640 Medium (Sigma-Aldrich, R8758) is used as culture media, supplemented with Insulin-Transferrin-Selenium liquid media supplement (ITS, Sigma-Aldrich, I3146), Fetal Bovine Serum (FBS, Sigma-Aldrich, F7524) and Penicillin Streptomycin solution (PS, Sigma-Aldrich, P4333).

Paraformaldehyde (PFA, Sigma-Aldrich, P6148) is used to fix cells. Bovine Serum Albumin (BSA, Sigma-Aldrich, A2153, 9048−46−8) is used to block nonspecific protein. Primary antipodocin antibody (Sigma-Aldrich, P0372), secondary antirabbit antibody (Alexa Fluor594, Cat: ab150080), 4′,6-diamidino-2-phenylindole (DAPI, Sigma-Aldrich, D9542) and Phalloidin (Invitrogen, Cat: A12379) are used for Immunocytochemical characterization.

Click-iT™ EdU Cell Proliferation Kit for Imaging, Alexa Fluor™ 488 dye (EdU, ThermoFisher scientific, C10337) is used to evaluate podocyte cells proliferation. CellEvent™ Caspase-3/7 Green Detection Reagent (ThermoFisher scientific, C10723) is used to detect alive from dead cells.

2. Fabrication of 3D Hydrolyzed Polyacrylamide Hydrogels

a) Hydrogel preparation:

AAM, BIS, Triton X-100, Sesame Oil, TEMED, APS are used to prepare emulsion in this exact order. 6 ml AAM:BIS mixture is introduced into 50 ml v-shape bottom falcon tube. 150 µl Triton X-100 is added and agitated for 1 min via vortex 2500 rpm. 6 ml of oil is added to the mixture and agitated manually for 1 min. 12 µl TEMED and 60 µl APS are added consecutively then agitated slowly. The mixture is transferred to 10 ml pipette and let to polymerize. After 30 minutes, the gel is extracted from the pipette and cut into 3 mm thick cylinder specimens along its length (3.5 cm makes 1 ml). Samples are soaked in Methanol for 24 hours, while changing the methanol 3 times to remove oil from the structure, then each 10 pieces are soaked in 4 ml NaOH 1M overnight. After doping, the gel is washed by DI water by soaking it in 100 ml of DI water in a Plastic Box. Water is changed twice per day (every 12 hours) until reaching full swelling and DI water initial pH (6-7). After full swelling the resulting hydrogels are soaked in 50 ml of PBS 1X, and changed once per day for 3 days.

For cell culture the initial gel is frozen at 80°C in O.C.T. compound bath for 30 min, and then sliced into 300 to 500 µm layer before being doped and swelled in PBS then in RPMI medium for podocyte cell culture.

Sesame oil is used as a pore-forming agent during the polymerization, and is removed from the gel after polymerization/crosslinking. Triton X-100 is used as surfactant or surface-active agent that forms a barrier between the phases and reduces the interfacial tension between them. Hydrophilic-lipophilic balance (HLB) value is 13.5 good for oil in water emulsion.

A general reaction scheme for the emulsion templating reaction is shown in Figure 1. Within these structures, the hydrophilic heads are directed outward towards the pregel solution, and the hydrophobic tails of the surfactants are pointed towards the interior of the micelle[13].

Oil-in-water (O/W) emulsion is formed by dispersing sesame oil droplets into the pre-gel aqueous solution by mechanical stirring. The phase-separated solution is shortly crosslinked to form a porous scaffold. The internal oil phase acts as the template around which polymerization

occurs. The oil phase is subsequently removed after the crosslinking to give a porous templated material.

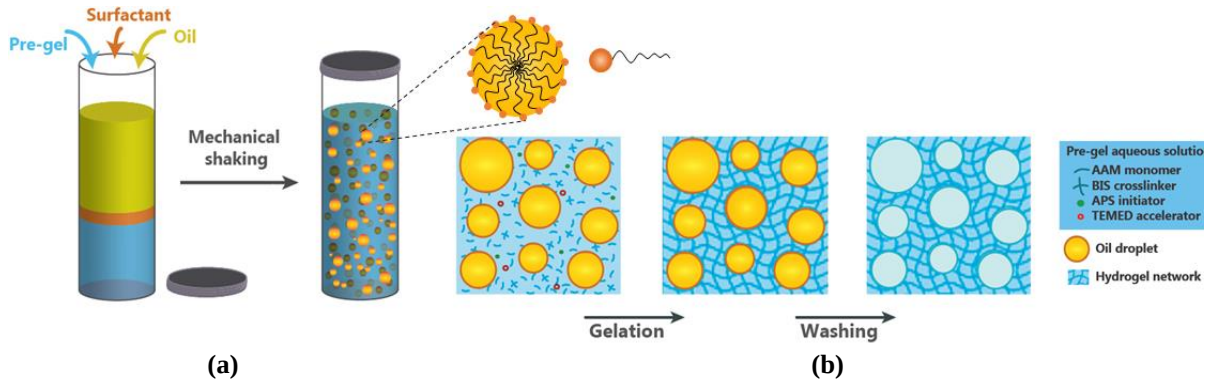

Figure 1. Schematic presentation of **(a)** the emulsion-templating methods used for the formation of 3D porous PAAM hydrogels and **(b)** the polymerization of the continuous phase and removal of the dispersed phase

Five sets of experiments are designed in order to test the effect of different parameters on the 3D Hydrogel properties.

In the first set, the effect of the "total liquid volume" is studied in a 50 ml tube. The pregel solution (1 ml "30:0.06 AAM:BIS ", 10 µl "APS", 2 µl "TEMED") presenting the water phase and the sesame oil are mixed at a ratio of 1/1 "O/W" at 3 different total volumes 6, 12 and 24 ml. The surfactant used is 1.4% of Triton X-100 (14 µl surfactant per 1 ml pregel).

In the second set, the effect of surfactant content is tested fixing the ratio of oil/pregel solution to 6/6, and using different Triton X-100 percentage of pregel solution volume (0.1, 0.35, 0.7, 1.4, 2.5 and 2.8%).

In the third set, the effect of oil/pregel ratio is evaluated by changing it as following (0/12, 2/10, 4/8, 6/6, 5/7, 8/4) using 2.5% of Triton X-100.

In the fourth set, the effect of crosslinking density is studied using the ratio 6/6 oil/pregel (1 ml "30:x AAM:BIS ", 10ml "APS", 2ml "TEMED") solution, 2.5% of Triton X-100 and changing the BIS percentage dissolved with 30% AAM (0.02, 0.06, 0.12, 0.18, 0.24 %).

Finally, in the fifth set, the effect of NaOH concentration is examined using the ratio 6/6 oil/pregel (1 ml "30:0.06 AAM:BIS", 10ml "APS", 2ml "TEMED") solution, 2.5% of Triton X-100 hydrolyzed in 0.0625, 0.125, 0.25, 1 and 2 Molar of NaOH.

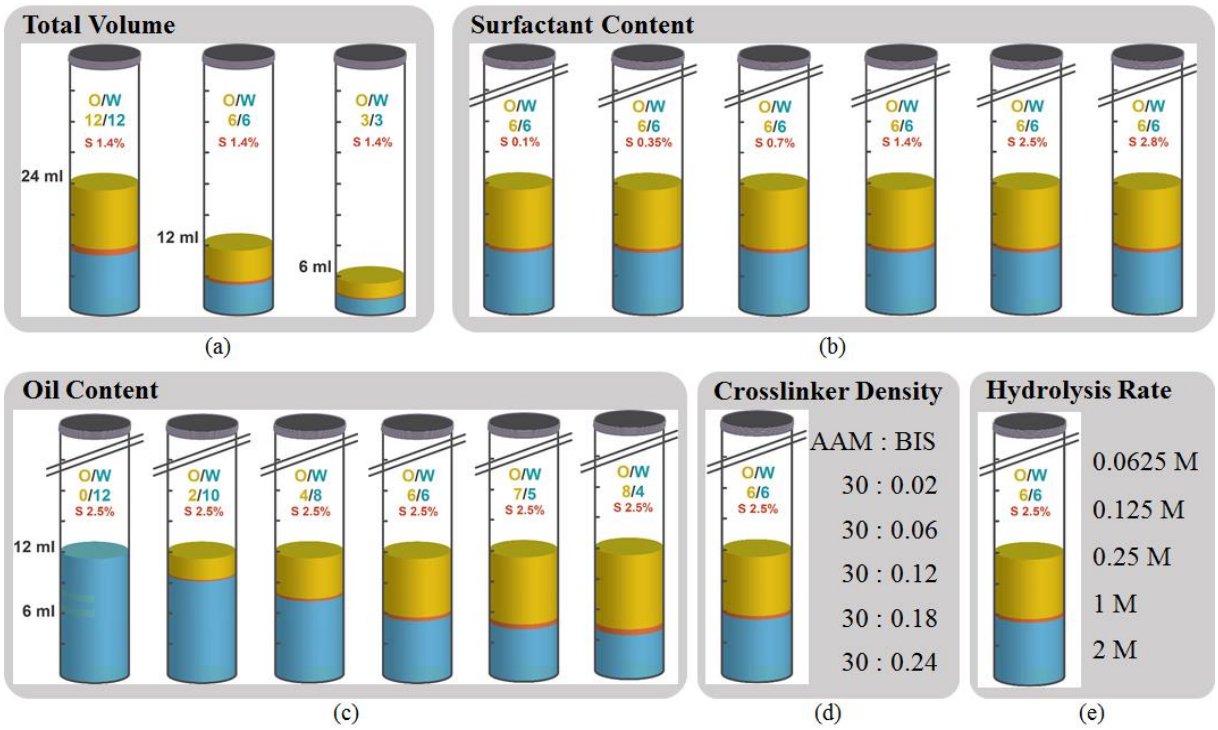

Figure 2. Schematic representation of five sets of experiments, designed in order to test the effect of different parameters on the 3D Hydrogel properties. **(a)** In the first set, the effect of the "total liquid volume" is studied in a 50 ml tube. The pregel solution (1 ml "30:0.06 AAM:BIS", 10 µl "APS", 2 µl "TEMED") presenting the water phase and the sesame oil are mixed at a ratio of 1/1 "O/W" at 3 different total volumes 6, 12 and 24 ml. The surfactant used is 1.4% of Triton X-100 in the pregel solution. **(b)** In the second set, the effect of surfactant content is tested fixing the ratio of oil/pregel solution to 6/6, and using different Triton X-100 percentage of pregel solution volume (0.1, 0.35, 0.7, 1.4, 2.5 and 2.8%). **(c)** In the third set, the effect of oil/pregel ratio is evaluated by changing it as following (0/12, 2/10, 4/8, 6/6, 5/7, 8/4) using 2.5% of Triton X-100. **(d)** In the fourth set, the effect of crosslinking density is studied using the ratio 6/6 oil/pregel (1 ml "30:x AAM:BIS", 10ml "APS", 2ml "TEMED") solution, 2.5% of Triton X-100 and changing the BIS percentage dissolved with 30% AAM (0.02, 0.06, 0.12, 0.18, 0.24 %). **(e)** Finally, in the fifth set, the effect of NaOH concentration is examined using the ratio 6/6 oil/pregel (1 ml "30:0.06 AAM:BIS", 10ml "APS", 2ml "TEMED") solution, 2.5% of Triton X-100 hydrolyzed in 0.0625, 0.125, 0.25, 1 and 2 Molar of NaOH.

Table I. Composition of the different sets of experiments.

	Pregel solution: 1 ml AAM:BIS, 10 µl APS, 2 µl TEMED				
	AAM:BIS	**Oil/Pregel**	**Surfactant**	**Total volume**	**NaOH**
Set 1 **Total liquid volume**	**30:0.06**	**1/1**	**14 µl**	6 ml 12 ml 24 ml	**1M**
Set 2 **Surfactant content**	**30:0.06**	**6/6**	1 µl 3.5 µl 7 µl 14 µl 25 µl 28 µl	**12 ml**	**1M**

Set 3 Oil content	**30:0.06**	0/12	**25 µl**	**12 ml**	**1M**
		2/10			
		4/8			
		6/6			
		8/4			
Set 4 Crosslinking density	30:0.02	**6/6**	**25 µl**	**12 ml**	**1M**
	30:0.06				
	30:0.12				
	30:0.18				
	30:0.24				
Set 5 Hydrolysis rate	**30:0.06**	**6/6**	**25 µl**	**12 ml**	0.0625 M
					0.125 M
					0.25 M
					1 M
					2 M

b) Polymerisation kinetic

The first step is to control the polymerization kinetic in order to maintain the emulsion stability during the polymerization. If the emulsion does not remain stable during the polymerisation, the phase separation can ruin the experiment. Since the polymerization of AAM is an exothermic reaction[14], the rate of heat release is considered to be proportional to the rate of polymerization[15]. The gelation kinetic can be followed by registering the temperature profile of the reactive solution during its polymerization. The interested part will be the induction phase, where the temperature is steady, which determine the correspondent duration before the polymerization starts[15]. This duration represents the minimum time required to maintain the emulsion stability before polymerization.

The temperature profile study is registered for 12 ml of pregel solution (1ml "30:0.06 AAM:BIS", 10 µl "APS", 2 µl "TEMED") without oil, to see the minimal time needed to manipulate the pre-gel solution before the polymerization starting point. The temperature polymerization kinetic of 12 ml of (1:1 oil:pregel solution) is also measured to see the time needed to maintain the emulsion stability before polymerization. The temperature profiles are recorded using a digital thermometer (OMEGA HH804U) attached to a thermocouple type Pt100. The temperature profiles are registered at a rate of one value per second with a precision of 0.1°C.

3. Hydrolysis and Swelling Measurement

After complete polymerization, the resulting gels are hydrolyzed in basic solutions of NaOH 1 M overnight and then placed in DI water for 10 days. The water is repeatedly changed to wash out most of the extractable materials and allow them to reach equilibrium volume. The resulting pH of the hydrated fully swelled gel in water is 6.8. Before cell culture process, fully swollen hydrogels are placed in a specific media depending on the type of cells.

The replacement of water by another media leads to a variation of the hydrogel's dimensions. This variation or shrinking is caused by the ions and molecules exchange between solvent and gel, to insure the electrostatic charge equilibrium. For this reason, the swelling and deswelling are measured in cell media.

Upon reaching swelling equilibrium, the resulting hydrogels are gently removed from water and placed in PBS solution. The PBS is changed twice a day for 3 days to reach the ion equilibrium. The swelling and deswelling capability of gels are defined as the weight of water (Medium) uptake per unit weight of dried polymers and is expressed as:

$$S = D = \frac{W_S - W_d}{W_d} \tag{1}$$

where W_s and W_d are the weight of the swollen hydrogel at equilibrium and the weight of dry hydrogel, respectively.

The weight of deswelled hydrogel W_d is measured after drying in the laboratory oven for 24 hours at 75℃, then for 2 hours at 105℃ over a Teflon paper to assure the complete evaporation of water.

4. Mercury Porosimetry

The pores size and volume of the swollen hydrogel are measured using Mercucy Intrusion Porosimetry (MIP) technique. These measurements are performed by Micromeritics AutoPore IV 9500 machine that characterizes a material’s porosity, with is the ratio of pore volume to its

total volume[16], by applying various levels of pressure to a sample immersed in mercury. The pressure required to intrude mercury into the sample's pores is inversely proportional to the size of the pores.

Since the samples should be dried to be characterized; the swollen hydrogels in PBS are frozen using liquid nitrogen for 4 hours, and subsequently lyophilized avoiding shrinkage during the drying process. The frozen hydrogels are freeze-dried using FreeZone 4.5 Liter Benchtop Freeze Dry Systems (LABCONCO, 7750030) under reduced pressure 0.09 mbar for 24 hours at -52°C. Lyophilization process of high water contents in hydrogels resulted in a macroporous sponge-like scaffolds. Each sample is transferred directly from the freeze-drier to the MIP avoiding humidification of the sample.

5. Scanning Electron Microscopy (SEM)

Hydrogel microstructure is evaluated using SEM (Hitachi S4800), before and after swelling. The middles of the samples are used for the characterization. First, the polymerized samples are soaked in methanol for 24 hours to remove oil from the structure to see the porosity clearly, then the gels are dehydrating in vacuum oven (France ETUVES, XF020) for 5 hours at room temperature to evaporate all the liquids before sputter-coating with gold.

The internal structure of the samples fully swelled in PBS is also determined by SEM. The swollen hydrogels in PBS are frozen using liquid nitrogen for 4 hours, freeze-dried for 24 hours and then sputter-coated with gold 1 hour before characterization, avoiding the humidification of the samples.

The pores size is determined by measuring their diameter from SEM images, considering a spherical shape of the pores. 40 different measurements are taken from three different specimens along the main cylindrical sample. The mean value of the pores diameter is calculated with the corresponding standard deviation.

The pore coverage area assessment is performed by image analysis using ImageJ software [ImageJ]. Image analysis of SEM images is done by pixel-based measurement once the microstructure is digitized. The pore coverage area over the total sample surface area is estimated in the percentage by masking the processed SEM microstructure as a binary image

with different thresholding levels. This method is accurately performed on three different SEM images of the specimens; the mean value and the uncertainty of the area fraction of porosity are quantified.

6. Optical Microscope

In order to compare the pore size of the swelled and freeze-dried hydrogels, thin layers of hydrogel are characterized using optical microscope (Nikon, TE2000) and the images are analyzed using [ImageJ] by measuring the pores diameter for 3 samples from each composition. The mean value of the pores diameter is calculated with the corresponding standard deviation.

7. Rheology of PAAM Hydrogel

An electromechanical material testing machine (zwickiLine Z5.0) is used to test samples in compression mode. The analyses are performed on four cylindrical samples from each composition. The samples are inserted between two horizontal plates and deformed with a rate of 2 $mm.min^{-1}$. Measurement time is of 3 min and within this short period of time the humidity of the sample is considered constant. The Young modulus is determined as a slope of the liner part of the stress-strain curve.

8. Cell Culture

Human podocyte cell line is purchased from the Faculty of Medicine, University of Bristol, U.K. Immortalized human podocytes are cultured on flasks according to the supplier protocol. Podocyte cells are cultured in RPMI−1640 Medium (Sigma-Aldrich, R8758) supplemented with 1% insulin-transferrin- Selenium liquid media supplement (Sigma-Aldrich, I3146), 10% fetal bovine serum (Sigma-Aldrich, F7524) and Penicillin Streptomycin solution (Sigma-Aldrich, P4333). Proliferation is induced when the cells are incubated at 33 °C and differentiation is induced by incubating the cells at 37 °C. After proliferation, cells are plated on the top of the hydrolyzed PAAm Hydrogel substrate having various properties. PAAM

Hydrogels having different oil content, crosslinker density and hydrolysis rate are used to test the effect of each condition on spheroid formation.

The hydrogel samples are autoclaved in glass scintillation vial closed with aluminium sheets in excess PBS. Autoclaved discs are introduced into 24 well plates, and stored overnight in RPMI media at 4 °C to insure complete media exchange. Transfer is always carried on flask under biological hood. Next day, fresh complete media (RPMI) is introduced into each well at 1 ml/well and left at 33°C for two hours.

5 millions of cells are suspended in 0.5 ml of RPMI; 20 µl (200 000 cells/well) is placed on the top of the samples after removing the media from the plate. The plate is placed carefully in the incubator for 1 hour, before adding media in order to maintain the rest of cells on the gel. After 0.5 ml of medium is added slowly in each plate and placed in the incubator at 33°C.

Podocytes cells are cultured on non-adhesive well plate (Costar® 24-well Clear Flat Bottom Ultra-Low Attachment Multiple Well Plates) and formed random aggregates. These aggregates are transferred to a normal well plate before 2 hours of the fixation in order to be used as control, and compare it to the culture on hydrogels.

9. Immunocytochemical characterization

Podocyte cells cultured on PAAm Hydrogels for 7 days are fixed with 2% of paraformaldehyde (PFA) (Sigma-Aldrich, P6148, 30525−89−4) for 15 min at room temperature. Then, cell permeablization is performed using 0.5% Triton X-100 (Sigma-Aldrich, X100, 9002− 93−1) for 15 min into the incubator (37 °C). Afterward, the nonspecific protein binding sites are blocked with 1% of Bovine Serum Albumin (BSA) (Sigma-Aldrich, A2153, 9048−46−8) and 0.5% of Triton X-100 in PBS for 1 hour at room temperature. Cells are then incubated overnight at 4 °C with a primary antipodocin antibody (Sigma-Aldrich, P0372). The samples are then rinsed with PBS and incubated with secondary antirabbit antibody (Alexa Fluor594, Cat: ab150080) for 1 h in dark at room temperature. Nucleus and actin cytoskeleton staining are done with DAPI (Sigma-Aldrich, D9542) and Phalloidin (Invitrogen, Cat: A12379), which are applied for 1 h in dark at room temperature. Image acquisition is achieved using Nikon TE2000 microscope.

10. Cell Proliferation Assay

Click-iT™ EdU Cell Proliferation Kit for Imaging, Alexa Fluor™ 488 dye (EdU, ThermoFisher scientific, C10337) is used to evaluate podocyte cells proliferation. After 9 days of culture on PAAm hydrogels, 500 µl of 10 µM EdU labelling solution is added to cells and incubated for 24h at 33°C. EDU solution is carefully removed and the sample is rinsed twice in PBS to remove EdU excess. The sample is incubated for 1h in dark at room temperature in DAPI 1/1000 then washed 3 times in PBS.

11. Live/Dead Cells Assay

A live and dead cell assay was implemented to measure the viability of the PAAM hydrogel. The Podocytes are seeded in PAAM hydrogel at a density of 200 000 cells/well and incubated in RPIM media. The RPMI is changed every 2-3 days. After 10 days of culture, the live and dead cell assay solution 2µM CellEvent™ Caspase-3/7 Green Detection Reagent (ThermoFisher scientific, C10723) is added to each cell-seeded hydrogel and incubated for 30 min at 33 °C, then washed 3 times in PBS.

IV. Results and Discussion

1. Polyacrylamide hydrogels properties

Polyacrylamide marcoporrous scaffolds are fabricated using emulsion templating technique; Sesame oil droplets are formed in pregel solution (AAM, BIS, APS and TEMED) stabilized using Triton X-100 as surfactant. After polymerization, the samples are sliced and hydrolyzed in NaOH solution. The influence on surfactant content, oil/AAM ratio, crosslinker density and hydrolysis rate on the mechanical and structural properties of the scaffold are tested.

A. Experimental conditions determination: Polymerisation kinetic, Total volume and Shaking method

a) Polymerisation kinetic

The first step is to control the polymerization kinetic in order to keep the emulsion stable during the gel polymerization. A short induction phase is not desirable since the mixture (pregel + oil) should be transferred to a pipette after mixing it. While long induction phase is also problematic since it can cause a phase separation. If a phase separation occurs before the gelation, the desirable porous structure is lost. Thus, an adequate quantity of APS and TEMED should be determined in order to have enough time to manipulate the mixture before gelation while preventing the emulsion instability.

The temperature profile presented in Figure 3, is registered for 12 ml of the pregel solution (1ml "30:0.06 AMM:Bis", 10 µl "APS", 2 µl "TEMED") without oil, and for 12 ml of 1:1 oil:pregel solution.

Figure 3 shows that the induction phase increases in the presence of oil, which slows down the polymerization. On one hand, the induction phase of "12/0" sample is 2 minutes which is enough to manipulate the solution (transfer it to the pipette). On the other hand, the emulsion stability should be maintained for 10 to 13 minutes, the time needed by the pregel solution of 6/6 to polymerize.

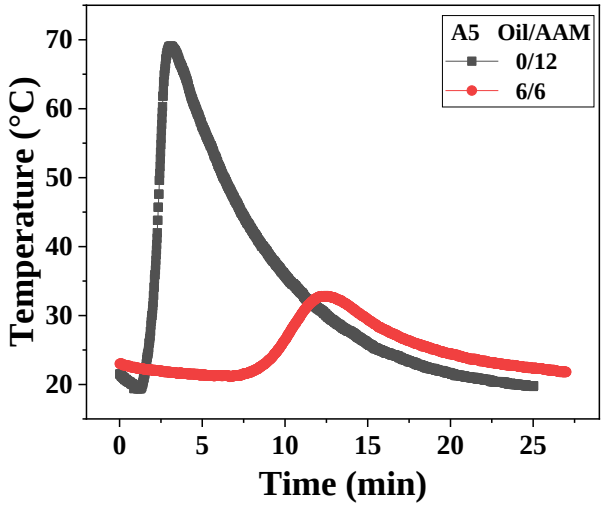

Figure 3. Variation of the temperature versus time of pregel solutions with a ratio of "12/0" and "6/6" pre-gel/oil samples during the polymerization.

Increasing the concentration of initiator or accelerator will decrease the time before the polymerization of pregel without oil, so the solution will polymerize before transferring it to the specific mold. Decreasing this concentration will slow down the polymerization, so the stability time of the emulsion should be increased. For that, the concentration of APS and TEMED is fixed on 10 and 2 µl respectively for 1 ml AAM/BIS.

b) Total filling volume

The optimum processing conditions for preparing O/W *emulsions* are investigated. After mechanical stirring a milky-white O/W emulsion is formed in the reaction vessel. The mechanical stirring conditions are optimized in order to obtain a stable emulsion for minimum duration of 15 minutes after the stirring ceasing. The polymerization kinetic indicates that the system is suitable for emulsion templating since the free-radical polymerization occurs before the emulsion became destabilized.

The effect of the reagents mixture's total volume on the resulting hydrogel properties is investigated. The pre-gel solution (1 ml "30:0.06 AMM:Bis", 10 µl "APS" and 2 µl "TEMED") considered as the water phase, the ratio of the water phase to oil (1/1) and the surfactant percentage (1.4%) are kept constant. The quantity used or the total volume was varied from 6 to 24 ml. SEM images of the resulting gels as prepared and the hydrogels after hydrolysis and full swelling in PBS are presented in Figure 4 (a) and (b).

The results show that the pore size increases when the total reagent quantity increases. The pores sizes that corresponds to 6 and 12 ml display a narrow distribution centred around a mode of about 85 and 95 µm respectively, whereas the 24 ml sample, present a broad pore size distribution, with a bigger pores volume of 180 ml/g over the total sample volume and larger pores which are around 120 µm.

This large distribution in pore size is attributed to the large filling volume of the 50 ml tube, especially after the foam formation on the top of the emulsion during the shaking process which increases the total filling volume of the tube. The large amount of foam formed increases the total filling volume.

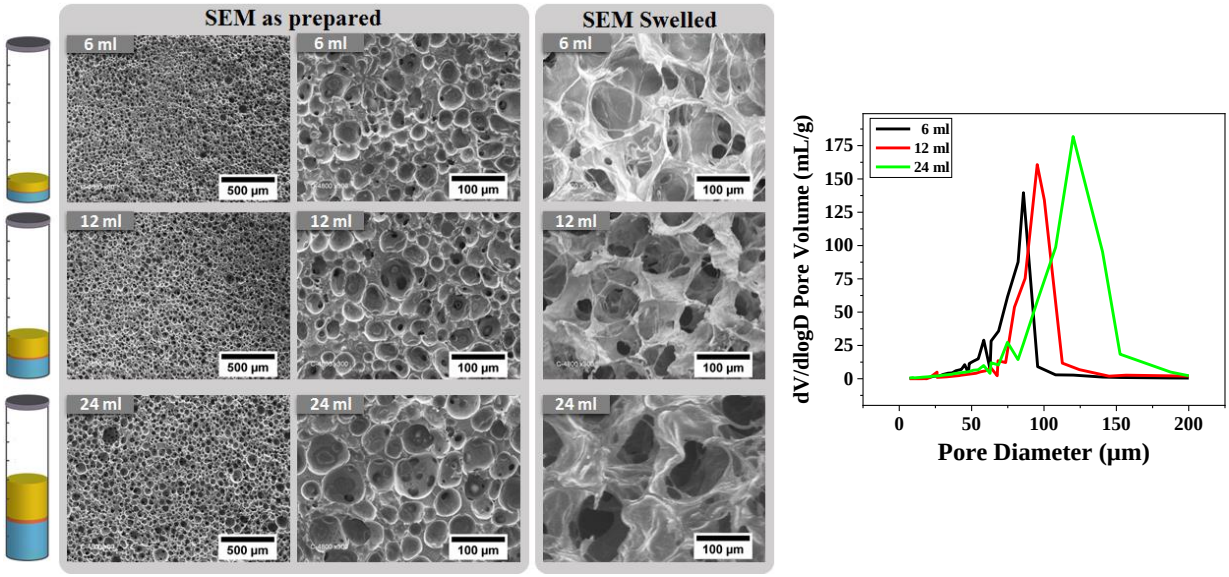

(a) **(b)** **(c)**

Figure 4. SEM images of hydrogels having same composition [(1 ml "30:0.06 AMM:Bis", 10 µl "APS", 2 µl "TEMED"), 1:1 oil:AAM ratio, 14 µl Trition X-100 in 1 ml AAM] , used at different quantities 6 ml, 12 ml and 24 ml in a 50 ml tube **(a)** as prepared after gelation and **(b)** after swelling in PBS. **(c)** The diameter and the volume of hydrogel pores prepared in different total volume 6 ml, 12 ml and 24 ml.

The increase in filling volume leads to a decrease in mass transfer between air and the liquid phases limiting the homogenization of the emulsion[21–24]. Likewise, at high filling volume the air– liquid interface came into contact with the cap of the container, which reduces the air liquid interface and therefore the mixture stability[25]. This explains the creaming on the top of the oil in water emulsion surface in the case of 24 ml filling volume which is not the case for the other samples (6 and 12 ml).

After swelling, the 12 ml samples represented the most interconnected and homogenous porosity. Therefore, it was adopted in the later experiments.

c) Effect of shaking method

Hand-shaking is a low-shear homogenization method normally used for the formation of micrometric size oil droplets emulsion[30–32]. The reproducibility and the homogeneity of this shaking technique is studied by preparing four different samples in two different days at two different times. The samples are prepared using 6/6 oil/pregel and a Trition X-100 concentration of 2.5%. The composition of the pre-gel solution (1 ml "30:0.06 AMM:Bis", 10 µl "APS" and

2 µl "TEMED"). After swelling, the samples are freeze-dried then analyzed using the Mercury porosimetry.

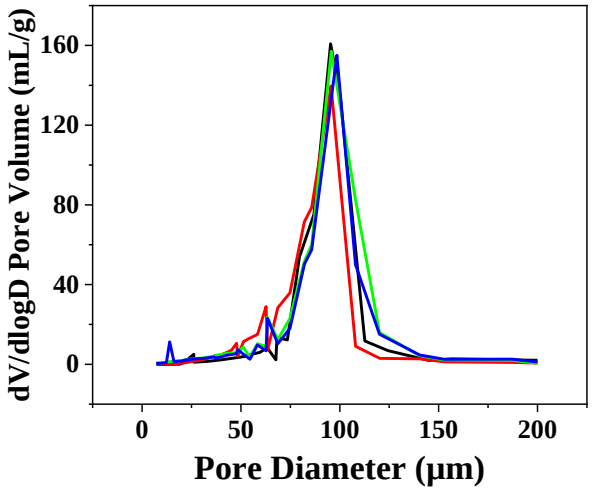

Figure 5. The diameter and volume of different PAAM hydrogel having the same composition and preparation technique

The result shows that the hand-shaking method is repetitive, and can be used for the formation of macrometric oil droplets in emulsion. After swelling, the pore size of the hydrogel displays a narrow distribution centred around a mode of about 100 µm, which proves the homogeneity of the pore size resulting from this adopted shaking method.

B. Determine the effect of different experiment parameters on the 3D PAAM Hydrogels properties

a) Effect of the surfactant content

Surfactants are amphiphilic molecules that minimize the energy required for the emulsion formation by reducing oil-water interfacial tension. The surfactant concentration is an important factor in the emulsion stability. Critical Micelle Concentration (CMC) is the minimum concentration of the surfactant in a solution at which micelle formation takes place[17]. So, a concentration above 0.014 wt%, ca. 2.4×10^{-4} mol/L (CMC of Triton X-100) is required for an emulsion formation; the percentage surfactant is given relative to the amount of water present in the solution[18].

In order to obtain an interconnected porosity with an average pore size of 150 to 250 µm[12], recommended for the formation of spheroids from Podocytes cells inside the 3D porous hydrogel. A wide range of surfactant percentage, ranging between 0.1 wt% (correspond to 6.6×CMC of Triton X-100[19]) and 2.8 wt% (200×CMC), is tested in order to study the effect of surfactant concentration on the emulsion stability of our mixture, and control the pores size and the porosity of the resulting hydrogels. Concentrations below 0.1 wt% did not while raising the surfactant percentage above 2.8 wt % produced an fused porous structure[20].

The emulsion stability is evaluated under the optical microscope (Nikon TE2000) for different surfactant/AAM ratios by measuring the droplet diameter immediately after emulsification formation and then after 5, 10 and 15 minutes. The emulsion was formed in a similar manner as that in the preparation of porous hydrogels; AAM and BIS solution is mixed to Sesame oil with a ratio o/w=1/1 and different concentrations of surfactant is added, without the APS and TEMED.

The results show that the oil droplets size decreases as a function of time, and this decrease become less important by increasing the surfactant concentration. Thus, a stable emulsion is maintained for 15 minutes which is enough time for polymerization, when the surfactant concentration is higher than 1.4%, which represent 100 × CMC of Triton X-100.

The effect of surfactants on the hydrogel properties is studied by changing the Triton X-100 concentration between 0.1 and 2.8% from the mix total volume (AAM+BIS). The pore size of the hydrogel is measured before swelling, in order to study the relation between pore size and the surfactant concentration and compare it to other studies working on effect of surfactants on the O/W emulsion stability and pore size.

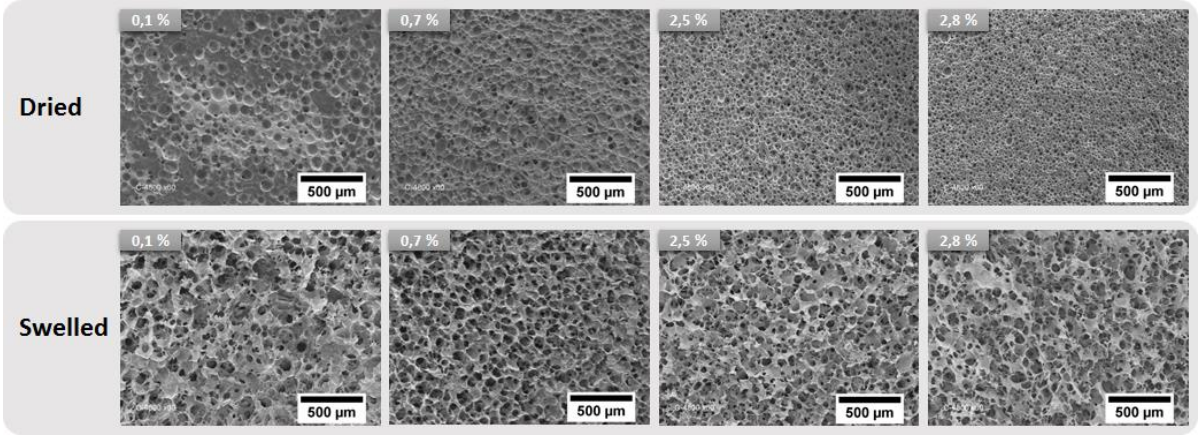

(a)

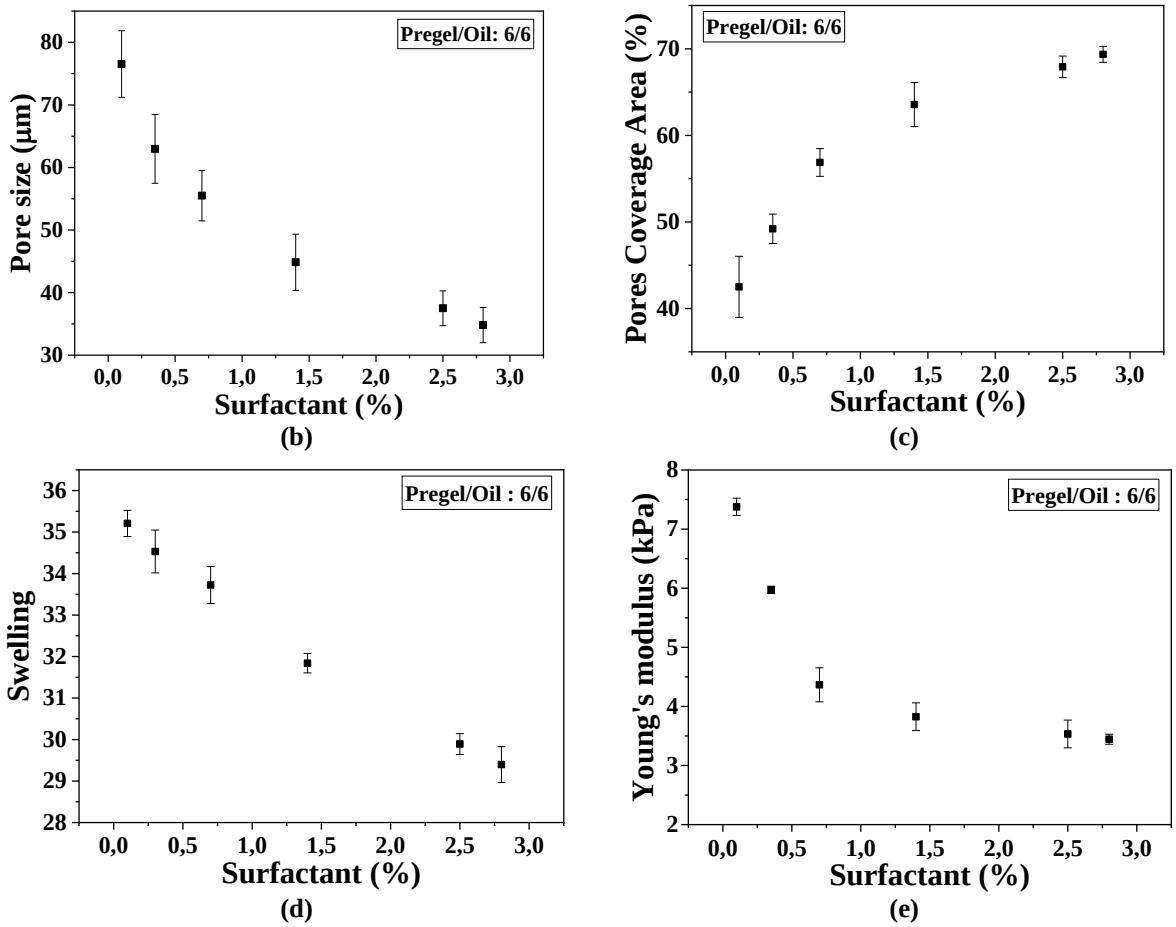

Figure 6. (a) SEM images of prepared samples [(1 ml "30:0.06 AMM:Bis", 10 µl "APS", 2 µl "TEMED"), 1:1 oil:pregel ratio] having different surfactant Trition X-100 percentage before and after swelling in PBS **(b)** Pore size and **(c)** pores coverage area in function of surfactant percentage in dry state. **(d)** Swelling ratio and **(e)** Young's modulus in function of surfactant percentage after full swelling in PBS.

In agreement to previous studies[26], SEM images of the gel before swelling show that the pore size decrease and the pore number increase while increasing the surfactant percentage. The results show that the pore coverage area and therefore the porosity increase from 42 to 71%, while the pore size decrease from 76 to 35 µm.

After swelling, the pores are more connected and well dispersed for high Triton X-100 content. Lowering the surfactant content produced a more closed structure whereas raising it produces an increasingly open, leading to an interconnected porous structure[20].

Fig. 6 (d, e) shows the swelling degree and the Young's modulus of the swelled porous hydrogels having different Triton X-100 percentage. All samples present a high equilibrium swelling ratios, indicating their good capability to absorb large amounts of water mostly after hydrolysis[27].

The hydrogel with 0.1 wt% of surfactant shows a swelling ratio about 35 and a Young's modulus of 7.4 kPa, while the hydrogel demonstrates a ratio of 29.7 and a modulus of 3.5 kPa when 2.8 wt% of Triton X-100 is used. Compared to the hydrogel without emulsion, it presents a Young's modulus of 40 kPa.

Overall, upon increasing the amounts of surfactant, the swelling ratios and the Young's modulus of macroporous hydrogels decrease. This behaviour is mainly attributed to the decreasing pore size and the increasing of hydrogels porosity for samples having a high concentration of surfactants. The smaller size of interconnected pores results low hydrogel swelling rate[28] and a softer structure[29].

During the mechanical test, the samples having high porosity start to leach out the water from the structure after applying a low compression force. This confirms that high interconnected porous structure cannot hold high water quantity. In the following 2.5% of surfactant is used for the other samples preparation, since it ensures with the 2.8% a highly connected porosity needed for the cell culture application.

b) Effect of the oil content

The effect of oil content on the hydrogel porosity is investigated. The gelation kinetic is followed by registering the temperature profile of the reactive solution during its polymerization.

The temperature profiles during the polymerization of pre-gel solutions having different Oil/pregel ratios are presented in the Figure 7 (a). The results show that while increasing the Oil/pregel ratio, the polymerization slows down and the maximum temperature decrease, and the area below the peak presents a linear decrease from a value of 318 for hydrogel without oil, to 66 for 8/4 Oil/pregel. The area below the peak represents the amount of heat released during polymerization, and it decreases with the increase of oil quantity in the mixture.

The heat is generated by the exothermic polymerization reaction of the pregel solution. When the proportion of the pregel solution in the mixture increase the generated heat increase. Since the reactive pregel increase the temperature of the solution, while the oil temperature maintains constant, the heat capacity of the pregel solution generated during the polymerization is

transferred to heat the oil, which decrease the total temperature of the mixture by increasing the oil content. Also the presences of oil at a stable temperature slow down the temperature increases and therefore the initiation of polymerization reaction, which explains the fact that for a high oil content, the deceleration of the temperature increase. This delay (>15 mins) affects the emulsion stability in the case of 7 and 8 ml oil in 12 ml solution, so the 1 cm of the top and the bottom of the gel are not used for characterization.

SEM images of the polymer before swelling show that the pore number increased with the increase of Oil content, while the pore size does not show a large difference. Indeed, the increase in oil content led to an increase of the total droplets volume and therefore the porosity from 36 to 70%[15].

After swelling, the samples are freeze-dried then analyzed using the Mercury porosimetry. The results show that pore sizes for the sample “2 ml oil / 10ml pregel” (12 ml of total volume) displays a broad pore size distribution and a large pores diameter, which are around 150 µm with a small porous volume about 50 ml/g. Whereas by increasing the oil content, the pore size and distribution decrease, to reach a narrow distribution centered around a mode of about 63 µm, with a bigger porous volume of 350 ml/g over the total sample volume for the sample having “8 ml oil / 4 ml pregel”.

So by increasing the oil content, the pores become smaller, more connected and more homogenous. This change between the pore size before and after swelling is due to the water quantity absorbed by the polymer. More the polymer absorbs water, more the structure is swelled and the pore size increases.

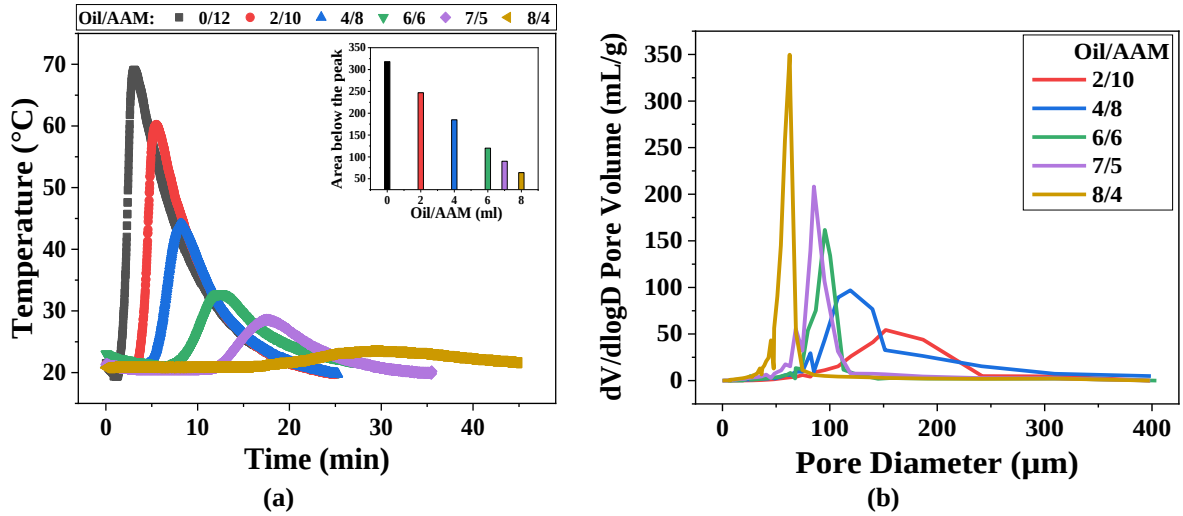

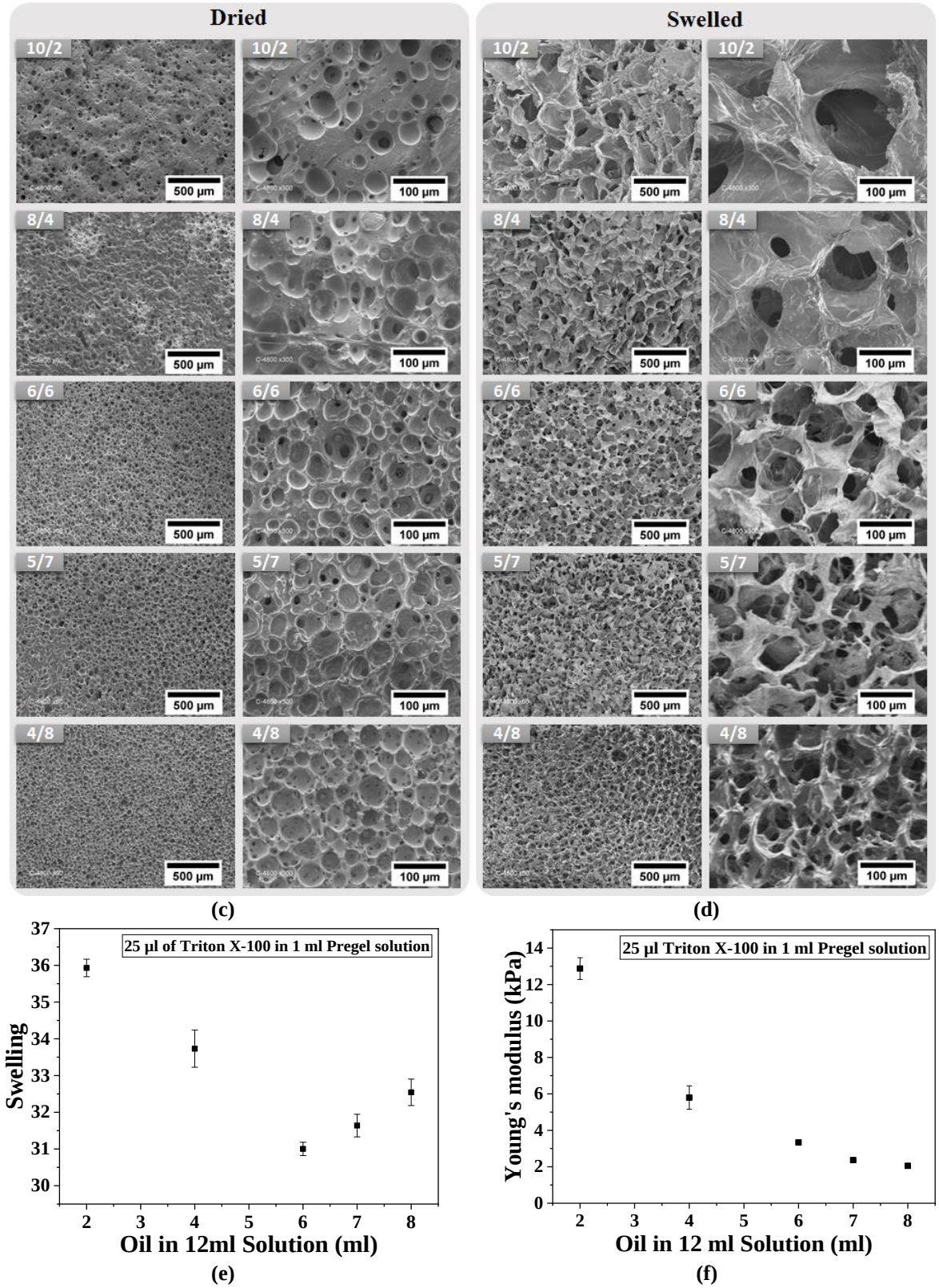

Figure 7. **(a)** Variation of the temperature versus time of pregel solutions during polymerization. **(b)** The diameter and the volume of hydrogel pores after swelling.
SEM images of prepared samples having different Oil/AAM ratio **(c)** before and **(d)** after swelling.
(e) Swelling ratio and **(f)** Young's modulus of hydrogel in function of Oil/AAM ratio after full swelling

The swelling of 3D samples is controlled by two main parameters; the polymer concentration by volume unit is which dominate in the first part of the curve, so by increasing the oil concentration, the polymer concentration decreases. So the swelling of the hydrogel decreases and therefore the pore size. On the other hand, increasing the oil content leads to a large connected porosity that can hold a large amount of water, which become dominant in the second part of the graph. This explains the divergence of the swelling values for an oil volume above 6 ml Figure 7 (e).

Figure 7 (f) shows that Young's modulus decreases with the increase of Sesame oil content. It presents a value of 13 kPa for the samples having 2/10 oil/pregel and decreases to 2 kPa for a higher oil content (8 ml in 12 ml total volume). Studies of the mechanical and elastic properties showed that the strength limit under compression, as well as the Young's modulus decrease with the increase of porosity[33,34].

Since the porosity of the hydrogel is related to oil/AAM ratio, this explains the decrease of Young's modulus with the increase of oil content which results a high interconnected porosity and a softer scaffold.

The sample having 6/6 Oil/AAM has shown a high porosity and a pore size about 100 µm, which makes it compatible for the formation of spheroids. 2/10 and 4/8 have an average pore size > 100 µm, but these pores are not interconnected which block the cell diffusion. Contrariwise, 7/5 and 8/4 samples have an interconnected porosity and a small pore size, limiting the formation of spheroids.

Despite that, all these samples will be used as a scaffold for spheroid formation in order to compare the spheroid formation under different scaffold conditions. The sample 6/6 is used in the following sections in order to determinate the efficiency of the crosslinker density and the hydrolysis rate on the mechanical and structural properties of the mocroporous PAAM hydrogel.

c) Effect of the crosslinking density

The extracellular matrix porosity is an important factor influencing the ability of cells to migrate and grow within the structure[35]. An increase of porosity in the 3D porous structure leads to a decrease of the Young's modulus according to the previous results, which is also a so important parameter for cell growth and attachment.

In this case, the Young modulus can be controlled by changing the composition of the pregel solution, and maintaining the high porosity by using 6/6 oil/AAM ratio and 2.5% of Triton X-100. The effect of crosslinker density of 3D hydrogel scaffold properties is studied.

SEM images of the polymer before swelling show that the porous structure has been loosened with a low crossliker concentration[36]. Well-defined spheres-like macrostructures were obtained for gels with the increase of BIS concentration (Fig. 8 (a)). Both pore size and pore coverage area did not show any significant change while changing the crosslinker density, it presents a pore diameter around 35 µm and a porosity volume around 70% of the total hydrogel volume.

After swelling, a highly connected structure is shown in the Figure 8 (b), more loosen for low crosslinker density and a more defined structure is maintained after swelling for high BIS concentration[36]. The pores size decreases from 120 to 60 µm with the increase of BIS concentration from 0.02 to 0.24 W%. Same for the swelling, it goes from 54 to 28 by increasing the BIS concentration. The pores size of the samples shows a decrease with the increase of crosslinker density, and this is related to the swelling ratio of each sample. For a high crosslinker concentration, the polymer network becomes less able to absorb water[37] due to the fact that the movement of the network chains is limited by the crosslinking nodes. So during the swelling of the network, the chains can extend between the nodes. More the nodes are close to each other less the chains can extend and less the gel can swell. This explains the decrease of the swelling by increasing the crosslinker density and therefore the pores size of sample at high concentration of Bis-acrylamide.

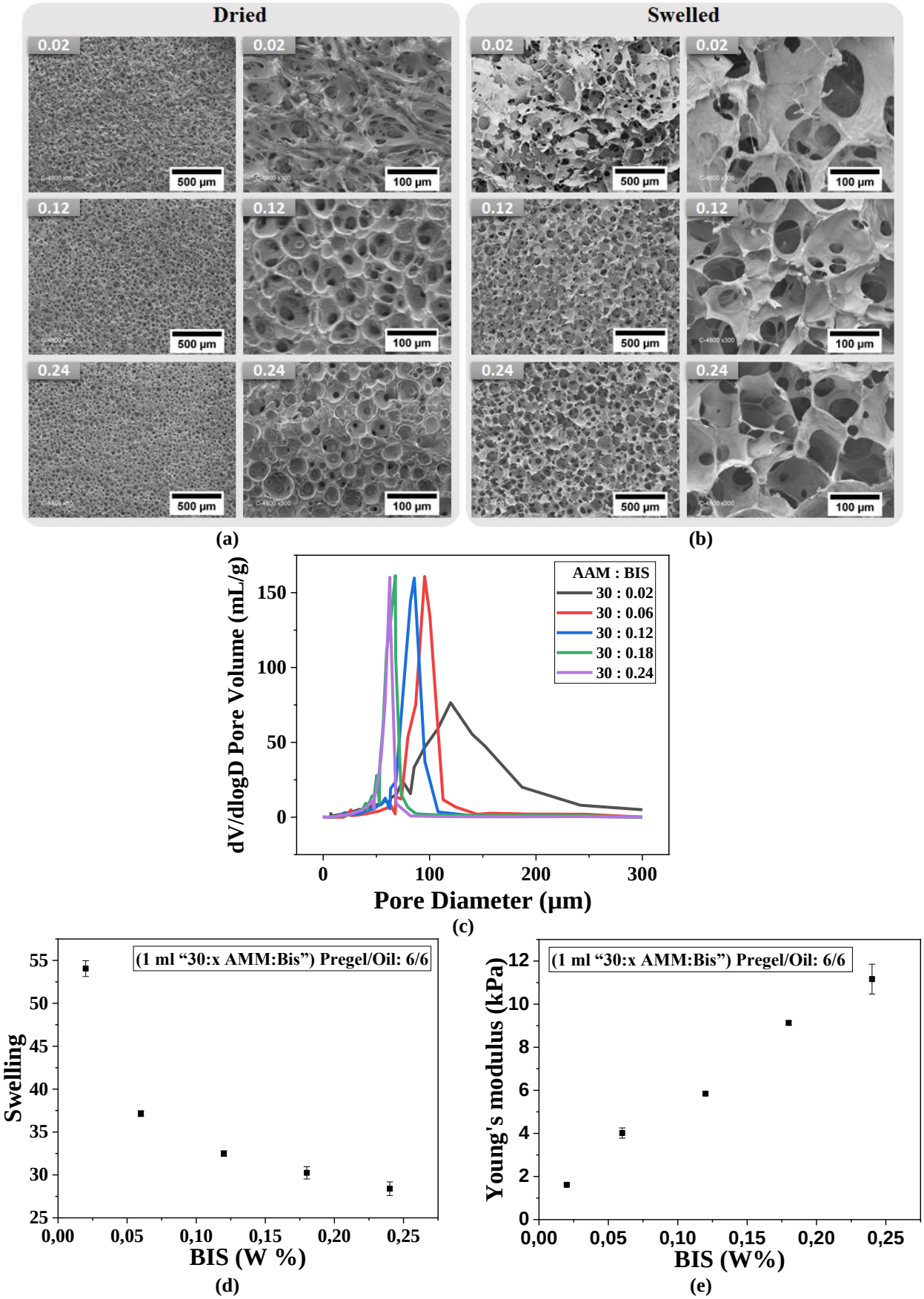

Figure 8. SEM images of prepared samples having different BIS concentration **(a)** before and **(b)** after swelling. **(c)** The diameter and the volume of hydrogel pores, **(d)** Swelling ratio and **(e)** Young's modulus in function of BIS concentration after full swelling.

As expected, the porous volume of hydrogels having different crosslinker density did not show any variation. This can explain the fact that by decreasing the crosslinker density, the total hydrogel volume increases, and both pores volume and polymer volume increases in the same proportion. In the case of 30:0.02 (AMM:Bis), because of its delicate structure, it shows some compact area after freeze-drying, which can explain the broad-pore size distributions and the low porous volume, compared to the other samples (Fig 8(c)).

Figure 8 (d) shows that Young's modulus increases from 1.5 to 11 kPa with the increase of Crosslinker density from 0.02 to 0.24 ml BIS over 30 ml AAM. This increase is due to the high connection between polymer chains surrounding the pores, which make the entire microstructure harder. A higher degree of crosslinker would reduce the average molecular weight between crosslinked point and thus, a rise of the gel stiffness.

We can conclude that the increase crosslinker density, the micromolecular chains between crosslinked points become shorter, which reveals a lower deformation ability and therefore an augmentation of stiffness and a decrease in the swelling ratio.

Since the cell sense, integrate and interpret the topography and the rigidity of ECM and therefore produce appropriate physiological responses regulating the cellular activities such as proliferation, migration, differentiation and apoptosis. All these samples will be used as a scaffolding material for cell culture in order to test the podocytes interaction on different samples rigidity.

d) Effect of the Hydrolysis rate

In order to determine the correlation between the concentration of doping ions and the swelling ratio, a samples having (1 ml "30:0.06 AMM:Bis", 10 µl "APS", 2 µl "TEMED") pregel solution with 6/6 oil/AAM ratio and 2.5% of Triton X-100 was prepared. This sample is hydrolyzed in a basic solution of NaOH of different molarities going from 0.0625 to 2 M.

The results show that pore size as well as the samples total volume and the swelling ratio increases from 16 to 35 with increasing NaOH concentration, due to the high concentration of doping ions. This increase is less significant for samples hydrolysed at a concentration of NaOH higher than 1 Molar.

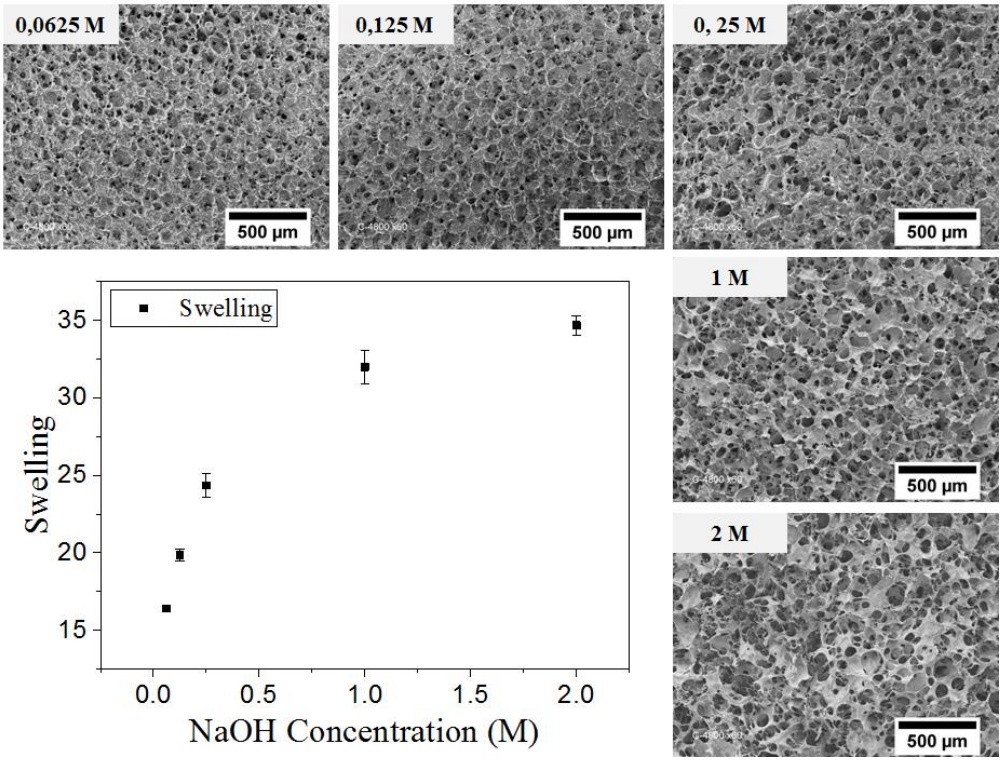

Figure 9. SEM images of hydrolysed samples with different NaOH concentration after swelling, and the swelling ratio of different samples

The mechanical and structural properties of 3D PAAM hydrogel can be tailored by changing hydrogel pregel composition, or the experimental condition such as emulsion components. Surfactant content is an essential parameter for maintaining the emulsion stability and it affects the pore size and porosity of the resulting hydrogel. Increasing the surfactant content, increase the stability time of the emulsion and lead to a small pore size and a very highly interconnected porosity. Swelling and Young's modulus are also affected by the surfactant content, it shows a decrease by raising Triton X-100 percentage in the emulsion solution.

Oil content can affect both polymerization kinetic and the properties of resulted polymer, increasing Oil/pregel ratio decrease pore size and increase the connection between pores with lead to a softer structure. The crosslinker density is a very important parameter to conserve the hydrogel structure and improve mechanical properties. For a high crosslinker concentration, the micromolecular chains between crosslinked points become shorter, which reveals a lower deformation ability and therefore an augmentation of stiffness and a decrease in the swelling ratio[37].

In the following section, all the samples prepared previously will be used as ECM for cell culture, in order to test the effect of the scaffold morphology and rigidity on the spheroids formation. These samples are characterized by different pore size and pores interconnection, and by different elasticity. The values of the pore size of the samples varies between 1.5 to 13 kPa which cover the range usually used for podocyte spheroids culture [38,39]. In addition, the pore size obtained in the microporous scaffold (60 to 150 µm) is suitable for spheroid formation [12,26,40,41].

2. Influence of the scaffold mechanical properties on podocytes cells

The ability of the scaffold to encapsulate and support proliferation of cells is an important requirement in tissue engineering. The encapsulated cells behavior is regulated via multiple micro and macro-environmental parameters, such as the mechanical stiffness and the structure of the hydrogel scaffolds that plays an important role in governing cells shape[42].

To investigate this, spheroids are formed by culturing podocytes cells in macroporous PAAM hydrogel, having different mechanical and structural properties. The values of the pore size of the samples varies between 1.5 to 13 kPa which covers the rage usually used for podocyte spheroids culture[38,39]. In addition, the pore size obtained in the microporous scaffold (60 to 150 µm) are suitable for spheroid formation[12,26,40,41].

Traditionally, cell culture on the two-dimensional tissue plastics has been used for cell biology studies. However, in 2D platform, cells are exposed to a rigid solid surface on the basal side and to a liquid at the apical surface. Studies have shown that two-dimensional cell culture cannot replicate real *in vivo* cell microenvironment because of lack of cell–cell and cell–matrix interactions and loss of specific tissue architecture, mechanical and chemical signals, which are essential for a function of real tissues in the human body. Three-dimensional spheroids have a complex architectural structure, dynamic cell–cell/cell–matrix interactions and bio-mimicking *in vivo* microenvironment[43].

In addition, the spheroid formation inside the scaffold porosity will avoid the cell detachment in case of a high flow rate inside the microfluidic device used for filtration applications.

In this section, the effect on hydrogel porosity, pore size and stiffness on spheroids formation is evaluated using the samples prepared with different oil/AAM ratios, different crosslinker density and hydrolyzed in different concentrations of NaOH solution.

A. Effect of hydrogel porosity on spheroid formation

The effect of hydrogel porosity on the spheroid formation is tested using samples prepared with different O/W ratio. Three of these samples are presented in the figure below (2/10, 6/6 and 8/4).

The results show that for both cases of 2/10 and 8/4 oil/AAM, the number of cells decreases after the second day of the culture. For the case of 2/10 sample, the cells stay on the pores located on the top of the sample and did not infiltrate inside the gel because of the low connection between pores. The podocytes form a small aggregation in these superficial pores, and since the PAAM hydrogel is non-adhesive the cell aggregation formed detached from the matrix while changing the media. For the sample 8/4 (O/W), the cells are easily and quickly infiltrate inside the hydrogel before even starting the aggregate formation and proliferate in the bottom of the well because of the large connection between pores. While for the case of 6/6 Oil/pregel, since the pores are also highly connected, podocytes start infiltrate inside the scaffold and form a small aggregation from day 1. Despite that, a large number of cells have also crossed the thin membrane and proliferate in the bottom of the well plate.

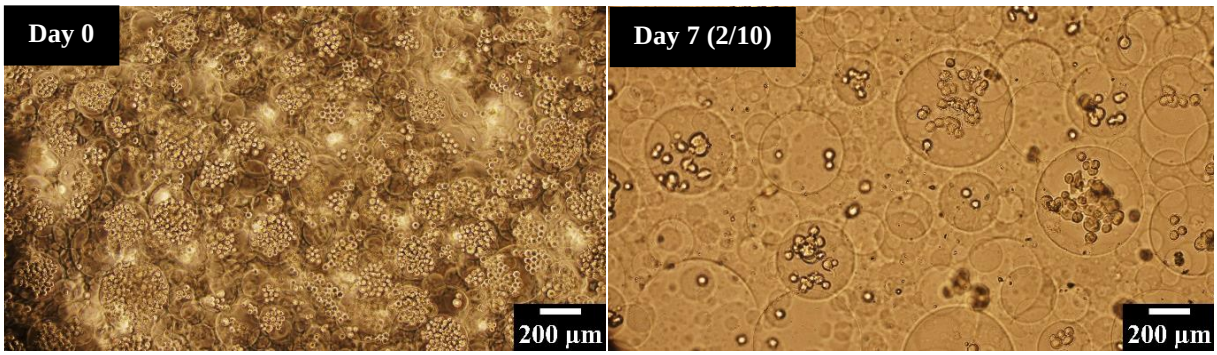

(a) **(b)**

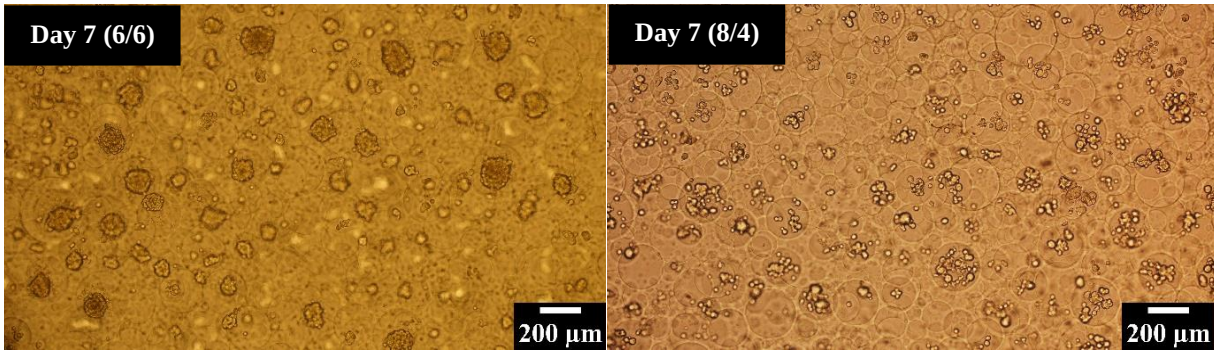

(c) **(d)**

Figure 10. Optical microscope images of podocytes inside the macropores of the hydrogel prepared with different Oil/AAM ratios **(a)** at day 0 and on **(b)** 2/10, **(c)** 6/6 and **(d)** 8/4 samples after 7 days of culture.

So by increasing the connection between pores, the cells can infiltrate inside the scaffold to form spheroids inside the pores and the large interconnected macropores ensure a sufficient nutrient and oxygen supply, and a waste extraction which promotes cell growth and enhances cell survival[16,44], but it risks that the cells cross the hydrogel without forming any spheroid for a very high-connected porosity.

B. Effect of mechanical properties of hydrogels on spheroid formation

Many studies show that the migration of cells in the case of 2D culture is influenced by the mechanical properties of their microenvironment[35,40], then the motile dynamics of multicellular spheroids might also be regulated by changes in ECM stiffness.

Wherefore, the effect of altered hydrogel stiffness on the podocytes cell is examined using all the prepared samples that have different crosslinker concentration. The increase of crosslinker density restricts deformation of the matrix and increase the local ECM stiffness around the cells.

After 2 days of the culture, encapsulated cells start forming spherical morphology instead of the random aggregation formed at the day 0 of the culture. The size of the spheroids formed increased at day 5 while maintaining the spherical morphology. After 7 days, spread spherical morphology was observed in hydrogels having high stiffness. The effect of the hydrogel mechanical properties on the morphology and the cytoskeleton reorganization of podocyte cells are characterized by visualizing the actin network using Phalloidin staining at the day 10 of the culture.

Figure 11 shows the spheroids formed in hydrogels having 2 different crosslinker density (30 : 0.06 (4 kPa) and 30 : 0.18 (9 kPa)), which shows during the cell culture two different cell response. These samples are compared to a control cultured on a well plate. For example, hydrogels having a Young's modulus of 4 kPa support circular morphology of podocytes cells aggregation located in the center of the pores, while for hydrogels having a Young's modulus of 9 kPa, the cells form spheroids having spread edges and these branches attach to the surface forming a barrier, for pores having initially a high cell concentration. For the pores having low initial cell concentration, the cell-cell interaction is low so cells proliferate and cover the inner surface of the pores, forming an empty sphere.

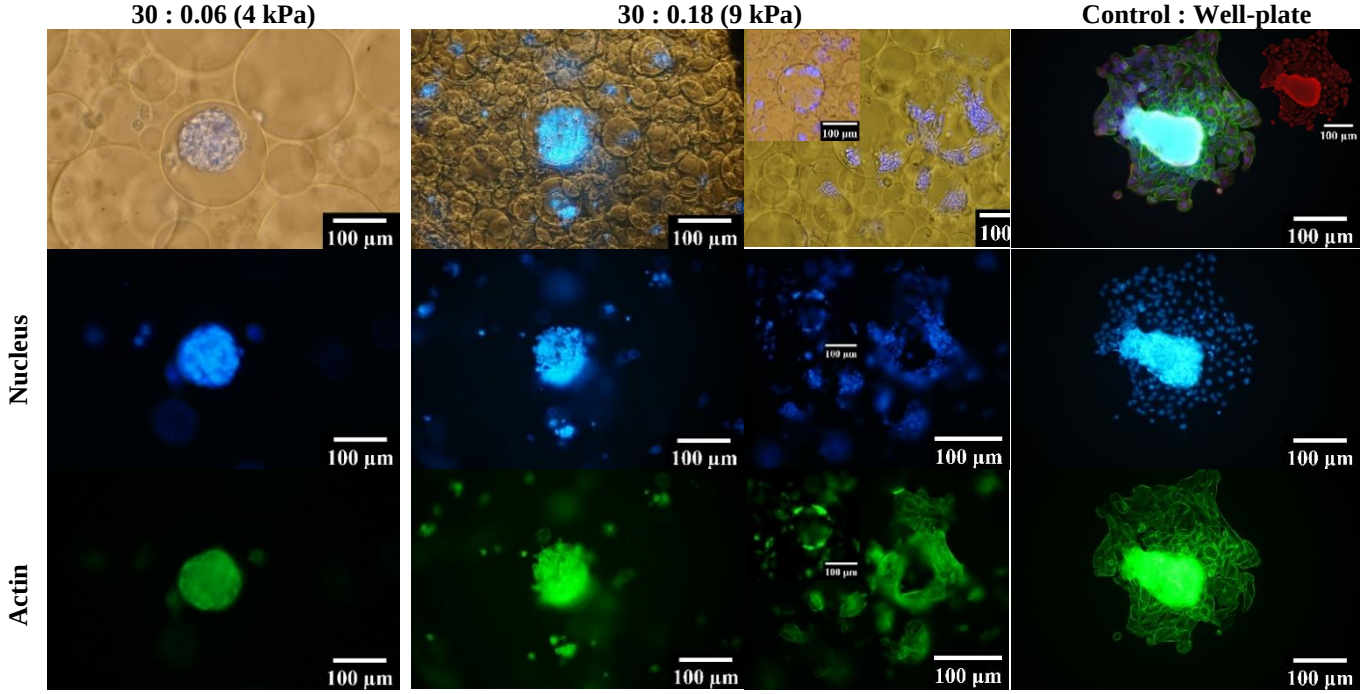

Figure 11. Representative immunofluorescence images of podocytes spheroids cultured on PAAM hydrogels prepared using 0.06 and 0.18% BIS after 10 days of culture. The cells are detected by staining the nucleus (DAPI-blue), and the actin cytoskeleton (Phalloidin-green).

It should be noted that the local stiffness of the hydrogel surrounding the spheroids it is not the same as stiffness of the total porous hydrogel. As shown in the chapter 2 (Fig 7b) the gel prepared with 0.18% of BIS have a Young's modulus of 40 kPa and 90 kPa for 0.6%, which is 10 times the Young's modulus of porous hydrogels having the same crosslinker density.

Encapsulated cells are able to sense and respond to external mechanical stimuli[42]. Increasing the matrix stiffness increase in the extension of the spheroids and facilitate their spreading and the formation of strong actin cytoskeleton [40,45–47].

C. Effect of hydrolysis rate of hydrogels on spheroid formation

PAAM hydrogel is hydrolyzed with different NaOH concentration in order to see their impact on cell growth. The results of cell proliferation show that the cells did not proliferate enough for low NaOH concentration (0.065 and 0.125 M) in addition to the high cell death that it is probably caused by the toxicity of the acrylamide monomer that stays in the structure. For gel hydrolyzed with a concentration above 0.25 M of NaOH, the cell growth was not affected and it did not show any difference on cell behavior from this value.

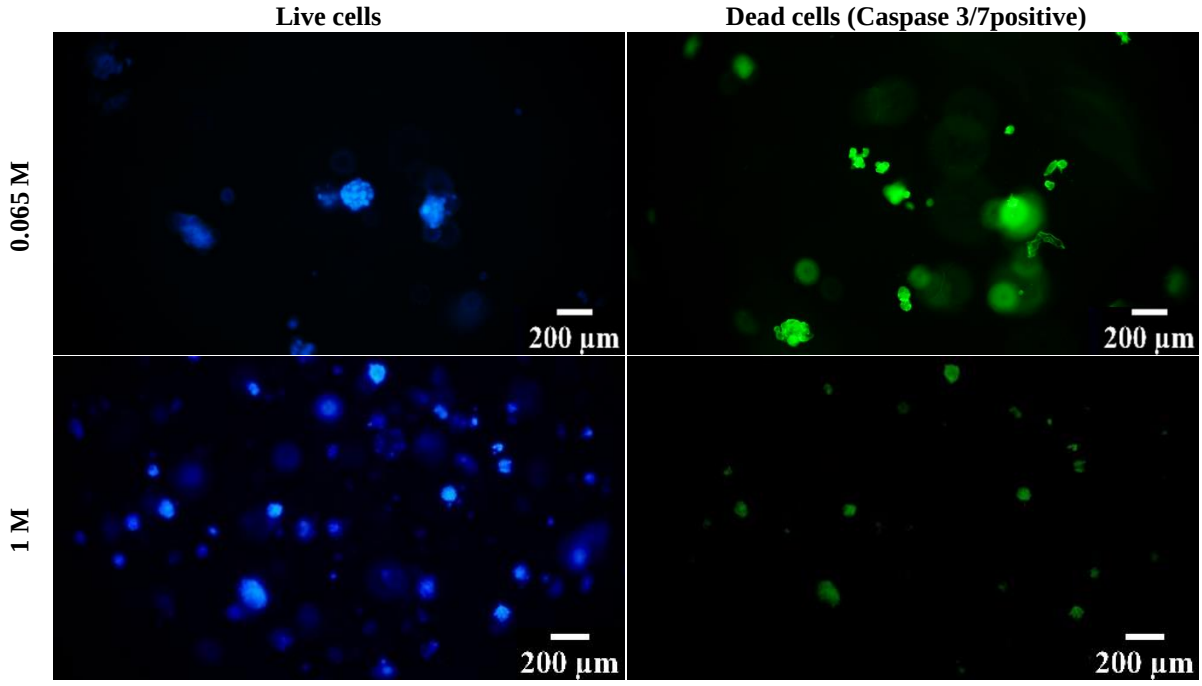

Figure 12. Detection of live/dead cells. Podocytes cells are treated with 2 µM caspase 3/7 for 30 minutes. Cells are stained with DAPI (blue), dead cells are detected with Caspase 3/7 502/530 nm (green).

Figure 12 shows that for 0.0065 M NaOH hydrolysis rate, that the number of dead cells (green) is more than live cells (bleu). However, the number of dead cells (green) in the sample hydrolyzed in 1 M NaOH is small compared to the number of living cells (bleu).

D. Effect of the hydrogels thickness on spheroid formation

The effect of Hydrogel thickness on spheroid preservation is studied. Since the cells are placed on the top of the porous hydrogel, the previous cases show a diffusion of single cells and even

small aggregation throw the membrane, and proliferate to the bottom of the plate. So increasing the hydrogel thickness may decrease the cells crossing throw the membrane.

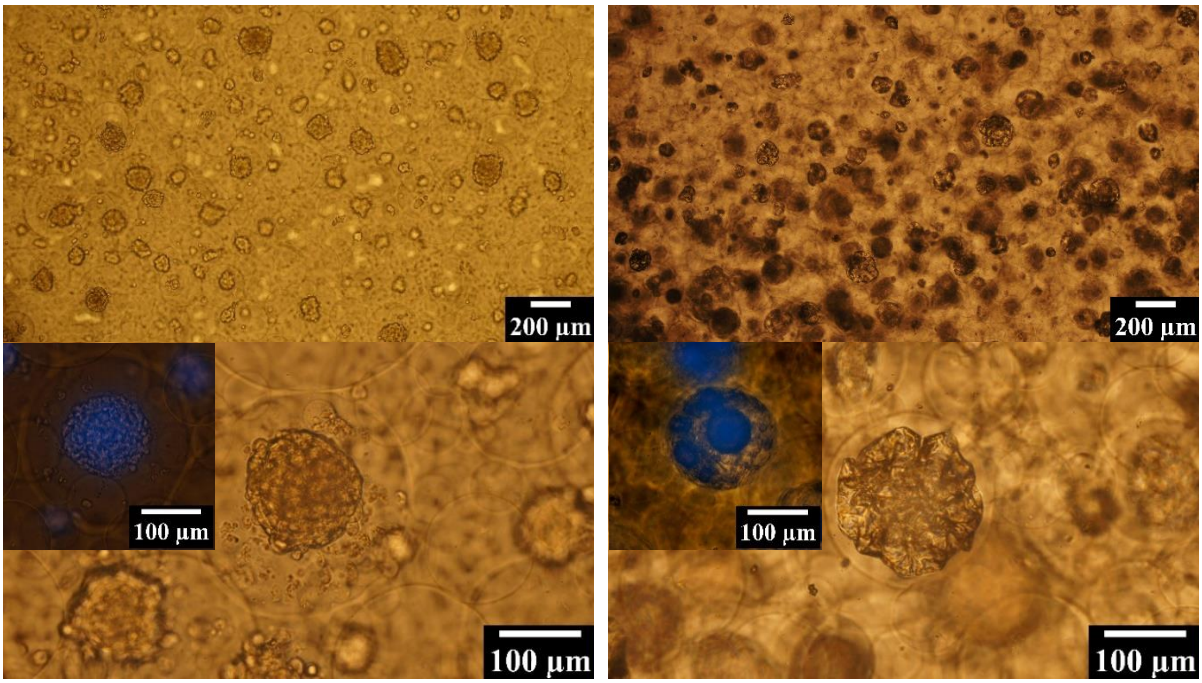

(a) **(b)**

Figure 13. Optical microscope images of podocytes inside the macropores of the hydrogel prepared with 30 : 0.06 AAM : BIS ratios cut at different thickness **(a)** 200 µm and **(b)** 500 µm at different magnification, and after staining the nucleus (DAPI-blue).

In addition, increasing the hydrogel thickness leads to a formation of deepest layers of spheroid and avoid the detachment of the spheroid formed on the top/bottom of the hydrogel in the case of the Immunocytochemical Characterization process or the filtration application. On the other hand, the hydrogel thickness has a big constraint for viewing under the microscope, so just the bottom of the hydrogel can be seen.

The results show an increase of the spheroid number with the increase of the hydrogel thickness (same cell number in the beginning). However, it was impossible to quantify the cells or spheroids number as in the case of 2D culture because the spheroids are formed in different level. In the thick hydrogel, cells need more time to cross the scaffold, so fewer cells cross the hydrogel to the bottom of the plate. In addition, a different shape of the spheroid is presented in the thick hydrogel, it shows a more compact nucleus aggregation and more spread actin.

More characterization should be realized to more understand the difference between spheroid shapes, such as SEM and TEM to closely see the cell-cell and cell-ECM interaction, and create slices to see deeply the inner layers of the spheroids.

E. Proliferation

The cell proliferation is tested on the day 10 of the culture. Since the spheroids in the gels are formed in different layers, and in the control culture they form a single layer, it is quite difficult to compare the proliferation between different culture conditions and the culture control. So the cell proliferation is evaluated to see if the cell still proliferates at this stage of the culture.

Figure 14. shows that the cells forming spheroids still proliferating after the day 10 of the culture. Among the living cells (bleu), the green marker indicates that the cells are still proliferating (EDU positive).

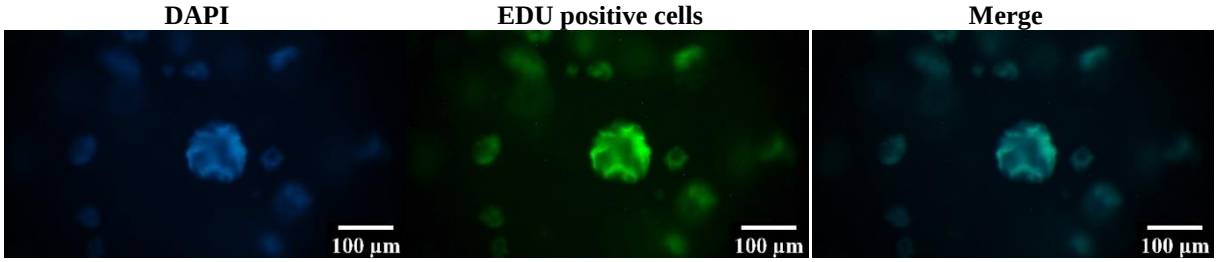

Figure 14. Detection of cell proliferation. Podocytes cells are treated with 10 µM EdU for 24 hours, then detected with Andy Fluor™ 488 azide (green), cells are counterstained with DAPI (blue).

This indicates that the cells still renewing themselves even after 10 days of the culture. During proliferation, cell number increase and maintain the balance between cell divisions and cell loss through cell death, which maintains a long lifetime of the culture.

F. Live/dead cells

Figure 15 shows the life and dead cell assay results of the 30:0.06 AAM:BIS hydrogel at the day 10 of the culture.

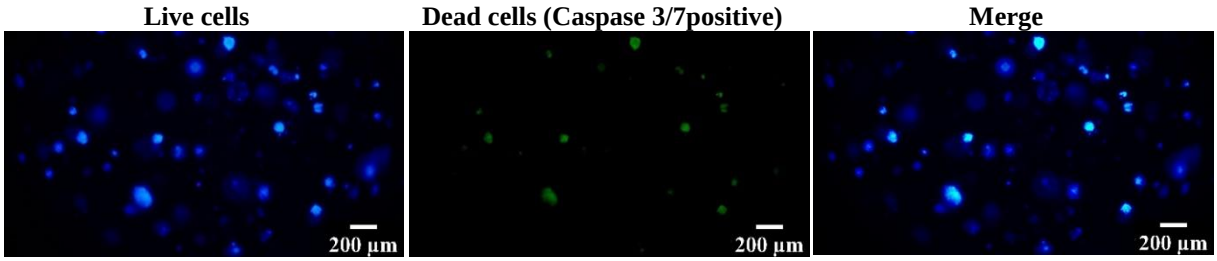

Figure 15. Detection of live/dead cells. Podocytes cells are treated with 2 µM caspase 3/7 for 30 minutes. Cells are stained with DAPI (blue), dead cells are detected with Caspase 3/7 502/530 nm (green).

The blue fluorescence from the live cells is detected, indicating that the cells had spread well in the PAAM hydrogel and prove its viability. Regarding the dead cells stained in green, they present a minority over the living cells even after 10 days of culture. This result in addition to the proliferation result, suggests that the PAAM hydrogels can provide a suitable 3D microenvironment for spheroid podocyte growth.

Three-dimensional spheroids have a complex architectural structure, dynamic cell–cell/cell–matrix interactions and bio-mimicking *in vivo* microenvironment[43]. In addition, spheroid formation inside the hydrogel macropores will avoid the cell detachment in case of a high flow rate inside the microfluidic device used for filtration applications.

The spheroids have shown different responses by changing the structural and mechanical properties of the hydrogel. The oil/AAM ratio affect the pore size and the porosity of the hydrogel. The results show that by increasing the connection between pores, the cells can infiltrate inside the scaffold to form spheroids inside the pores and the large interconnected macropores ensure a sufficient nutrient and oxygen supply, and a waste extraction which promotes cell growth and enhances cell survival[16,44], but it risks that the cells cross the hydrogel without forming any spheroid for a very high-connected porosity.

The crosslinker density has an important role for spheroid formation, because it affects the hydrogel stiffness and therefore the cell-ECM interaction. Encapsulated cells are able to sense and respond to external mechanical stimuli[42]. Increasing the matrix stiffness increase in the extension of the spheroids and facilitate their spreading and the formation of strong actin cytoskeleton[40,45–47]. The spheroids formed inside the pores of (30 : 0.18) form a barrier on the inner surface of the pore which makes this hydrogel a promising membrane to replace kidney filtration. The hydrolysis rate affects the cells live and proliferation; a low concentration of NaOH solution cannot eliminate all toxins existing inside the PAAM scaffold, which lead to cell death.

IV. Conclusion

Polyacrylamide micro and macro structure can be tailored depending on the application. Hand-shaking is a repetitive low-shear homogenization method used for the formation of micrometric size oil droplets emulsion[30–32]. 3D porous PAAM scaffolds are formed using emulsion templating technique, in order to form an interconnected marcro-porosity of an average pore size of 150 to 250 µm[12] suitable for spheroid cell culture.

The mechanical and structural properties of 3D PAAM hydrogel can be tailored by changing hydrogel pregel composition, or the experimental condition such as emulsion components. Surfactant content is an essential parameter for maintaining the emulsion stability and it affects the pore size and porosity of the resulting hydrogel. Increasing the surfactant content, increase the stability time of the emulsion and lead to a small pore size and a very highly interconnected porosity. Swelling and Young's modulus are also affected by the surfactant content, it shows a decrease by raising Triton X-100 percentage in the emulsion solution.

Oil content can affect both polymerization kinetic and the properties of resulted polymers, increasing Oil/pregel ratio decrease pore size and increase the connection between pores with lead to a softer structure.

Crosslinker density is a very important parameter to conserve the hydrogel structure and improve mechanical properties. For a high crosslinker concentration, the micromolecular chains between crosslinked points become shorter, which reveals a lower deformation ability and therefore an augmentation of stiffness and a decrease in the swelling ratio[37].

PAAM hydrogel is a suitable scaffold for cell culture, due to the high water content, the biocompatibility, non-toxicity and the facility of controlling its mechanical and structural properties. Both structural and mechanical properties of porous PAAM hydrogels affect the Podocyte spheroid formation and proliferation. Spheroid's formation is affected by the hydrogel porosity; increasing the interconnection between pores allows the cells to infiltrate and form spheroids inside the hydrogel and ensure a sufficient nutrient and oxygen supply and a waste extraction [16,44], but it risks that the cells cross the hydrogel without forming any spheroid for a very high-connected porosity.

Encapsulated cells are able to sense and respond to external mechanical stimuli[42]. Increasing the matrix stiffness increase in the extension of the spheroids and facilitate their spreading and the formation of strong actin cytoskeleton [40,45–47].

PAAM 3D macroporous hydrogel properties, such as water content, stiffness and porosity, can be easily controlled in order to mimic spheroids environment and improve the cell-cell and cell-ECM interaction. The oil/AAM ratio affect the pore size and the porosity of the hydrogel, and therefore the spheroid formation. Increasing the connection between pores, the cells can infiltrate inside the scaffold to form spheroids inside the pores and the large interconnected macropores ensure a sufficient nutrient and oxygen supply, and a waste extraction which promotes cell growth and enhances cell survival [16,44], but it risks that the cells cross the hydrogel without forming any spheroid for a very high-connected porosity.

The crosslinker density has an important role for spheroid formation, because it affects the hydrogel stiffness and therefore the cell-ECM interaction. Encapsulated cells are able to sense and respond to external mechanical stimuli[42]. Increasing the matrix stiffness increase in the extension of the spheroids and facilitate their spreading and the formation of strong actin cytoskeleton [40,45–47]. The hydrolysis rate affects the cells live and proliferation; a low concentration of NaOH solution cannot eliminate all toxins existing inside the PAAM scaffold, which lead to cell death.

Macroporous PAAM hydrogel is a suitable scaffold for spheroid formation, due to its structural and mechanical properties that can be easily controlled to form a favorable environment for cells. The spheroids formed inside the pores of (30 : 0.18) form a barrier on the inner surface of the pore which makes this scaffold a promising membrane to replace kidney filtration. A microfluidic device encapsulating a PAAM hydrogel cultured with podocytes, will be used as a “filtration unit” in our future bioartificial kidney.

V. References

1. Yue, B. Biology of the Extracellular Matrix: An Overview. *Journal of Glaucoma* **23**, S20–S23 (2014).
2. Naba, A. *et al.* The extracellular matrix: Tools and insights for the “omics” era. *Matrix Biology* **49**, 10–24 (2016).

3. Ying, G. *et al.* Aqueous Two-Phase Emulsion Bioink-Enabled 3D Bioprinting of Porous Hydrogels. *Advanced Materials* **30**, 1805460 (2018).

4. Caló, E. & Khutoryanskiy, V. V. Biomedical applications of hydrogels: A review of patents and commercial products. *European Polymer Journal* **65**, 252–267 (2015).

5. Abdallah, M. Développer des hydrogels et étudier les effets des propriétés mécaniques sur les activités biologiques des podocytes. (Université de Montpellier, 2019).

6. Haque, Md. A., Kurokawa, T. & Gong, J. P. Super tough double network hydrogels and their application as biomaterials. *Polymer* **53**, 1805–1822 (2012).

7. Sergeeva, A., Vikulina, A. S. & Volodkin, D. Porous Alginate Scaffolds Assembled Using Vaterite CaCO3 Crystals. *Micromachines* **10**, 357 (2019).

8. Du, B., Yu, M. & Zheng, J. Transport and interactions of nanoparticles in the kidneys. *Nature Reviews Materials* **3**, 358–374 (2018).

9. Reiser, J. & Altintas, M. M. Podocytes. *F1000Research* **5**, 114 (2016).

10. Greka, A. & Mundel, P. Cell Biology and Pathology of Podocytes. *Annual Review of Physiology* **74**, 299–323 (2012).

11. Qu, Y. *et al.* A nephron model for study of drug-induced acute kidney injury and assessment of drug-induced nephrotoxicity. *Biomaterials* **155**, 41–53 (2018).

12. Hale, L. J. *et al.* 3D organoid-derived human glomeruli for personalised podocyte disease modelling and drug screening. *Nature Communications* **9**, (2018).

13. Rhein, L. Surfactant Action on Skin and Hair: Cleansing and Skin Reactivity Mechanisms. in *Handbook for Cleaning/Decontamination of Surfaces* 305–369 (Elsevier, 2007). doi:10.1016/B978-044451664-0/50009-7.

14. Y. Abu-Thabit, N. Thermochemistry of Acrylamide Polymerization: An Illustration of Auto-acceleration and Gel Effect. *World Journal of Chemical Education* **5**, 94–101 (2017).

15. Bassil, M., El Haj Moussa, G. & El Tahchi, M. Templating polyacrylamide hydrogel for interconnected microstructure and improved performance. *Journal of Applied Polymer Science* **135**, 46205 (2018).

16. Bäcker, A. *et al.* Silk scaffolds connected with different naturally occurring biomaterials for prostate cancer cell cultivation in 3D: BÄCKER et al. *Biopolymers* **107**, 70–79 (2017).

17. Williams, J. J. Formulation of Carpet Cleaners. in *Handbook for Cleaning/Decontamination of Surfaces* 103–123 (Elsevier, 2007). doi:10.1016/B978-044451664-0/50004-8.

18. Valdés-Díaz, G. *et al.* Effects of gamma radiation on phase behaviour and critical micelle concentration of Triton X-100 aqueous solutions. *Journal of Colloid and Interface Science* **311**, 253–261 (2007).

19. Tehrani-Bagha, A. R. Cationic gemini surfactant with cleavable spacer: Emulsion stability. *Colloids and Surfaces A: Physicochemical and Engineering Aspects* **508**, 79–84 (2016).

20. Pulko, I. & Krajnc, P. High Internal Phase Emulsion Templating - A Path To Hierarchically Porous Functional Polymers. *Macromolecular Rapid Communications* **33**, 1731–1746 (2012).

21. Zhang, X. *et al.* Use of Orbital Shaken Disposable Bioreactors for Mammalian Cell Cultures from the Milliliter-Scale to the 1,000-Liter Scale. in *Disposable Bioreactors* (eds. Eibl, R. & Eibl, D.) vol. 115 33–53 (Springer Berlin Heidelberg, 2009).

22. Maier, U., Losen, M. & Büchs, J. Advances in understanding and modeling the gas–liquid mass transfer in shake flasks. *Biochemical Engineering Journal* **17**, 155–167 (2004).

23. Zhu, L. *et al.* Fluid dynamics of flow fields in a disposable 600-mL orbitally shaken bioreactor. *Biochemical Engineering Journal* **129**, 84–95 (2018).

24. Klöckner, W. & Büchs, J. Advances in shaking technologies. *Trends in Biotechnology* **30**, 307–314 (2012).

25. Zhu, L. *et al.* Studies on fluid dynamics of the flow field and gas transfer in orbitally shaken tubes. *Biotechnology Progress* **33**, 192–200 (2017).

26. Pichot, R., Spyropoulos, F. & Norton, I. T. O/W emulsions stabilised by both low molecular weight surfactants and colloidal particles: The effect of surfactant type and concentration. *Journal of Colloid and Interface Science* **352**, 128–135 (2010).

27. Bassil, M. *et al.* Electrochemical and electromechanical properties of fully hydrolyzed polyacrylamide for applications in biomimetics. *Smart Materials and Structures* **17**, 055017 (2008).

28. Liu, S. *et al.* High internal phase emulsions stabilised by supramolecular cellulose nanocrystals and their application as cell-adhesive macroporous hydrogel monoliths. *Journal of Materials Chemistry B* **5**, 2671–2678 (2017).

29. Annabi, N. *et al.* Synthesis of highly porous crosslinked elastin hydrogels and their interaction with fibroblasts in vitro. *Biomaterials* **30**, 4550–4557 (2009).

30. Mable, C. J. *et al.* ABC Triblock Copolymer Worms: Synthesis, Characterization, and Evaluation as Pickering Emulsifiers for Millimeter-Sized Droplets. *Macromolecules* **49**, 7897–7907 (2016).

31. Arditty, S., Whitby, C. P., Binks, B. P., Schmitt, V. & Leal-Calderon, F. Some general features of limited coalescence in solid-stabilized emulsions. *The European Physical Journal E* **11**, 273–281 (2003).

32. Frelichowska, J., Bolzinger, M.-A. & Chevalier, Y. Effects of solid particle content on properties of o/w Pickering emulsions. *Journal of Colloid and Interface Science* **351**, 348–356 (2010).

33. Jelitto, H. & Schneider, G. A. Fracture toughness of porous materials – Experimental methods and data. *Data in Brief* **23**, 103709 (2019).

34. Garlea, E. *et al.* Variation of elastic mechanical properties with texture, porosity, and defect characteristics in laser powder bed fusion 316L stainless steel. *Materials Science and Engineering: A* **763**, 138032 (2019).

35. Abdallah, M. *et al.* Influence of Hydrolyzed Polyacrylamide Hydrogel Stiffness on Podocyte Morphology, Phenotype, and Mechanical Properties. *ACS Applied Materials & Interfaces* **11**, 32623–32632 (2019).

36. Zhang, L. *et al.* Pullulan dialdehyde crosslinked gelatin hydrogels with high strength for biomedical applications. *Carbohydrate Polymers* **216**, 45–53 (2019).

37. Hu, X. *et al.* Preparation and characterization of a novel pH-sensitive Salecan-g-poly(acrylic acid) hydrogel for controlled release of doxorubicin. *Journal of Materials Chemistry B* **3**, 2685–2697 (2015).

38. Embry, A. E. *et al.* Biochemical and Cellular Determinants of Renal Glomerular Elasticity. *PLOS ONE* **11**, e0167924 (2016).

39. Jansen, K., Schuurmans, C. C. L., Jansen, J., Masereeuw, R. & Vermonden, T. Hydrogel-Based Cell Therapies for Kidney Regeneration: Current Trends in Biofabrication and In Vivo Repair. *Current Pharmaceutical Design* **23**, (2017).

40. McKenzie, A. J. *et al.* The mechanical microenvironment regulates ovarian cancer cell morphology, migration, and spheroid disaggregation. *Scientific Reports* **8**, (2018).

41. Lee, J., Cuddihy, M. J., Cater, G. M. & Kotov, N. A. Engineering liver tissue spheroids with inverted colloidal crystal scaffolds. *Biomaterials* **30**, 4687–4694 (2009).

42. Jaiswal, M. K. *et al.* Mechanically Stiff Nanocomposite Hydrogels at Ultralow Nanoparticle Content. *ACS Nano* **10**, 246–256 (2016).

43. Cui, X., Hartanto, Y. & Zhang, H. Advances in multicellular spheroids formation. *Journal of The Royal Society Interface* **14**, 20160877 (2017).

44. Zhang, K., Yan, S., Li, G., Cui, L. & Yin, J. In-situ birth of MSCs multicellular spheroids in poly(l -glutamic acid)/chitosan scaffold for hyaline-like cartilage regeneration. *Biomaterials* **71**, 24–34 (2015).

45. Imaninezhad, M., Hill, L., Kolar, G., Vogt, K. & Zustiak, S. P. Templated Macroporous Polyethylene Glycol Hydrogels for Spheroid and Aggregate Cell Culture. *Bioconjugate Chemistry* **30**, 34–46 (2019).

46. Mason, B. N., Starchenko, A., Williams, R. M., Bonassar, L. J. & Reinhart-King, C. A. Tuning three-dimensional collagen matrix stiffness independently of collagen concentration modulates endothelial cell behavior. *Acta Biomaterialia* **9**, 4635–4644 (2013).

47. Wang, C., Tong, X. & Yang, F. Bioengineered 3D Brain Tumor Model To Elucidate the Effects of Matrix Stiffness on Glioblastoma Cell Behavior Using PEG-Based Hydrogels. *Molecular Pharmaceutics* **11**, 2115–2125 (2014).

General Conclusion

Kidney have an essential role for a normal body function. Kidney filtration membrane (basement membrane, endothelium, and podocytes) is responsible of normal kidney filtration. Chronic Kidney Disease (CKD) reduce their efficiency to filter the blood of 10% to 15% of the population worldwide and few of them receive treatment (Dialysis, transplantation and Microfluidic Bioartificial Kidney).

The challenge for researchers nowadays is to reduce the socio-economical burdens on the societies and the patients suffering from kidney disease, by developing an implantable or portable dialysis device that can replace the tissue function, and specially the kidney function in case of loss or failure.

Microfluidics Bioartificial Kidney, is a promising technology to treat the loss or malfunction of kidney, despite all the limitations they still facing. Microfluidic kidney encapsulates a filtration membrane based usually on hydrogel seeded with podocytes in order to closely mimic the kidney filtration function. PAAM hydrogel is an ionic gel used in cell culture, because its high fluid contents, its possibility of cells adhesion without the need of protein and its non-toxicity. The properties of this hydrogel such as swelling, porosity and stiffness can be controlled to mimic cell environment for better conditions for cell growth.

The ultimate goal of this work is to develop a biocompatible implantable bioartificial kidney that mimic the work of a natural kidney. In this thesis, we aim to develop several “filtration units” each having a specific filtration function and serving as building blocks of the future bioartificial kidney.

A single microchip “filtration unit” is designed to replicate the in vivo model and works as a miniaturized dialysis machine. The “filtration unit” consist of PDMS layers encapsulating a hydrogel membrane or a hydrogel extracellular matrix seeded with podocyte and endothelial cells. Controlling the hydrogel physicochemical properties will help monitoring the filtration ability and efficiency of the “filtration unit”. The PAAM hydrogel properties can be controlled by changing the gel composition or the fabrication method of the hydrogel. The swelling and the mesh size decrease by increasing the crosslinker density, and this is due to the small distance between the network nodes and reduce the capacity of the gel to absorb water. As the network density increases, the average molecular weight between crosslinked point decreases and leads to a rise of the gel stiffness.

Hydrogels have a potential not just as filtration membrane but also they can be used as extracellular membrane for kidney regeneration. Hence the importance to study the filtration ability of PAAM hydrogel as new candidate to be used as a basement membrane for kidney replacement.

2D PAAM hydrogels have shown a good efficiency in small molecules clearance (< 500 Da), but it blocks the passage of medium and large molecules, so a fabrication of nanoporous hydrogel is required to eliminate molecules having a molecular weight between 1 and 69 kDa. The diffusion of small molecules can be controlled by changing the hydrogel composition or the experimental parameters. Increasing the flow rate as well as the crosslinker density slows down the diffusion of molecules through the membrane. Controlling the hydrogel physicochemical properties will help monitoring the filtration ability and efficiency of the "filtration unit". (As an example: controlling the pore size of the hydrogel matrix will allow monitoring the size selectivity or the molecular weight cutoff while controlling the porosity will help controlling the speed of solute diffusion across the matrix).

Polyacrylamide micro and macro structure can be also tailored depending on the application. 3D porous Hydrogel scaffold is required for cell culture application due to its resemblance to natural tissue. 3D porous PAAM scaffolds are formed using emulsion templating technique, in order to form an interconnected marcro-porosity of an average pore size of 150 to 250 µm suitable for spheroid cell culture. Hand-shaking is a repetitive low-shear homogenization method used for the formation of micrometric size oil droplets emulsion.

The mechanical and structural properties of 3D PAAM hydrogel can be tailored by changing hydrogel pregel composition, or the experimental condition such as emulsion component. Surfactant content is an essential parameter for maintaining the emulsion stability and it affects the pore size and porosity of the resulting hydrogel. Increasing the surfactant content, increase the stability time of the emulsion and lead to a small pore size and a very high interconnected porosity. Swelling and Young's modulus are also affected by the surfactant content, it shows a decrease by raising Triton X-100 percentage in the emulsion solution.

Oil content can affect both polymerization kinetic and the properties of resulted polymer, increasing Oil/pregel ratio decrease pore size and increase the connection between pores that lead to a softer structure.

Crosslinker density is a very important parameter to conserve the hydrogel structure and improve mechanical properties. For a high crosslinker concentration, the micromolecular chains between crosslinked points become shorter, which reveals a lower deformation ability and therefore an augmentation of stiffness and a decrease in the swelling ratio.

PAAM hydrogel is a suitable scaffold for cell culture, due to the high water content, the biocompatibility, non-toxicity and the facility of controlling its mechanical and structural properties. Both structural and mechanical properties of porous PAAM hydrogel affect the Podocyte spheroids formation and proliferation. Spheroids formation is affected by the hydrogel porosity; increasing the interconnection between pores allow the cells to infiltrate and form spheroids inside the hydrogel and insure a sufficient nutrient and oxygen supply and a waste extraction, but it risks that the cells cross the hydrogel without forming any spheroid for a very high connected porosity.

Encapsulated cells are able to sense and respond to external mechanical stimuli. Increasing the matrix stiffness increase in the extension of the spheroids and facilitate their spreading and the formation of strong actin cytoskeleton.

PAAM 3D macroporous hydrogel properties, such as water content, stiffness and porosity, can be easily controlled in order to mimic spheroids environment and improve the cell-cell and cell-ECM interaction.

Using hydrogels having different properties, seeded or not with podocytes will lead the generation of different filtration units each having a specific function and imitating a specific renal activity.

Finally, the future bioartificial kidney could be an assembly of several filtration units working in parallel, each unit having a specific filtration function. Developing such device would be an epic advance in medicine and could address a chronic shortage of donor kidneys needed. Therefore, the perspective of this study will be to fabricate a nanoporous PAAM hydrogel that will eliminate all molecules having a molecular weight between 10 and 69 kDa, and work as a second “filtration unit” in the bioartificial kidney in parallel with the device encapsulating 2D PAAM hydrogel membrane that eliminate small molecules. Furthermore, testing the filtration efficiency of PAAM hydrogel seeded with podocytes spheroids will be the future objective of

this work, after studying the interaction podocytes/PAAM. In addition, the filtration efficiency and the biofouling will be tested for a long duration (more than 1 week), in order to minimize the frequency of the patient's visit to the hospital in the case of device implantation. The assembly of different “filtration units” working in parallel will be tested in order to assess the replication of normal renal function.

Abstract

Microfluidics is a promising technology for improving biology and medicine research. Artificial kidney is a microfluidic device that replaces kidney filtration function by minimizing the whole dialysis system, consist of a filtration membrane placed inside a device prepared from biocompatible materials. Bioartificial kidneys provide an extension to conventional artificial kidneys, by incorporating tissue engineering with living cellular and tissue, in an order to better mimic normal kidneys. Hydrogels are three-dimensional, hydrophilic, polymeric networks capable of absorbing large amounts of biological fluids. Due to their high water content, porosity and soft consistency, hydrogels closely simulate natural living tissue, and are widely used as an extracellular matrix (ECM). The use of porous hydrogels as ECM in microfluidic devices provides a soft and controllable mechanical properties of the matrix, improve the cell-cell and cell-ECM interaction and enables the embedding of cells, as oxygen and nutrients are able to diffuse through their structure and provide the proper environment for cell culture. The hydrolyzed polyacrylamide hydrogel was chosen for tissue engineering due to its mechanical properties, its easy shaping and its viscoelasticity. The thesis aim was to develop a Polyacrylamide hydrogel used as a filtration membrane in microfluidics system forming a "filtration unit" in order to block the passage of molecule above a specific size due to their controllable mesh size. Macroporous Polyacrylamide hydrogel is prepared using emulsion technique, and used as extracellular matrix for podocytes spheroids formation. Controlling the hydrogel structural and mechanical properties leads to different responses of podocytes spheroids. Macroporous Polyacrylamide hydrogel holding podocytes spheroids will be used as filtration basement membrane encapsulated in a microfluidic device forming another "filtration unit". The assembly of different filtration units encapsulating hydrogels seeded with podocytes cells or not, working in parallel will form the bioartificial kidney that replace the normal kidney function.

Résumé

La microfluidique est une technologie prometteuse pour l'amélioration de la recherche en biologie et en médecine. Le rein artificiel est un dispositif microfluidique qui remplace la fonction de filtration rénale en minimisant l'ensemble du système de dialyse, constitué d'une membrane de filtration placée à l'intérieur d'un dispositif préparé à partir de matériaux biocompatibles. Les reins bioartificiels offrent une extension aux reins artificiels conventionnels, en incorporant l'ingénierie tissulaire avec des cellules et des tissus vivants, afin de mieux imiter les reins normaux. Les hydrogels sont des réseaux polymériques hydrophiles tridimensionnels capables d'absorber de grandes quantités de fluides biologiques. En raison de leur teneur élevée en eau, de leur porosité et de leur consistance molle, les hydrogels simulent étroitement les tissus vivants naturels et sont largement utilisés comme matrice extracellulaire (MEC). L'utilisation d'hydrogels poreux comme MEC dans les dispositifs microfluidiques fournit des propriétés mécaniques douces et contrôlables de la matrice, améliore l'interaction cellule-cellule et cellule-MEC et permet l'enrobage des cellules, car l'oxygène et les nutriments sont capables de se diffuser à travers leur structure et fournir l'environnement approprié pour la culture cellulaire. L'hydrogel de polyacrylamide hydrolysé a été choisi pour l'ingénierie tissulaire en raison de ses propriétés mécaniques, sa facilité de mise en forme et sa viscoélasticité. L'objectif de la thèse est de développer un hydrogel de Polyacrylamide utilisé comme membrane de filtration microfluidique, formant une « unité de filtration » afin de bloquer le passage de molécule au-dessus d'une taille spécifique en raison de leur taille de maille contrôlable. L'hydrogel de polyacrylamide macroporeux est préparé à l'aide de la technique d'émulsion et utilisé comme matrice extracellulaire pour la formation de sphéroïdes de podocytes. Le contrôle des propriétés structurelles et mécaniques de l'hydrogel conduit à différentes réponses des sphéroïdes de podocytes. Un hydrogel de Polyacrylamide macroporeux contenant des sphéroïdes de podocytes sera utilisé comme membrane basale de filtration encapsulée dans un dispositif microfluidique formant une autre « unité de filtration ». L'assemblage de différentes unités de filtration encapsulant des hydrogels ensemencés ou non de cellules de podocytes, travaillant en parallèle formera le rein bioartificiel qui remplace la fonction rénale normale.